

AD-A129 858

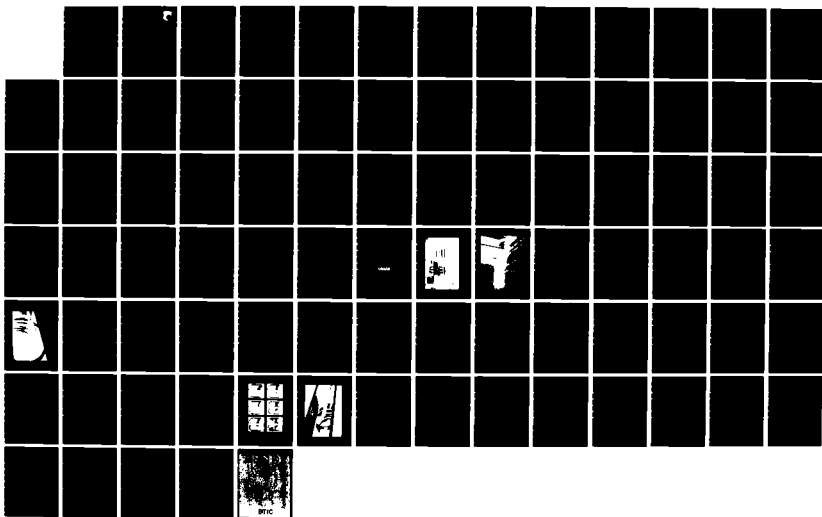
THREE-DIMENSIONAL TEST EXPERIENCE WITH A TRANSONIC
ADAPTIVE-WALL WIND TUNNEL(U) DAYTON UNIV OH RESEARCH
INST D J HARNEY MAR 83 AFWALLTR-83-3028

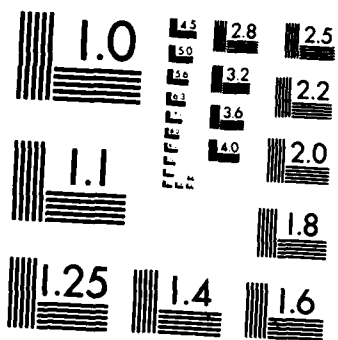
1/1

UNCLASSIFIED

F/G 14/2

NL





MICROCOPY RESOLUTION TEST CHART
NATIONAL BUREAU OF STANDARDS-1963-A

ADA 1 29858

AFWAL-TR-83-3028



THREE-DIMENSIONAL TEST EXPERIENCE WITH A TRANSONIC
ADAPTIVE-WALL WIND TUNNEL

Donald J. Harney
Aerospace Engineer

Experimental Engineering Branch
Aeromechanics Division
and
University of Dayton
Research Institute

March 1983

Final Report for Period April 1981 - December 1982

Approved for public release; distribution unlimited

JUN 2 1983

DTIC FILE COPY

FLIGHT DYNAMICS LABORATORY
AIR FORCE WRIGHT AERONAUTICAL LABORATORIES
AIR FORCE SYSTEMS COMMAND
WRIGHT-PATTERSON AIR FORCE BASE, OHIO 45433

83 06 00 025

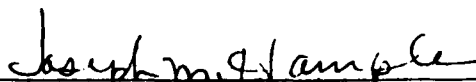
NOTICE

When Government drawings, specifications, or other data are used for any purpose other than in connection with a definitely related Government procurement operation, the United States Government thereby incurs no responsibility nor any obligation whatsoever; and the fact that the government may have formulated, furnished, or in any way supplied the said drawings, specifications, or other data, is not to be regarded by implication or otherwise as in any manner licensing the holder or any other person or corporation, or conveying any rights or permission to manufacture use, or sell any patented invention that may in any way be related thereto.

The report has been reviewed by the office of Public Affairs (ASD/PA) and is releasable to the National Technical Information Service (NTIS). At NTIS, it will be available to the general public, including foreign nations.

The technical report has been reviewed and is approved for publication.


MAURICE R. CAIN
Mechanical Engineer


JOSEPH M. HAMPLE, Chief
Experimental Engineering Branch
Aeromechanics Division

FOR THE COMMANDER


JOHN R. CHEVALIER, Colonel, USAF
Chief, Aeromechanics Division
Flight Dynamics Laboratory

If your address has changed, if you wish to be removed from our mailing list, or if the addressee is no longer employed by your organization please notify AFWAL/FIMN, Wright-Patterson AFB, OH 45433 to help us maintain a current mailing list.

Copies of this report should not be returned unless return is required by security consideration, contractual obligations, or notice on a specific document.

UNCLASSIFIED

SECURITY CLASSIFICATION OF THIS PAGE (When Data Entered)

REPORT DOCUMENTATION PAGE		READ INSTRUCTIONS BEFORE COMPLETING FORM
1. REPORT NUMBER AFWAL-TR-83-3028	2. GOVT ACCESSION NO. AD-A129 858	3. RECIPIENT'S CATALOG NUMBER
4. TITLE (and Subtitle) THREE-DIMENSIONAL TEST EXPERIENCE WITH A TRANSONIC ADAPTIVE-WALL WIND TUNNEL		5. TYPE OF REPORT & PERIOD COVERED Final Technical Report April 1981-December 1982
		6. PERFORMING ORG. REPORT NUMBER
7. AUTHOR(s) Donald J. Harney		8. CONTRACT OR GRANT NUMBER(s) F33615-79-C-3030
9. PERFORMING ORGANIZATION NAME AND ADDRESS University of Dayton 300 College Park Avenue Dayton, Ohio 45469		10. PROGRAM ELEMENT, PROJECT, TASK AREA & WORK UNIT NUMBERS P.E. 62201F, Project 2404 Task 240413 Work Unit 24041303
11. CONTROLLING OFFICE NAME AND ADDRESS Flight Dynamics Laboratory (AFWAL/FIMN) Air Force Wright Aeronautical Laboratories, AFSC Wright-Patterson Air Force Base, Ohio 45433		12. REPORT DATE March 1983
14. MONITORING AGENCY NAME & ADDRESS (if different from Controlling Office)		13. NUMBER OF PAGES 88
		15. SECURITY CLASS. (of this report) Unclassified
		15a. DECLASSIFICATION/DOWNGRADING SCHEDULE
16. DISTRIBUTION STATEMENT (of this Report) Approved for public release; distribution unlimited		
17. DISTRIBUTION STATEMENT (of the abstract entered in Block 20, if different from Report)		
18. SUPPLEMENTARY NOTES		
19. KEY WORDS (Continue on reverse side if necessary and identify by block number) Wind tunnels Transonic wind tunnels Wall interference Adaptive walls		
20. ABSTRACT (Continue on reverse side if necessary and identify by block number) A square 9-inch wind tunnel with solid sidewalls and flexible upper and lower rod walls capable of 3-D contouring was used to test an axisymmetric and a winged lifting model at M=0.50 to 0.95. The simple, direct analytical method for wall contouring uses the model geometry for solid blockage and iterative model force data to adapt for lift and for wake blockage. Solid sidewall effects and the convergence of the adaptation scheme are evaluated. Linear and nonlinear theory for solid blockage is compared. Interesting comparisons are also made between 2-D and 3-D wall contouring.		

DD FORM 1 JAN 73 1473 EDITION OF 1 NOV 65 IS OBSOLETE

UNCLASSIFIED

SECURITY CLASSIFICATION OF THIS PAGE (When Data Entered)

TABLE OF CONTENTS

SECTION		PAGE
I	INTRODUCTION	1
II	FACILITY DESIGN AND PERFORMANCE	5
	1. Overall Configuration	5
	2. Nozzle and Test Section Design	5
	3. Wall Boundary Layer Displacement Effects	9
	4. Wall Adaptation Methods	13
III	AXISYMMETRIC PRESSURE MODEL	15
	1. General	15
	2. Analytical Methods	15
	3. Solid Sidewall Effects	17
	4. Two-Dimensional Versus Three-Dimensional Contouring	20
	5. Additional Observations	21
IV	LIFTING MODEL TESTS	23
	1. General	23
	2. Analytical Methods	23
	3. Solid Sidewall Effects	26
	4. Self Adaptive Wall Streamlining	28
	5. Two-Dimensional Versus Three-Dimensional Contouring	29
V	CONCLUDING REMARKS	30
	REFERENCES	33

LIST OF ILLUSTRATIONS

FIGURE		PAGE
1	Overall Schematic of Facility	37
2	Cross Section through the Center of the Test Region	38
3	Display of Flexible Wall Test Section with Sidewall Removed	39
4	Details of Motorized Jacking Station	40
5	Rodwall Boundary Layer Development through the Nozzle Contraction to the Center of the Test Section	41
6	Sidewall Boundary Layer Development	42
7	Estimated Effect of Model Induced Pressure Gradient on the Wall Boundary Layer Displacement Thickness	43
8	Test Section Empty Calibration after Correction for Wall Boundary Layer	44
9	Wall Adaptation Scheme Showing Sequence of Operations	45
10	Parabolic-Arc Body of Revolution Pressure Model	46
11	Selected Comparisons of Free-Air Center Streamlines at the Wall Comparing Linear and Nonlinear Potential Flow Calculations	47
12	Comparison of Peak Streamline Deflections versus Mach Number Comparing Linear and Nonlinear Calculation Methods	48
13	Centerline Rod Deflection Including Boundary Layer Displacement and Solid Sidewall Effects	49
14	Pressure Distributions on the Axisymmetric Model for Varying Values of the Solid Sidewall Factor	50
15	Pressure Distribution for a Solid Sidewall Factor of 2.0 Comparing Nonlinear and Linear Methods of Calculation	51
16	Solid Sidewall Factor and Peak Streamline Deflection Required to Match the Theoretical Pressure Distribution on the Axisymmetric Body	52
17	Model Pressure Distributions with Variations in the Two-Dimensional Wall Setting	53
18	Pressure Distributions on a Parabolic-Arc Body of Revolution, Walls Contoured Using Linear Theory Corrected for Solid Sidewalls. Includes Comparisons of 2-D and 3-D Contours (a) $M = 0.500$	54

LIST OF ILLUSTRATIONS (continued)

FIGURE		PAGE
18	(b) $M = 0.700$	55
18	(c) $M = 0.800$	56
18	(d) $M = 0.850$	57
18	(e) $M = 0.900$	58
18	(f) $M = 0.925$	59
18	(g) $M = 0.945$	60
19	High Mach Number Model Pressure Distribution with Walls Expanded to Relieve Tunnel Choking	61
20	Relief of Tunnel Choking with a Slight Reduction in Mach Number of 0.005	62
21	Data Comparison Between a 10% and 20% Thick Model Illustrating a Double Compression	63
22	Schlieren Photographs of Axisymmetric Flow Ranging from Critical Flow to Tunnel Choking	64
23	Lifting Model Installed In Tunnel	65
24	Sectioning of Lifting Model Showing Locations of Representative Singularities	66
25	Refined Sectioning of Model for Solid Blockage Effects Using a Distribution of Doublets	67
26	Typical Three-Dimensional Rod Contouring for the Lifting Model	68
27	Convergence of Output Coefficients Using Zeros for Initial Input and Measured Values for Iterating	69
28	Variation of Convergence with Angle of Attack	70
29	Comparison of Three-Dimensionally Streamlined Wall Output Coefficients with AEDC 4T Data	71
	(a) $M = 0.50$	
29	(b) $M = 0.80$	72
29	(c) $M = 0.90$	73
29	(d) $M = 0.95$	74
30	Effect of Varying 2-D Wall Contours in Relation to a 3-D Contour	75
31	Comparison of the Area Displacement of 2-D and 3-D Wall Contours	76
32	Additional Comparisons of 2-D and 3-D Contouring at $M = 0.90$	77

LIST OF SYMBOLS

A	Cross-sectional area of the tunnel test section
A, B, C	Coefficients in Equation 9
C_f	Skin friction coefficient
C_D	Drag coefficient
C_L	Lift coefficient
C_m	Pitching moment coefficient
C_p	Pressure coefficient, $(p-p_\infty)/q_\infty$
d_s	Sting diameter
D	Drag force
\bar{D}	$D/q_\infty = C_D S$
h	Height of wind tunnel nozzle
H	Boundary layer form factor, δ^*/θ
K	Axisymmetric transonic similarity parameter, $(1 - M_\infty^2)/(M_\infty \tau)^2$
L	Lift force
\bar{L}	$L/q_\infty = C_L S$
m	Coefficient of skin friction term in Equation 2
M	Mach number
M_∞	Freestream Mach number
n	Empirical coefficient in Equation 4
p	Static pressure
q	Dynamic pressure
r_i, R_i	Cylindrical and compressible-polar radial coordinates (See Table I)
Re	Reynolds number
RE/FT, Re/ ℓ	Unit Reynolds number, Re per foot
s	Arc length along rodwall surface
S	Wing platform area
SSF	Solid sidewall factor
u, v, w	Perturbation velocities
U	Local flow velocity
V	Volume of an incremental segment of a model

LIST OF SYMBOLS (continued)

x, y, z	Cartesian coordinates
x_j, y_j, z_j	Cartesian coordinates of potential flow singularities
α	Angle of attack
β	Compressibility similarity parameter, $(1-M_\infty^2)^{1/2}$
δ^*	Boundary-layer displacement thickness
Δ^*	Wall deflection to account for wall boundary-layer displacement effects
θ	Boundary-layer momentum thickness
ϕ	Perturbation velocity potential

SUBSCRIPTS

i	Location, strength or effect of a potential flow singularity
s, d, v	Related to a source, doublet or vortex
th	Value at the nozzle throat
o	Upstream starting point of wall deflection calculation
$x, y, z,$	First derivative with respect to x, y and z
xx, yy, zz	Second derivative with respect to x, y and z
∞	Freestream value

SECTION I

INTRODUCTION

Plans for an improved wind tunnel capability at the Flight Dynamics Laboratory (FDL) of the Air Force Wright Aeronautical Laboratories led to the initiation of this project in 1973. The requirement to be satisfied was a tunnel of adequate size (approximately 50 x 50-inch test section) to conduct subsonic and transonic research and exploratory development on aircraft and missile configurations. Versatility was also desirable; this included a capability to test two-dimensional airfoils and both half- and full-span three-dimensional models with full visual coverage for Schlieren optics, oil flow studies, laser anemometry, etc. For the type of research envisioned, minimizing or absolutely eliminating wall interference effects was not an overriding consideration. This requirement was viewed as being more of a need for major test centers where the final aerodynamic data must be suitable for accurate extrapolation to free flight. Adaptive test section walls were included in this design principally to maximize the size of models. This could provide improved model accuracy, ease and variety of both instrumentation and optical observation as well as a higher test Reynolds number. Hopefully all of these desirable features might be attained cost effectively with a reasonably low level of wall interference.

The wind tunnel described in this report was designed and constructed as an 18% pilot scale facility to evaluate an adaptive wall concept and provide the necessary design criteria for a new and larger facility described above. With its size partially determined by some available major components, the pilot became the FDL 9-inch Pilot Self-Adaptive Wall (SAW) Wind Tunnel. A symmetric, square cross-section was adopted only because there appeared to be no definitive criteria for selecting any other test section geometry when one considered the desired variety of two- and three-dimensional test configurations. At the time of the design of the FDL 9-inch Pilot, two concepts of adaptive walls had been reported and had been or were being implemented in two-dimensional wind tunnels. Both concepts had the intriguing feature that nothing needed to be known about the model under test but did require extensive measurements at or near the upper and lower wind tunnel walls.

The first concept is described in Ref. 1 where the impressive pioneering work of Lock and Beavan is reported on airfoil tests in a 20 x 8-inch two-dimensional tunnel with flexible walls. The technique employed, which has a simplified theoretical foundation, was to adjust the walls to a constant pressure which would be equivalent to a free-jet tunnel and then set the walls to about one-half the distance between the constant pressure position and a "straight" wall which was corrected for wall boundary layer displacement effects. Wall shapes also compare favorably with those calculated using linear compressible subsonic theory with, for example, solid blockage effects being represented by a doublet or a distribution of singularities representing an ellipse that more closely represents the geometry of an airfoil section. Wake blockage is represented by a properly located source and lift by a vortex having a strength determined by the measured lift coefficient. The authors concluded that standard methods of streamlining the wall are satisfactory up to speeds at which the shock from the airfoil first reaches the wall. The final recommended method of wall setting is a hybrid scheme using the wall pressures to empirically correct for solid and wake blockage and a calculated correction for lift derived from pressure measurements on the airfoil or on the upper and lower walls. In retrospect, this method is not unlike the simplified methods that are evaluated in the present study where solid blockage is calculated from the model geometry and the wake blockage and lift contributions to the wall streamlining are iteratively determined from balance measurements of forces and moments.

The second concept reported was directed primarily to ventilated wind tunnels and an iterative process using two measured variables at or near the wind tunnel walls. The variables may be perturbation velocities, flow angles or static pressures. From one measured variable a virtual, external free-air flow field may be calculated producing a calculated second variable which is then compared with the measured value of the second variable. In principle, adjustments may then be made to the flow through the wall until the calculated free-air value and the measured value agree. Descriptions of this concept have been reported by Ferri and Baronti in Ref. 2 and by Sears in Ref. 3. Reference 3 also describes the experimental program in progress at Calspan using segmented plenums to control the flow through a perforated wall.

Although other research was underway at the time, it was limited to the simple case of two-dimensional flow. It was in this atmosphere of very limited information on two-dimensional and practically none on three-dimensional adaptive walls that a wall design concept for the FDL 9-inch Pilot Tunnel was selected. It has three-dimensional characteristics in that the top and bottom walls can be streamlined in the transverse as well as the axial direction. A full three-dimensional capability is compromised by the use of straight sidewalls which satisfies the desire for full optical coverage and a variety of test configurations. The test program was planned to proceed directly to three-dimensional testing since it was believed that the demonstration of the two-dimensional case was receiving adequate attention and, indeed, the desired capability being sought was a wind tunnel to be used predominately to test three-dimensional models. The simplified wall adaptation scheme developed to evaluate the wall concept used linear compressible subsonic theory to calculate streamlines in the plane of the flexible walls. Solid blockage is predetermined from the geometry of the model, and the adaptation and iteration uses measurements from the model in the form of lumped parameters such as lift, drag, and pitching moment coefficients rather than extensive distributed parameters or variables in the plane of the wall such as pressure and flow angle measurements. The measured coefficients establish the strength of distributed singularities that represent the model. These measurements should, in part, reflect the nonlinear effects that occur with the onset of supercritical flow. Thus, although the methodologies described in Refs. 1, 2, and 3 permit, in principle, wall adjustments to the free-air case with no knowledge needed about the model, the simple three-dimensional method used here makes maximum use of what is known about the model and about the forces that it experiences. No particular claims are made for the advantages of the methods used here which are probably oversimplified. However, the approach did provide a means for evaluating the three-dimensional flexible wall concept which need not be tied to any particular computational scheme.

In the meantime, extensive research has been completed and reported on a variety of adaptive walls (Refs. 6 through 23) including some three-dimensional results (Refs. 18 through 23). Most have employed the iterative

use of two variables as measured and calculated at or near the wall as suggested by Ferri and Sears. In Refs. 20, 21, and 22 this is replaced by the use of one variable in two planes between the model and each wall which appears attractive for the application of a laser anemometer for the measurement of a single perturbation velocity component. Parallel efforts are in progress to improve the methods of correcting wind tunnel data for the effects of wall interference effects. All of this research is being aided by improvements in computational fluid dynamics and by the application of the computer to data acquisition and processing as well as to automated operation and control of the wind tunnels. Other relevant studies not referenced in this report have recently been catalogued in a NASA bibliography, Ref. 35.

In Section II the 9 x 9-inch Pilot facility is described along with performance and calibration information. Section III outlines a simplified wall adaptation method using an analytical and experimental test program on an axisymmetric parabolic-arc body of revolution. The purpose is to assess the analytical methods for correcting for solid blockage and the effects of solid sidewalls, and to compare 2-D versus 3-D contouring of the flexible walls. Section IV, which also includes experimental test results, employs a lifting aircraft configuration to further evaluate the analytical wall contouring methods including lift and wake blockage, the convergence of the iterative scheme using measured force and moment balance data, and an additional comparison of 2-D versus 3-D contouring of the flexible walls. Finally, in Section V the study is summarized, important results highlighted and recommendations made for additional research and for facility design criteria based upon the research thus far completed.

SECTION II
FACILITY DESIGN AND PERFORMANCE

1. OVERALL CONFIGURATION

Figure 1 illustrates the overall pilot facility configuration. It is a blowdown-to-atmosphere wind tunnel fed from a nominally 3000 psi air storage system having a storage capacity of 15,000 cubic feet. Air throttles and regulators take the pressure down to a maximum of a little over four atmospheres in the stilling or settling chamber. This provides a reasonably high unit Reynolds number of about 20-million per foot at Mach 1.

A settling chamber containing a conical baffle and anti-turbulence screens is 57-inches in diameter providing a 31-to-1 area contraction ratio. Downstream of the test section the flow is exhausted to atmosphere through a silencer to attenuate the high noise levels from air flow rates that can be of the order of 100-pounds per second.

Flow through the tunnel is controlled by the upstream P_0 valve which is the primary control for Reynolds number and a downstream choke valve used to set the Mach number. Reynolds number, Mach number and the angle of attack corrected for balance deflection were displayed digitally on the operator's console; no problems were encountered in manually setting these parameters to the desired value and accuracy. Although the introduction of automatic control of most of the tunnel operating parameters is straightforward, manual control proved quite acceptable for the short duration blowdown runs used for most of the testing. Provisions are included for modulating the pressure and flow in the plenum that surrounds the test section although this feature has yet to be required nor its potential assessed for operating the tunnel in the slot ventilated configuration.

2. NOZZLE AND TEST SECTION DESIGN

Before describing the flexible rodwall design some discussion on the use of solid sidewalls for three-dimensional testing is in order. There are obvious advantages to the use of solid sidewalls which include the simplicity of the mechanical design, a wide range of optical observation

and versatility of permissible test configurations. The aerodynamic effects of solid sidewalls are not so obvious. During the design of this facility the results from Ref. 29 instilled some confidence in the use of solid sidewalls. In Ref. 29 Ongarato showed that the force and moment data from a variety of aircraft models in a slotted-wall transonic tunnel was very nearly the same for either solid or slotted sidewalls if the total open area of the ventilated test section is maintained at 5.7%. In support of the present study a similar series of tests on the full configuration of the lifting model described in Section IV was conducted in the Flight Dynamic Laboratory's Trisonic Gasdynamic facility. This uses a square, 15-inch variable-slot transonic test section having interchangeable solid and slotted sidewalls. As reported in Ref. 30 the force and moment data for solid sidewalls with the upper and lower walls set at 12% open area is nearly the same as for all four walls set at 6% open area. The results are not identical. However, the differences are comparable with those of tunnel-to-tunnel correlations on this same model in much larger wind tunnels where wall interference effects are expected to be negligible. For the present study of a flexible-wall tunnel an analogous result might be a close correlation of data for the two cases of full 3-D wall streamlining and partial 3-D wall streamlining of just the upper and lower walls with deflections about doubled to account for the effects of the solid sidewalls.

The case for solid sidewalls is not clear cut. Some studies support the results of Refs. 29 and 30 while others seem to argue against solid sidewalls. In Ref. 23 it appears that wall interference is significantly reduced at $M = 0.90$ and 0.95 for perforated wall configurations having the sidewalls set to a porosity that is two to seven times that of the upper and lower walls which also differ for the case with lift. A numerical study described in Ref. 31 concludes that for a constant longitudinal slotted tunnel the stream curvature effects are minimized when the sidewall has a ventilation that is eight times that of the upper and lower walls.

Other numerical results are presented in Reference 32 which includes the cases of solid sidewalls with upper and lower walls both slotted and contoured. Even for the situation where the flow at the solid sidewalls is supercritical the pressure distribution at the mid-semispan of a lifting

rectangular wing that spans two-thirds of the tunnel width is quite close to that of the free air case. Additional support for the use of solid sidewalls is presented in Ref. 22. There, numerical simulation of a three-dimensional adaptive-wall tunnel demonstrated that free air conditions can be approximated by adjusting only the upper and lower walls. Finally, from a practical viewpoint, the solid sidewall transonic tunnel, in particular NASA's 8-foot Transonic Pressure Tunnel at the Langley Research Center, has produced a wealth of quality aerodynamic data over a span of many years.

The flexible wall design is best illustrated by the cross sectional sketch of Fig. 2. To satisfy the requirement for a laterally as well as an axially flexible wall, the top and bottom walls are each composed of nine cylindrical rods which are 7/8-inch in diameter. Flexible followers back up the rods and act as seals for a non-ventilated wall. The original design also included a capability to fix the followers and position the rods to provide variable distributed slot ventilation. This latter capability was not used except for some preliminary tests with the slots fully opened which provides an open area of 12.5%. In fact, it was found that there was significant air leakage through the flexible wall in the non-ventilated configuration caused by a mismatch in the elastic properties of the rods and seals and the lack of inter-jack spring loading of the seals or flexible followers. Because of this it was necessary to defer the variable slotted capability by installing silicone rubber rod stock in the slots between the rods to eliminate the air leakage. Thus, although the air leakage problem was solvable it would have required a major redesign and modification. The temporary fix was satisfactory since the non-ventilated configuration was of primary interest. All of the test results in this report represent the non-ventilated case with positive sealing between the rods.

Each rod is a constant diameter circular cylinder of silicone rubber molded about a steel insert that varies in thickness to satisfy the varying flexibility requirement along the length of the test section. The curvature or flexibility requirement is greatest in the neighborhood of the model. Here the steel insert is thinnest and jacking stations are more closely spaced. Details of the mechanical design and stress analysis are covered by Cain in Refs. 26 and 27.

The cross section of Fig. 2 is at a position in the center of the working region of the test section. This shows the solid sidewalls which, in this case, are large optical quality windows. One inner window may be replaced by a pressure instrumented metallic insert which includes static pressure orifices and a centrally located boundary-layer pitot-probe rake. One inner window may also be replaced by a half-span model support and a design is available for replacing both inner windows with a full-span airfoil support with partial optical observation. The outer chambers between the inner and outer windows and the plenums above and below the flexible walls are all vented together.

A more comprehensive picture of the nozzle and test section is shown in Fig. 3. The nozzle contraction from the settling chamber takes place in two steps. First there is a three-dimensional contraction from the 57-inch diameter settling chamber to a rectangular section which is 26-inches high and 9-inches wide. From here the top and bottom rod walls contract to a 9 x 9-inch throat. Note that the rod shape extends forward into the rectangular contraction to prevent the introduction of strong flow disturbances that would be produced by transitioning the wall from a flat to rodded shape in the vicinity of the throat. The flexible elements begin at the throat and are first controlled by three manual jacks that contour all nine rods simultaneously. Following this there are ten electric jack stations on top and bottom. At each of these stations the rods may be individually contoured to provide three-dimensional streamlining or may be set to the same position to simulate a two-dimensional flexible wall. This important feature has been used extensively in this study to evaluate the benefits of three-dimensional contouring as compared to the significantly simpler two-dimensional flexible plate wall used in conjunction with three-dimensional models.

A diffuser section downstream of the flexible walls has flaps to modulate the plenum pressure and contains a sting crescent having a pitch range of -3° to $+10^\circ$.

Figure 4 displays the electro-mechanical features of one lower jacking station. The maximum allowable displacement of each jack is ± 1.250 -inches. A typical accuracy of jack setting is ± 0.001 -inch.

3. WALL BOUNDARY-LAYER DISPLACEMENT EFFECTS

In the design and operation of a wind tunnel such as this, it is essential to include in the wall adaptation scheme, as best one can, the displacement effects of the nozzle and test section wall boundary layer. These effects become of particular importance in the transonic regime where small geometrical changes produce large gradients in static pressure and Mach number.

The non-ventilated, streamlined-wall tunnel has some advantage over the ventilated wall facility in analytically estimating these viscous effects. Nevertheless, the analysis still may have a variety of complications. In Ref. 1 the wall streamlining to correct for the wall boundary layer appeared to be a strong function of Mach number. It was subsequently found that the boundary layer effects were relatively insensitive to Mach number and that the observed effects were due primarily to the condensation of atmospheric water vapor, the wind tunnel being of the in-draft type. In the present study the wind tunnel is of the blowdown type which uses very dry air from a high pressure air storage system. Although water condensation is of no concern, the blowdown process introduces another problem: in a typical run the wall temperature exceeds the adiabatic wall temperature and, hence, the boundary-layer displacement thickness is increased by wall heating. This is in addition to a similar effect due to energy dissipation in high-speed boundary layers. The magnitude of the heat transfer to the wall boundary layer varies from run to run depending upon the air storage temperature, the initial wall temperature, and the length of the test run. It also differs on the rodwalls which are thermal insulators from that on the sidewalls which are metallic thermal conductors. Generally, the rodwalls should be close to adiabatic while the sidewalls provide a higher level of boundary-layer heating.

An added complication of this rodwall geometry is the increase in the wetted area of the wall which is very nearly 1.5 times that of a flat plate. This factor will be used in estimating the boundary-layer growth rate on the rodwalls as compared to the flat sidewalls.

Usually it is quite acceptable for a wind tunnel design of this type to assume that the wall boundary layer is turbulent and equivalent to a flat

plate boundary layer starting at the throat or at the end of the subsonic contraction. However, if the model induced pressure gradient substantially affects the boundary-layer growth rate as is shown in Refs. 12 and 16 for the case of two-dimensional flexible-wall tunnel testing, then a better estimate of the boundary-layer thickness in the neighborhood of the model may be needed. That is, the simplification of assuming that the boundary layer begins at the throat may be inadequate. Thus, an attempt is made here to estimate the size of the displacement thickness at the throat and throughout the nozzle.

Because of the varied and complex nature of measuring or calculating the wall boundary-layer displacement effects, the approach will attempt to include most of the physical features but with approximate engineering estimates of each. The eventual wall streamlining method will be based on an equivalent flat plate boundary layer having a starting point upstream of the throat. The calculation of the boundary layer thickness at the throat includes the upstream acceleration on the rodwalls and sidewalls and the streamline contraction effects on the sidewalls. The analysis is based on the momentum integral equation of a turbulent boundary layer which may be expressed in terms of the growth of the boundary layer momentum thickness, θ , on a plate in the presence of a pressure gradient as

$$\frac{d\theta}{dx} + (H + 2) \frac{\theta}{U} \frac{dU}{dx} = \frac{1}{2} C_f \quad (1)$$

Assuming incompressible flat plate values for the form factor, $H = \delta^* / \theta = 1.30$, and a skin friction coefficient based on Reynolds number of $C_f = 0.230 (Re_x)^{-.139}$, the growth rate of the displacement thickness, δ^* , may be approximated as

$$\frac{d\delta^*}{ds} = .00780 m (Re_{\delta^*})^{-.161} - 3.30 \frac{\delta^*}{U} \frac{dU}{ds} - \frac{\delta^*}{h} \frac{dh}{dx} \quad (2)$$

where m in the skin friction term accounts for differences in the wetted area: it is assumed equal to 1.0 for the flat sidewalls and equal to 1.5 for the rodwalls. The coordinate s is the arc length along the rodwall surface; for the sidewall $ds = dx$. The third factor on the right-hand side of Eq. 2 has been added to account for the streamline contraction which is

applied only to the flat sidewalls in the nozzle contraction. That is, to first order the boundary-layer thickness tends to increase in proportion to the surface area contraction along the sidewalls, i.e., in proportion to the reduction of the height of the nozzle sidewall, h .

Equation 2 has been numerically integrated to obtain a rough estimate of the size of the boundary layer displacement thickness at the throat. In the absence of any measurements near or upstream of the throat, a wide range of initial values of δ^* were assumed at the start of the rodwall contraction varying all the way from zero to unrealistically large values. As seen in Fig. 5, which is the calculation for the rodwall, the competing effects of skin friction and acceleration give a value at the throat of $\delta^* = 0.038$ inches regardless of what is assumed for the initial thickness. This value in turn locates the leading edge of a virtual flat plate that would give the same value of the displacement thickness at the throat. In this case the leading edge is approximately 14.6 inches upstream of the throat.

A similar numerical integration on the sidewall produced the result shown in Fig. 6. In this case $\delta^* = 0.034$ inches at the throat which is close to the value for the rodwall. The leading edge of a virtual flat plate is 20.5 inches upstream of the throat. Continuing the flat plate calculation to the center of the test section, there is surprising agreement between the calculated value of $\delta^* = 0.082$ inches and the experimental result at $M = 0.90$ using a sidewall mounted pitot rake that gave $\delta^* = 0.081$. Such close agreement is probably fortuitous considering the approximations and simplifications used in the analysis. However, the calculated results appear quite realistic, and from here the effect of model induced pressure gradients may now be evaluated.

The model induced pressure gradient effect on the sidewall boundary layer uses free-flight pressures in the plane of the sidewall as calculated in the following section of this report for a parabolic-arc body of revolution at $M = 0.90$. With the upper and lower walls contoured, the pressure gradients on the sidewalls are greater, and those on the top and bottom walls are less, than the calculated values. Nevertheless, the calculated pressure gradient and the modulation of the boundary layer is considered to be

typical of the average effect on all four walls. Again Eq. 2 is numerically integrated, this time in the test region where $ds = dx$, $m = 1$, $dh/dx \approx 0$ and $\frac{1}{U} \frac{dU}{dx} \approx -\frac{1}{2} \frac{dC_p}{dx}$. The result which is compared to the test section empty or zero pressure gradient flat plate result is illustrated in Fig. 7. The maximum perturbation from the zero pressure gradient displacement thickness of about 8% occurs near the center of the model. Of more importance is a comparison of this perturbation with the wall deflection to correct for the solid blockage of the model. Looking ahead to Fig. 13 and noting that the upper and lower wall deflections must account for the total area perturbation of all walls, the pressure gradient could amount to a 13% increase in the effective deflection to correct for solid blockage. Although this may be significant the effect is included as a small part of the factor which is derived experimentally in the following section to account primarily for the effects of solid sidewalls. Nevertheless, this pressure gradient effect appears to be deserving of further study to isolate its magnitude and variation and possibly to derive an approximate method to account for this feature on a day-to-day basis without extensive instrumentation.

In all of the model testing reported here the boundary-layer displacement thickness was calculated at each rodwall jacking station using the equation

$$\delta^* = 0.01738(Re/\ell)^{-0.139} (x+x_{th})^{0.861} \text{ ft.} \quad (3)$$

Re/ℓ is the unit Reynolds number per foot, x is the distance measured from the throat and x_{th} is the distance from the throat to the leading edge of a virtual flat plate which is taken as the average of the values shown in Figs. 5 and 6, or $x_{th} = 1.462$ ft.

The actual wall deflection,

$$\Delta^* = n (\delta^* - \delta_{th}^*) \quad (4)$$

where the throat value, δ_{th}^* , must be subtracted since the deflection at the throat, which is fixed, must be zero. The factor n , which is derived experimentally, accounts in most part for the requirement to correct for

all four walls using just the top and bottom walls, and, considering the additional wetted area of the rodwall, it may be expected to have a value of about 2.5. Using the equivalent flat plate starting point given above and varying the value of n until the test region Mach number gradient is zero in an empty test section produces a value of $n = 2.70$.

The empty test section calibration, then, is shown in Fig. 8 where variations in Mach number in the test region are typically within $\pm .002$ of the indicated freestream Mach number, M_∞ . While the variability of the local Mach number increases with the freestream Mach number as might be expected, the Mach number gradient in the test region remains negligible over the range of freestream Mach numbers from $M_\infty = 0.50$ to 0.95. This appears to justify the simplification of neglecting the effect of Mach number and energy dissipation on the growth rate of the boundary-layer displacement thickness. However, while this effect should be measurable, it may be dominated by wall heat transfer in a blowdown facility. This anomaly could be the subject of additional experiments and further analyses.

Finally, after considering a number of the many variables that affect the wall streamlining to account for the displacement effect of the wall boundary layer the simple method of adjusting the wall for zero pressure or Mach number gradient assuming a turbulent flat plate boundary layer appears to provide a practical first approximation.

4. WALL ADAPTATION METHODS

The scheme of adapting or streamlining the upper and lower walls is described by the diagram of Fig. 9 in terms of the sequence of operations. The diagram may be viewed in some generality. That is, the aerodynamic input data need not be model data as used here but rather extensive measurements taken at or near the walls which is then used to calculate freeflight or unbounded streamlines that serve as the boundary condition for a virtual external flow field.

A number of devices are used to implement the operations. All calculations for facility control and data reduction and interpretation are performed by a dedicated Hewlett-Packard 21MX minicomputer. The main storage device is a 5-megabyte disk drive with tape backup. I/O devices include a

Tektronics and a Teletype terminal. Input may also be made using a card reader. Hard copy output is delivered by a Versatek printer/plotter. A 180-channel wall-contour controller drives the electromechanical jacking system pictured in Fig. 4. More detailed information on the devices and their operation are described in Ref. 28 while the operations related to stress analysis are treated in Ref. 27.

The type of aerodynamic input data used in the present study and the methods of calculating wall streamlines are described in the following two sections on the analysis and testing of an axisymmetric model and a winged lifting model. Briefly, the input data includes the geometry of the model which establishes the streamlining to correct for solid blockage. The other basic aerodynamic data which are interactive may be model pressures or force and moment balance measurements. Although these aerodynamic calculation methods may be considered simplistic by today's standards, they do appear to be adequate to evaluate some fundamental characteristics of a complex three-dimensional test configuration.

SECTION III

AXISYMMETRIC PRESSURE MODEL

1. GENERAL

An axisymmetric pressure model was designed to provide:

- a. a detailed evaluation of the blockage effects of the solid sidewalls
- b. a comparison of wall streamline calculations using linearized compressible flow and non-linear transonic finite-difference methods, and
- c. an analysis of 2-D vs 3-D wall contouring.

The model shown in Fig. 10 is a 20% thick, 8-inch long parabolic-arc body of revolution which is truncated at 85% of its length to accommodate a sting support. In this tunnel the area blockage ratio of the parabolic body is approximately 2.5%, very nearly the same as the Microfighter force-and-moment model described in the following section. There are two axial rows of pressure orifices on the model, eighteen on top and eighteen on the side; all are read by one Scanivalve using a 5 psid transducer. The scan marches downstream in a top-side, top-side sequence.

2. ANALYTICAL METHODS

All of the experimental model pressure distributions are referenced to predicted values computed by a finite-difference relaxation method. Numerical results are solutions to the potential equation for transonic small disturbance flow. The method is described in Ref. 33. In this reference comparisons are made with data on similar axisymmetric bodies with models that range from 8 to 17% thick. The present study on a 20% model could be considered an extension beyond the demonstrated validity of the computational code. However, most of the test conditions of this study fall within the experimentally validated range of the transonic similarity parameter used in the analysis of Ref. 33. The accuracy of the predicted pressure distributions for Mach numbers of 0.7 and above are considered reasonable for the present purposes even though these studies are a reversal of the usual roles of computational and experimental aerodynamics. Here the computational results are used to validate wind tunnel data and develop the experimental methods.

Two methods are used to generate the inviscid streamlines in the plane of the upper and lower test-section walls. One method employs the same non-linear finite-difference scheme used to calculate the predicted model pressure distribution. This is described in Ref. 33 except for the additions to the computer program which provide streamline information for wall contouring and flowfield data which is correlated to the wind tunnel instrumentation.

The second method uses linear compressible theory similar to that used to calculate the solid and wake blockage for the lifting force-and-moment model described in the next section. The parabolic body is represented by sixteen doublets equally spaced along the axis and the sting is represented by a single source located at 95% of the length of the body. The strength of each doublet is proportional to the volume segment that it represents. Although approximate closed-form solutions may be used for this simple parabolic geometry it was most desirable to evaluate the method of finite volume elements which is used in the next section to calculate the solid blockage of more complex bodies. The source produces a half body which is asymptotic to the sting diameter. Other source contributions representing drag are neglected.

In both cases the wall is streamlined by integrating the vertical velocity component or upwash in the plane of the wall in the axial direction, multiplying the calculated displacement by a factor that accounts primarily for the interference of the solid sidewalls, and adding to this the displacement effects of the wall boundary layers. Some sample results of the two methods of calculating the inviscid wall streamlines, in this case only the deflection of the center rod on the top wall, are shown in Fig. 11. What is actually plotted is the wall shape based upon the elastic properties of the rods matched to the calculated positions at the ten jack stations between $x = 21$ and $x = 52$ inches. The result is practically identical to the streamline calculations except at $M = 0.99$ where the flexible properties of the wall produce some small changes such as the slight undershoot of the wall for the linear case forward of station 30. Although the $M = 0.99$ case is displayed, it was found (as will be shown below) that this is beyond the range of accurate data for this size of model. Excellent results have been demonstrated up to $M = 0.925$ for this 2.5% blockage model; with a modest amount of additional research this should be expandible to $M = 0.950$.

Peak streamline deflections are just about equal at a Mach number of 0.90. At lower Mach numbers the linear method produces higher peak deflections and at higher Mach numbers the roles are reversed. This variation is better illustrated in Fig. 12. Model pressure distributions appear to be predominately influenced by the peak wall deflection as compared to the axial distribution. For example, the differences between the two methods cannot be distinguished at $M = 0.90$ (See Fig. 15).

Now, to these inviscid calculations must be added the displacement effects of the nozzle boundary layer and some factor to account for the blockage effects of the solid sidewalls. Boundary-layer displacement effects have been discussed earlier and the next section considers the solid sidewall effects. Before continuing, Fig. 13 illustrates these additional considerations by adding a deflection to account for the wall boundary-layer displacement effects and multiplying the calculated inviscid streamlines that are shown in Fig. 11 by a factor of two to reduce the blockage effects of the solid sidewalls. The solid sidewall factor (SSF) of $SSF = 2.0$, which might be considered as the intuitive value, works nicely at $M = 0.90$ but varies with Mach number for both methods of streamline calculation as will be seen in the following.

3. SOLID SIDEWALL EFFECTS

For simplicity, the previously described analytical methods calculate free flight or unbounded streamlines. Although the top and bottom wall can be deflected to minimize their own wall interference they must also be used to reduce the blockage effects of the solid sidewalls.

An empirical approach is adopted to establish a solid sidewall factor (SSF) or multiplier that provides a best match to the theoretical pressure distribution on the model. As an example of the procedure Fig. 14 shows the pressure distributions* at $M = 0.90$, first for the case of $SSF = 1.0$, i. e.,

* Note that the frame of reference for the axial coordinate is not unique. Tunnel calibrations and flexible wall contours are referenced to nozzle stations having their origin at the nozzle throat. In Fig. 14 and subsequent plots of model pressure distributions the axial coordinates are referenced to the center of the parabolic-arc body of revolution. Figure 21 is an exception because of the comparison with a figure from an earlier document (Ref. 33) which references the nondimensional axial coordinate to the nose of the model where $x/L = 0$.

with the wall deflected to the calculated free flight streamline and, secondly, for a value of the solid sidewall factor of $SSF = 3.0$. Obviously, a value in between these two provides a best match to the theoretical pressure distribution. In this case, an interpolated value of $SSF = 2.0$ provides a good correlation as shown in Fig. 15. Also shown is a comparison between the linear and nonlinear methods of calculating streamlines. At this particular Mach number there is no distinguishable difference due to the different methods of calculation.

Using varying values of SSF at fixed Mach numbers and interpolating to obtain a value that closely matches the theoretical pressure distribution in the same way as was shown for $M = 0.90$, appropriate values of SSF were established for $M = 0.50, 0.70, 0.80, 0.85, 0.90,$ and 0.925 . The schedule of values versus Mach number is shown in Fig. 16. For $0.70 \leq M \leq 0.95$ the values are nearly equal for both the linear and nonlinear methods of calculating streamlines but are widely different at $M = 0.50$. The difficulty here may be due to overextending the range of validity of the transonic nonlinear theory which is used to compute the predicted pressure distribution. Beyond about $M=0.70$ the peak inviscid streamline deflection required to match the theoretical pressure distribution is pretty much the same; this is also displayed in Fig. 16. Actually, the peak streamline deflection between $M = 0.70$ and 0.95 does not change drastically. It varies only by $\pm 7\%$ about a value of 0.104 inches. Using the schedule of SSF shown in Fig. 16 and linear theory to calculate the wall streamlining the resulting pressure distributions are shown on the left side of Figs. 18(a) through (g). (The right side of these figures show comparative results for two-dimensionally contoured walls which will be discussed in the following subsection). Quite good correlation with the theoretically predicted pressure distribution is possible up to $M = 0.925$. Above this Mach number the experimental results obtained by varying the solid sidewall factor can be extrapolated to a value that should match the predicted pressure distribution. For the data used for Fig. 18 an extrapolated value of $SSF = 1.9$ should produce a match to the predicted pressure distribution at $M = 0.945$. However, for this 2.5% blockage model the tunnel becomes fully choked at this condition and it is necessary to further deflect the wall to unchoke the flow by using a value

of $SSF = 2.2$. This effect is shown in Fig. 16 where above $M = 0.925$ the open symbols represent the desired wall contour and the cross-filled symbols represent a contour expanded to prevent the tunnel from choking. Figure 18(g) shows the $M = 0.945$ case using the higher value of the solid sidewall factor. The correlation is reasonably good but the location of the terminal shock wave is beginning to move forward of the predicted location. By further expanding the flexible walls, data was obtained at upstream Mach numbers as high as $M = 0.99$ giving a model pressure distribution as illustrated in Fig. 19. Although the freestream (upstream) is at $M = 0.99$ the terminal shock wave is significantly forward of its predicted location: the pressure distribution is typical of a freestream value of more like $M = 0.92$.

Tunnel choking onsets abruptly. In addition to relieving a choked condition by expanding the wall contour, the same result is obtained under certain conditions by a slight reduction in Mach number for a given wall setting. A choked pressure distribution is shown in Fig. 20(a) and a typical flow pattern is illustrated in Fig. 22(f). A slight reduction of Mach number from $M = 0.950$ to $M = 0.945$ gives the unchoked pressure distribution of Fig. 20(b). In both cases the theoretical distribution is for $M = 0.950$.

The mode and onset of tunnel choking appears to be controlled by the tunnel wall and model configuration downstream of the maximum cross-sectional area of the model. Although time schedules did not permit a follow-on experimental evaluation, it is believed that useful data can be obtained at higher freestream Mach numbers by fine tuning the wall contour downstream of the maximum model thickness to compress the flowfield back to subsonic Mach numbers.

As a final review of solid sidewall effects it should be noted that the solid sidewall factor displayed in Fig. 16 is an empirical factor used to calculate flexible wall contours that produce a close correlation of the experimental and theoretical pressure distributions on the axisymmetric model. Although the magnitude of this factor should be strongly influenced by the requirement to relieve the blockage effects of the solid sidewalls, it is recognized that other important effects may also be included. For example, as described in Section I and shown in Fig. 7, the thickness of

the wall boundary layer in the neighborhood of the model is modulated by the model-induced pressure gradient which, in turn, varies with Mach number. Another effect that has not been fully evaluated is the reliability of the theoretical model pressure distribution and the nonlinear streamline calculations at the lower Mach numbers. These numerical calculations are based on axisymmetric small disturbance theory using the empirical transonic similarity parameter $(1 - M_\infty^2)/(M_\infty \tau)^2$ which should produce good results near $M_\infty = 1$ but must fail at the singular condition of $M_\infty = 0$. Ideally, all of the physical and analytical features that might affect the solid sidewall factor displayed in Fig. 16 should be defined and evaluated individually. This is beyond the scope of this study.

One simplification that is suggested by the peak streamline deflection of Fig. 16 may be invoked. This simplification, based upon the global effects illustrated in Fig. 16, is that the peak streamline deflection and possibly a single approximate wall contour can accommodate all solid blockage effects from $M_\infty = 0.70$ up to the tunnel choke point.

4. TWO-DIMENSIONAL VERSUS THREE-DIMENSIONAL CONTOURING

Experimental studies included an evaluation of the benefits of three-dimensional wall contouring as compared to two-dimensional contouring. Here, the 2-D contouring is accomplished by setting all nine rods on the upper and lower walls at a given axial jacking station to the same contour. This simulates the simpler configuration of a flexible-plate wall.

The walls were placed in the two-dimensional configuration by setting all rods to the calculated contour of one of the upper wall rods 1, 2, 3, 4 or 5, where rod 1 is an outermost rod adjacent to the wall and rod 5 is a centerline rod. For this axisymmetric configuration the reflections of these five rods determine the full 18-rod contour. Analysis of the resulting pressure distributions then determines which value best matches the predicted model pressure distribution. As a sample case for a nominal Mach number of 0.925, Fig. 17(a) shows the pressure distribution on the model with the upper wall set to the rod number 2 contour and Fig. 17(b) for the wall set to the rod 4 contour. The lower wall, of course, is a reflection of the upper wall. A match to the predicted model pressure distribution lies

somewhere between these two values. The final value that resulted from an extensive variation of test conditions was the contour for an imaginary rod number of 2.75. This represents a wall streamline at 2.25 inches from centerline or just at mid-semispan of the test section. The result which appears valid throughout the present range of experimental Mach numbers is demonstrated on the right side of Figs. 18(a) through 18(g). The data comparisons are surprisingly close and there is no observable change between the top and side row of pressure taps. A similar result will be demonstrated on a limited scale in the following section on a winged lifting model. Note that this correlation between 2-D and 3-D contouring has been demonstrated only for a square test section. How this result may be generalized for, say, a rectangular cross section remains to be resolved.

In summary, the results suggest that for a square test section two-dimensional flexible-plate upper and lower walls that are contoured to the mid-semispan streamline reproduce quite accurately the results produced by three-dimensional contouring of the upper and lower wall.

5. ADDITIONAL OBSERVATIONS

The top and side rows of model pressure taps give nearly identical results for both cases of 2-D and 3-D wall contouring. In general, the top and side row pressures at the most forward location and those over the aft portion of the model are about equal. In between, the absolute magnitude of the pressure coefficient of the side row is higher than that of the top row which may be indicative of the effect of the solid sidewalls.

One interesting observation of the pressure distribution on the axisymmetric model appeared to be most pronounced in the Mach number neighborhood of $M_{\infty} = 0.9$, see for example Fig. 15. There is a definite flow compression upstream of the maximum thickness of the model, giving the appearance of a double shock phenomenon. However, the upstream disturbance is not a full shock recompression to subsonic speeds. Both top and side model pressure taps show the same result which occurs at a model location of about $x/L = 0.4$. This premature compression which was initially thought to be a pressure transducer problem was confirmed by the Schlieren photographs of Figs. 22(c) and (d). It was then believed to be a phenomenon related to the present model/tunnel configuration and such a large blockage model of

2-1/2%. However, in reviewing the experimental results of Ref. 34 the same phenomenon appears in the model pressure distributions on similar parabolic-arc bodies of revolution. For example, a 10% thick model with a comparatively low blockage ratio of 0.19% produced the results shown in Fig. 21(a). The Mach number is much higher than for the comparative results of the present study shown in Fig. 21(b). However, the transonic similarity parameter which is a combination of Mach number and thickness ratio used in Ref. 33 is about the same. The theoretical results shown in Fig. 21(a) are from Ref. 33. At this time no explanation is offered for the observed double compression which is not predicted by the transonic finite-difference relaxation calculation. Other qualitative observations of the axisymmetric flow are given in Fig. 22. The Schlieren photos cover the Mach number from $M = 0.850$, which should be close to the onset of supercritical flow at the maximum diameter of the model, up to tunnel choking at $M = 0.943$ for this wall setting. In addition to the double compression phenomenon discussed above which is most apparent at $M = 0.90$ and 0.925 the photos illustrate the appearance of supercritical flow occurring between $M = 0.850$ and 0.875 . Just short of tunnel choking at $M = .935$ there is a strong, nearly normal shock which can be seen penetrating the upper and lower wall boundary layer with no apparent interaction except possibly for some thickening of the wall boundary layer downstream of the shock. As the tunnel chokes, in this case at $M = .943$, the flow abruptly transitions to supersonic flow throughout the test section downstream of the model, and the model shock transitions to an oblique shock wave.

One final observation of the axisymmetric model study is that it would be desirable to test the same or the same size model in a much larger transonic wind tunnel to establish an experimental data base with low or negligible wall interference to supplement the theoretical free-air baseline data used for correlations in this study. This could provide

- a.) added confidence in the use of linearized compressible flow theory for streamlining the wall to correct for solid blockage,
- b.) additional analyses of the separate and combined effects of the solid sidewalls and the wall boundary layer without concern for the limits of the theoretical prediction, and
- c.) further correlation between 2-D and 3-D wall contouring.

SECTION IV

LIFTING MODEL TESTS

1. GENERAL

A lifting model representative of a fighter aircraft was selected to evaluate the three-dimensional flexible-wall wind tunnel. As was also addressed in the preceding section on an axisymmetric model, the evaluation included the relief of solid blockage effects in a solid sidewall tunnel and a limited study of two-dimensional versus three-dimensional contouring of the upper and lower walls. Additional goals of the lifting model tests were to study self streamlining or adaptive methods to account for wake blockage and lift using the measured force and moment data from a standard six-component balance.

The model shown in Figs. 23 and 24 is a low aspect ratio (1.53) fighter with a wing span of 6.3-inches. In this tunnel the blockage ratio is about 2.5%, the same value as for the axisymmetric model described in the preceding section. The full model of this Microfighter aircraft has vertical tails mounted at the wing tips. Here the model excludes the vertical tails only because the comparative data available from the AEDC 4-T wind tunnel with a fared-over engine inlet was also without vertical tails. The important point is the use of the fared-over inlet since data on this model using a flow-through inlet in a variety of wind tunnels produced peculiar drag measurements and comparisons, due probably to a very complex flow pattern at the base of the model. The upper surface of the wing was grit-stripped at approximately 10% of chord aft of the leading edge. This is believed to be standard for all other comparative data.

All of the data obtained in the present test series was read from a standard 6-component Task Corporation balance. Only 3-components are actually used; lift, drag, and pitching moment.

2. ANALYTICAL METHODS

The simplified methods of calculating wall streamlines for the rodwall tunnel being evaluated uses as input the model geometry and measured forces

and moments. This information, together with linear compressible flow theory, is used to determine the strengths of a distribution of singularities that represent the model. Model geometry provides a distribution of doublets each with a strength proportional to the volume element represented. This is identical to one of the two analytical methods used for the axisymmetric model to calculate the solid blockage contribution to the flexible wall contour. A distribution of vortices of vanishing span represents lift and pitching moment with strengths determined from measured values and certain assumptions about how the lift is distributed, for example, assuming an elliptical lift distribution on the wing. Drag and wake blockage may be represented by a distribution of sources with strengths related to measured drag. The sting support may also be represented by a source having a strength proportional to the sting diameter.

Note that the solid blockage contouring is predetermined except for variations due to angle of attack while the lift and wake blockage are determined from iterative force measurements which hopefully account in part for the nonlinear effects that become important with the onset of supercritical flow.

The degree of detail required for the distribution of singularities is not known in advance but is certainly a function of the size of the model relative to the size of the test section. If the model is relatively very small a single source, doublet and vortex located at the center of the model should be an adequate representation of the model for contouring the walls. For two-dimensional airfoil testing, Ref. 1 suggests that wall streamlining using a single source, doublet and vortex, provides reasonable results for rather large models with supercritical flow if the two-dimensional source is properly located in the chordwise direction.

A distribution of minimal detail for the model/test-section configuration of this study is illustrated in Fig. 24. A five point distribution is certainly a major improvement over the single point representation for typical aircraft configurations. This next higher level of complexity may be used to account for model deflections of ailerons, flaps, elevators or stabilators and, with a vertically oriented vortex, the rudder deflections.

For these tests the outer wing panel is one-half of the semispan and lift is divided between points 1, 2 and 3 based upon an elliptical lift distribution. In a more conventional transport or bomber configuration with a separately defined empennage the lift contributions from the wing and tail may be readily separated using measurements of lift and pitching moment and the model geometry. The distribution of drag was quite arbitrary with six-tenths being assigned to the central section, Section 1, and one-tenth to the other four points. The additive effects of lift and drag on the wall streamlines produced smoothly varying contours. A similar attempt to divide the volume of the model into five elements represented by doublets at the five points was totally unproductive. In fact, this minimal doublet representation produced modulation of the wall streamlines that exceeded the allowable stress levels of the flexible rods. A more successful distribution of doublets, comparable to that used for the axisymmetric model, is based on a division of the model volume into nine fuselage elements and ten wing elements as shown in Fig. 25. The source, doublet and vortex used here are itemized in Table I. Written in terms of the perturbation velocity potential, ϕ , they are solutions to the linearized equation of the velocity potential.

$$(1-M_{\infty}^2)\phi_{xx} + \phi_{yy} + \phi_{zz} = 0 \quad (5)$$

Perturbation velocities then are given by

$$u = \phi_x, \quad v = \phi_y, \quad w = \phi_z$$

The perturbation velocities at x, y, z are due to singularities located at x_i, y_i, z_i . The strength of the singularities are proportional to measured values of drag, volume, and lift as shown in Table I. Not shown is an approximate representation of the model support sting as was used for the axisymmetric body of the previous section. There a source was placed at 95% of the length of the parabolic-arc body. The source produces a semi-infinite, axisymmetric half body which rapidly but asymptotically approaches the diameter of the sting. The equations for the source are the same as in Table I with the substitution

$$\bar{D}_i = \pi d_s^2 / 2 \quad (6)$$

where d_s is the sting diameter.

In this study the axial perturbation velocity has been used to calculate pressure coefficients at or near the plane of the walls using the small perturbation equation,

$$C_p = - 2 \frac{u}{U} \quad (7)$$

The lateral perturbation, v/U , is neglected at all four walls. The vertical perturbation velocity or upwash, w/U , is used to calculate freeflight streamlines in the plane of the upper and lower wall; these are calculated by integrating with respect to x the sum of the vertical velocity perturbations separately for the sources, doublets and vortices. For example, for the source contributions, the streamline deflection is

$$\Delta z_s = \int_{x_0}^x \left[\sum \frac{w_i}{U} \right]_s dx \quad (8)$$

where x_0 is taken to be a point upstream of the model where the contributions from the model are negligible. In this case, two tunnel widths, or 18-inches, upstream of the model is a suitable starting point for the integration. Similar integrals are used for the doublet and vortex contribution to the streamlines. The streamline deflections are calculated separately for each class of singularity so that the relative magnitudes of each may be displayed on command as a programming check during testing. Alternatively, all of the upwash contributions could be summed first requiring only one integration per rod.

3. SOLID SIDEWALL EFFECTS

Again, the effects of the solid sidewalls must be evaluated and factors applied to the calculated streamline deflections produced by the distributed singularities and the displacement effect of the wall boundary layer. The equation of a rod streamline ($y = \text{constant}$) is

$$z = z_0 + A \Delta z_s + B \Delta z_d + C \Delta z_v + n\Delta^* \quad (9)$$

where z_0 is the tunnel half-height at the throat. The additive streamline deflections Δz_s , Δz_D and Δz_v , which are functions of x , are the contributions of the distributed sources, doublets, and vortices. The factors A, B, C, and the factor n contained in Δ^* (see Eq. 4) are derived to account largely for the effects of the solid sidewalls and the fact that all wall contouring to minimize wall interference effects must rely on flexing of the upper and lower walls only. A more detailed analysis of the wall boundary-layer effect and value of n was given in Section II and of the solid blockage effects, $B = SSF$, in Section III. After considerable preliminary experimentation on the lifting model where the values of the factors A, B, and C were varied independently and in combination with a goal of matching available data from the AEDC 4T Tunnel, the following constant values were adopted for the data presented in this section:

PHYSICAL PHENOMENON	SOLID BLOCKAGE	WAKE BLOCKAGE	LIFT	BOUNDARY LAYER
FACTOR	A	B	C	n
VALUE	3.0	2.0	2.0	2.7

Intuitively it might be expected that a value of each factor except for lift should be close to 2.0. However, as discussed in Section II, the boundary-layer factor could be closer to 2.5 and from Section III the solid blockage factor appears to be a function of the freestream Mach number, varying from a value of 4.0 at $M_\infty = 0.500$ to a value of 2.0 at $M_\infty = 0.925$. For the lifting model tests an intermediate constant value of $A = SSF = 3.0$ is used which should be appropriate for $M_\infty = 0.70$. However, the selection of a constant value of $A = 3.0$ from the experiments on the lifting model is not derived as a median value from the results of the axisymmetric tests since the two series of tests are not presented in accordance with the chronological order of the tests. The axisymmetric model tests which were conducted last are presented first in this report only because of the simpler and more fundamental nature of the study. Tests on the lifting model chronologically preceded those on the axisymmetric model because the instrumentation

was simpler. If the order of the tests had been reversed, some accounting of the Mach number variation of the solid blockage factor may have been included in the lifting model tests, possibly resulting in different values for the factors for wake blockage and lift. Finally, it is not apparent at this time why a value for the lift factor, C , of 2.0 provides an improved level of data correlation.

Typical rod contours for the lifting model at four degree angle of attack are illustrated in Fig. 26.

4. SELF-ADAPTIVE WALL STREAMLINING

The self-adaptive feature of the analytical method of this study for wall contouring uses the measured values of lift, drag, and pitching moment to iterate and hopefully converge on a contour that approximates the streamlines of free flight.

An example of this feature is shown in Fig. 27 for the case of the lifting model at $M_\infty = 0.90$ and an angle of attack of four degrees. The initial input or zeroth iteration sets the lift, drag and pitching moments to zero so that the contouring of the wall includes only the solid blockage effects of the model and the displacement effects of the wall boundary layer. Setting the initial input to zero is certainly an overly severe test; experience or rough engineering calculations could give approximate but much better input values. Nevertheless, the output converged in three iterations. Note that this is a test for convergence and rate of convergence; the output coefficients do not necessarily converge to the correct interference-free values. Here they converge to the same value that results from using as input the data from the AEDC 4T Transonic Wind Tunnel, and for this case the differences between the final input/output are illustrated in Fig. 29(c).

Expanding on this result at $M = 0.90$, additional values of angle of attack give essentially the same result as shown in Fig. 28. It is apparent that the initial output values using zeroes for input are diverging rapidly with angle of attack and could present a problem at higher angle of attack, thus, requiring a more reasonable estimate of the initial input.

Since the AEDC 4T data is close enough to give the converged output, this is used directly as the input to compare the present three-dimensionally

streamlined wall results with the 4T data over a range of Mach numbers from 0.50 to 0.95. These results are shown in Fig. 29(a) through (d). The present data is at a higher Reynolds number; a somewhat lower constant value could have been used, however, at $M = 0.95$ this blowdown-to-atmosphere tunnel requires a minimum total pressure of about 20 psia for operation. This gives a minimum unit Reynolds number of 7×10^6 per foot.

Considering the coarseness of the mathematical model and the use of linearized theory, the comparisons with the AEDC 4T data is reasonably good and not dissimilar to other tunnel-to-tunnel comparisons for this same model. But, then, this is to be expected since the values of the factors in Eq. (9) were empirically selected to give an acceptable degree of correlation.

5. TWO-DIMENSIONAL VERSUS THREE-DIMENSIONAL CONTOURING

Having established a simplified but workable mathematical model for contouring the upper and lower walls, a limited number of tests were conducted to compare two-dimensionally contoured walls with the foregoing results on three-dimensional contouring. By setting all nine rods on the upper, and all of the nine on the lower wall to the upper and lower streamlines calculated for various lateral positions, the results are as shown in Fig. 30. As was the case for the axisymmetric model, two-dimensional walls set to the calculated mid-semispan streamline matches the data obtained from a three-dimensionally contoured wall. Figure 31 illustrates another interesting result. Along the full length of the test section, the cross-sectional area that is displaced by the two-dimensional wall is nearly identical to the area displaced by the three-dimensional wall. Again it is noted that these results are demonstrated only for a square test section with solid sidewalls.

In Fig. 32 the result is expanded to other angles of attack at $M = 0.90$.

SECTION V
CONCLUDING REMARKS

A unique flexible-wall wind tunnel is described. The wind tunnel was designed as a pilot scale facility for a proposed larger subsonic and transonic facility which would provide a wide range of test capabilities for aerodynamic research and exploratory development. Although the rod and seal design allows for three-dimensional contouring of the upper and lower walls, a full three-dimensional wall configuration is compromised by the use of solid sidewalls. In addition to simplifying the mechanical design, the solid sidewalls provide full optical observation of the test region and allow for a variety of test configurations including two-dimensional airfoil tests and both full-span and half-span model tests.

In a flexible-wall wind tunnel the correction for the wall boundary layer can be a large part of the total deflection to minimize wall interference effects. Additional research could productively be applied to refinements of the effects of the wall boundary layer including pressure gradients and heat transfer. Nevertheless, it was found that the application of a simple flat plate turbulent boundary-layer equation with an empirical factor that minimized test section Mach number gradients was adequate at least for calibrating the empty test section.

Because of the complexity of the three-dimensional configuration, including the use of solid sidewalls and the difficulties of pressure instrumenting the upper and lower rodwalls, the analysis and instrumentation regressed to comparatively simple methods. The approach uses subsonic compressible flow theory, a minimum of instrumentation and considerable knowledge of the model configuration and the forces that it experiences.

The freeflight streamlines in the plane of the wall are calculated from a distribution of singularities representing the model. Relief of solid blockage is calculated from the model geometry represented by a distribution of doublets which are proportional to the distribution of the volume of the model. This linear method compares favorably with the results for an axisymmetric model using a nonlinear finite-difference relaxation scheme over

a range of Mach number of $0.70 \leq M_\infty \leq 0.95$. For both methods the effect of solid sidewalls which appears to be Mach number dependent must be included.

Comparing a two-dimensionally contoured wall with three-dimensional contouring it was found that the pressure distributions on a parabolic-arc body in a square test section are nearly identical if the two-dimensional walls are contoured to the streamline calculated for the mid-semispan of the test section.

While the solid blockage contribution to the wall streamlining is established from the model geometry prior to testing, the lift and wake blockage is self-adaptive. In this evaluation of the tunnel concept, balance force measurements on a fighter-type aircraft model have been used to determine the strengths of a distribution of vortices and sources. Thus, lift and wake blockage contributions to the wall streamlining may be derived from measured lift, pitching moment and drag in an iterative adaptation scheme. Over a limited range of test conditions it is shown that the output coefficients of lift, drag and pitching moment converge in just three iterations starting from initial input values of zero.

Using empirically derived factors that account primarily for the solid sidewalls and contouring only the upper and lower walls to correct for solid blockage, wake blockage, lift and the wall boundary layer, reasonably good correlation is obtained with data obtained on this same model in the AEDC 4T wind tunnel.

Although the two-dimensional wall tests on the lifting model are not as extensive as on the axisymmetric model, the same result is demonstrated. The measured force and moment data in this case is nearly identical to the three-dimensionally contoured results if the two-dimensional walls are contoured to the mid-semispan streamline of a square test section.

This study was not directed toward producing an optimum wall adaptation method. It is believed, however, that the simplified methods employed are reasonably effective and allowed an evaluation of the three-dimensional flexible wall concept. As recommendations for further use of this type of direct calculation of the wall contours, it appears that the modeling of solid blockage with a distribution of doublets related to the volume

distribution of the test article is acceptable at the level of detail used in this report. Refinements should be made to the vortex representation of lifting surfaces and to the source distribution representing the drag since the coarse distribution used here on the lifting model is probably at the lowest level of acceptability for this low aspect ratio model and simplistic for a high aspect ratio model.

A number of follow-on studies with this pilot facility could be productive. These would be, for the most part, additions and refinements to the analysis and testing already completed. For example, a fine tuning of the wall contours downstream of the maximum area of the model might lead to higher useable freestream Mach numbers prior to tunnel choking. Further experimental studies could evaluate the possible simplification of using a fixed wall contour to correct for solid blockage over the transonic range from $M = 0.70$ to tunnel choking. One additional major test sequence of considerable interest would employ a half-span or wing-on-sidewall model to further study the effects of solid sidewalls and the comparative advantage of two-dimensional versus three-dimensional wall streamlining.

Finally, since the original purpose of this research on a pilot-scale facility was to develop design criteria for a larger flexible-wall wind tunnel, some comments should be expected on this point. Based upon the results from the pilot tunnel to date, a recommended configuration should seriously consider the use of two-dimensional, flexible-plate walls for three-dimensional testing. At the very least, it is recommended that further research should pursue this possibility.

REFERENCES

1. Lock, C. N. H. and Beavan, J. A., "Tunnel Interference at Compressibility Speeds Using the Flexible Walls of the Rectangular High Speed Tunnel," British ARC R. & M. 2005, 1944.
2. Ferri, A. and Baronti, P., "A Method for Transonic Wind-Tunnel Corrections," AIAA Journal Vol. 11, No. 1, January 1973, pp. 63-66.
3. Sears, W. R., "Self-Correcting Wind Tunnels," The Sixteenth Lanchester Memorial Lecture of the Royal Aeronautical Society, London, May 1973, and the Aeronautical Journal, February 1974, pp. 80-89.
4. Vidal, R. J., Erickson, J. C., Jr., and Catlin, P. A., "Experiments With a Self-Correcting Wind Tunnel," AGARD-CP-174, October 1975; also Calspan Report No. RK-5070-A-4, October 1975.
5. Sears, W. R., Vidal, R. J., Erickson, J. C., Jr., and Ritter, A., "Interference-Free Wind-Tunnel Flows by Adaptive-Wall Technology," ICAS Paper No. 76-02, 10th Congress of the International Council of the Aeronautical Sciences, Ottawa, Canada, 3-8 October 1976; also Journal of Aircraft, Vol. 14, No. 11, pp. 1042-1050, November 1977.
6. Vidal, R. J. and Erickson, J. C., Jr., "Experiments on Supercritical Flows in a Self-Correcting Wind Tunnel," AIAA Paper No. 78-788, AIAA 10th Aerodynamic Testing Conference, San Diego, California, 19-21 April 1978.
7. Vidal, R., Jr. and Erickson, J. C., Jr., "Research on Adaptive-Wall Wind Tunnels," AEDC Report No. AEDC-TR-78-36, November 1978.
8. Erickson, J. C., Jr., Wittliff, C. E., and Daughtery, D. C. "Further Investigations of Adaptive-Wall Wind Tunnels," AEDC Report No. AEDC-TR-80-34, October 1980.
9. Chevallier, J.-P., "Soufflerie Transsonique a Parois-Adaptables," AGARD-CP-174, October 1975; also translated into English as European Space Agency Report ESA-TT-326, October 1976, available at NASA Accession No. N77-13085.
10. Capelier, C., Chevallier, J.-P., and Bouniol, F., "A New Method for Correcting Wall Interference," La Recherche Aerospaciale, 1978, No. 1, January-February 1978, pp. 1-11; also translated into English as European Space Agency Report ESA-TT-491, August 1978, available as NASA Accession No. N79-11997.
11. Archambaud, J. P. and Chevallier, J.-P., "Utilisation de Parois Adaptables pour les Essais en Cournat Plan," AGARD Fluid Dynamics Panel Specialists' Meeting on Wall Interference in Wind Tunnels, London, 19-20 May 1982., AGARD CP-335, September 1982.

12. Goodyer, Michael J., "The Self-Streamlining Wind Tunnel," NASA TM X-72699, August 1975.
13. Goodyer, M. J., "A Low-Speed Self-Streamlining Wind Tunnel," AGARD-CP-174, October 1975.
14. Goodyer, M. J. and Wolf, S. W. D., "The Development of a Self-Streamlining Flexible Walled Transonic Test Section," AIAA Paper No. 80-0440, AIAA 11th Aerodynamic Testing Conference, Colorado Springs, Colorado, 18-20 March 1980, also AIAA Journal, Vol. 20, No. 2, February 1982, pp. 227-234.
15. Wolf, S. W. D., Cook, I. D., and Goodyer, M. J., "The Status of Two- and Three-Dimensional Testing in the University of Southampton Transonic Self-Streamlining Wind Tunnel," AGARD Fluid Dynamics Panel Specialists' Meeting on Wall Interference in Wind Tunnels, London, 19-20 May 1982, AGARD CP-335, September 1982.
16. Newman, P. A. and Anderson, E. C., "Numerical Design of Streamlined Tunnel Walls for a Two-Dimensional Transonic Test," NASA Technical Memorandum 78641, April 1978.
17. McDevitt, J. B., Polek, T. E., and Hand, L. A., "A New Facility and Technique for Two-Dimensional Aerodynamic Testing," AIAA Paper No. 82-0608, AIAA 12th Aerodynamic Testing Conference, Williamsburg, Virginia, 21-24 March 1982.
18. Ganzer, U., "On the Use of Adaptive Walls for Transonic Wind Tunnel Testing," AGARD Fluid Dynamics Panel Specialists' Meeting on Wall Interference in Wind Tunnels, London, 19-20 May 1982, AGARD CP-335.
19. Ganzer, U., "Adaptable Wind Tunnel Walls for 2-D and 3-D Model Tests," ICAS Paper No. 23-3, 12th Congress of the International Council of the Aeronautical Sciences, Munich, Germany, 12-17 October 1980.
20. Bodapati, S., Schairer, E., and Davis, S., "Adaptive-Wall Wind Tunnel Development for Transonic Testing," AIAA Paper 80-441, Colorado Springs, Colorado, April 1980.
21. Davis, S. S., "A Compatibility Assessment Method for Adaptive-Wall Wind Tunnels," AIAA Journal, Vol. 19, No. 9, September 1981, pp. 1169-1173.
22. Schairer, E. T. and Mendoza, J. P., "Adaptive-Wall Wind Tunnel Research at Ames Research Center," AGARD Fluid Dynamics Panel Specialists' Meeting on Wall Interference in Wind Tunnels, London, 19-20 May 1982.
23. Parker, R. L., Jr., and Sickles, W. L., "Application of Adaptive Wall Concept in Three-Dimensions," Journal of Aircraft Vol. 18, No. 3, March 1981, pp. 176.

24. Kemp, W. B., Jr., "Toward the Correctable-Interference Transonic Wind Tunnel," AIAA Paper No. 76-1794, AIAA 9th Aerodynamic Testing Conference, Arlington, Texas, 7-9 June 1976.
25. Murman, E. M., "A Correction Method for Transonic Wind Tunnel Wall Interference," AIAA Paper No. 79-1533, AIAA 12th Fluid and Plasma Dynamics Conference, Williamsburg, Virginia, 24-26 July 1979.
26. Cain, M. R., "Facility Air Control Systems Design for a Pilot Transonic Wind Tunnel," AFFDL-TM-79-53-FXN, Air Force Flight Dynamics Laboratory, Wright-Patterson Air Force Base, Ohio, May 1979.
27. Cain, M. R., "Mechanical Design and Control of a Variable Geometry, Adaptive Wall Test Section for a Pilot Transonic Wind Tunnel," AFWAL Technical Report (to be published), Flight Dynamics Laboratory, Wright-Patterson Air Force Base, Ohio.
28. Ballard, B. L., "Development of a 180-Channel Controller for the Automatic Adjustment of a 9 x 9-inch Self-Adaptive Wall Wind Tunnel," AFWAL Technical Memorandum (to be published), Flight Dynamics Laboratory, Wright-Patterson Air Force Base, Ohio.
29. Ongarato, J. R., "Wind Tunnel Wall Interference Studies at High Subsonic Speeds," Journal of Aircraft, Vol. 6, No. 2, March-April 1969.
30. Harney, D. J. and White, H. L., "An Assessment of Solid and Ventilated Sidewalls for Transonic Wind Tunnels," Data Report FX 79-1, September 1979.
31. Steinle, F. W., Jr. and Pejack, E. R., "Toward an Improved Transonic Wind-Tunnel-Wall Geometry - a Numerical Study," AIAA Paper No. 80-0442, AIAA 11th Aerodynamic Testing Conference, 18-20 March 1980.
32. Newman, P. A. and Klunker, E. B., "Numerical Modeling of Tunnel-Wall and Body-Shape Effects on Transonic Flow over Finite Lifting Wings," NASA SP-347, Paper No. 41, pp. 1189-1212, March 1975.
33. Krupp, J. A. and Murman, E. M., "Computation of Transonic Flows Past Lifting Aerofoils and Slender Bodies," AIAA Journal, Vol. 10, No. 7, July 1972, pp. 880-886.
34. Taylor, R. A. and McDevitt, J. B., "Pressure Distributions at Transonic Speeds for Parabolic-Arc Bodies of Revolution Having Fineness Ratios of 10, 12, and 14," NASA TN 4234, March 1958.
35. Tuttle, M. H. and Plentovich, E. B., "Adaptive Wall Wind Tunnels, A Selected, Annotated Bibliography," NASA TM 84526, November 1982.

TABLE I
VELOCITY POTENTIAL AND DISTURBANCE VELOCITIES
FOR ISOLATED SINGULARITIES IN COMPRESSIBLE SUBCRITICAL FLOW

	<u>SOURCE</u>	<u>DOUBLET</u>	<u>VORTEX</u>
$\frac{\phi_i}{U}$	$-\frac{\bar{D}_i}{8\pi} \frac{1}{R_i}$	$\frac{V_i}{4\pi} \frac{x-x_i}{R_i^3}$	$\frac{\bar{L}_i}{8\pi} \frac{z-z_i}{r_i^2} \left[1 + \frac{x-x_i}{R_i} \right]$
$\frac{v_i}{U}$	$\frac{\bar{D}_i}{8\pi} \frac{(x-x_i)}{R_i^3}$	$\frac{V_i}{4\pi} \left[\frac{1}{R_i^3} - 3 \frac{(x-x_i)^2}{R_i^5} \right]$	$-\frac{\bar{L}_i}{8\pi} \frac{z-z_i}{r_i^2} \left[\frac{1}{R_i} - \frac{(x-x_i)^2}{R_i^3} \right]$
$\frac{v_i}{U}$	$\frac{\bar{D}_i}{8\pi} \frac{\beta^2(y-y_i)}{R_i^3}$	$-\frac{3V_i}{4\pi} \left[\frac{\beta^2(x-x_i)(y-y_i)}{R_i^5} \right]$	$-\frac{\bar{L}_i}{8\pi} \left\{ \frac{2(y-y_i)(z-z_i)}{r_i^4} \left[1 + \frac{x-x_i}{R_i} \right] + \frac{\beta^2(x-x_i)(y-y_i)(z-z_i)}{r_i^2 R_i^3} \right\}$
$\frac{w_i}{U}$	$\frac{\bar{D}_i}{8\pi} \frac{\beta^2(z-z_i)}{R_i^3}$	$-\frac{3V_i}{4\pi} \left[\frac{\beta^2(x-x_i)(z-z_i)}{R_i^5} \right]$	$\frac{\bar{L}_i}{8\pi} \left\{ \frac{(y-y_i)^2 - (z-z_i)^2}{r_i^4} \left[1 + \frac{x-x_i}{R_i} \right] - \frac{\beta^2(x-x_i)(z-z_i)^2}{r_i^2 R_i^3} \right\}$

where $r_i^2 = (y-y_i)^2 + (z-z_i)^2$

$R_i^2 = (x-x_i)^2 + \beta^2 r_i^2$

$\bar{D}_i = \frac{D_i}{q}$

$\bar{L}_i = \frac{L_i}{q}$

$V_i =$ Incremental Volume

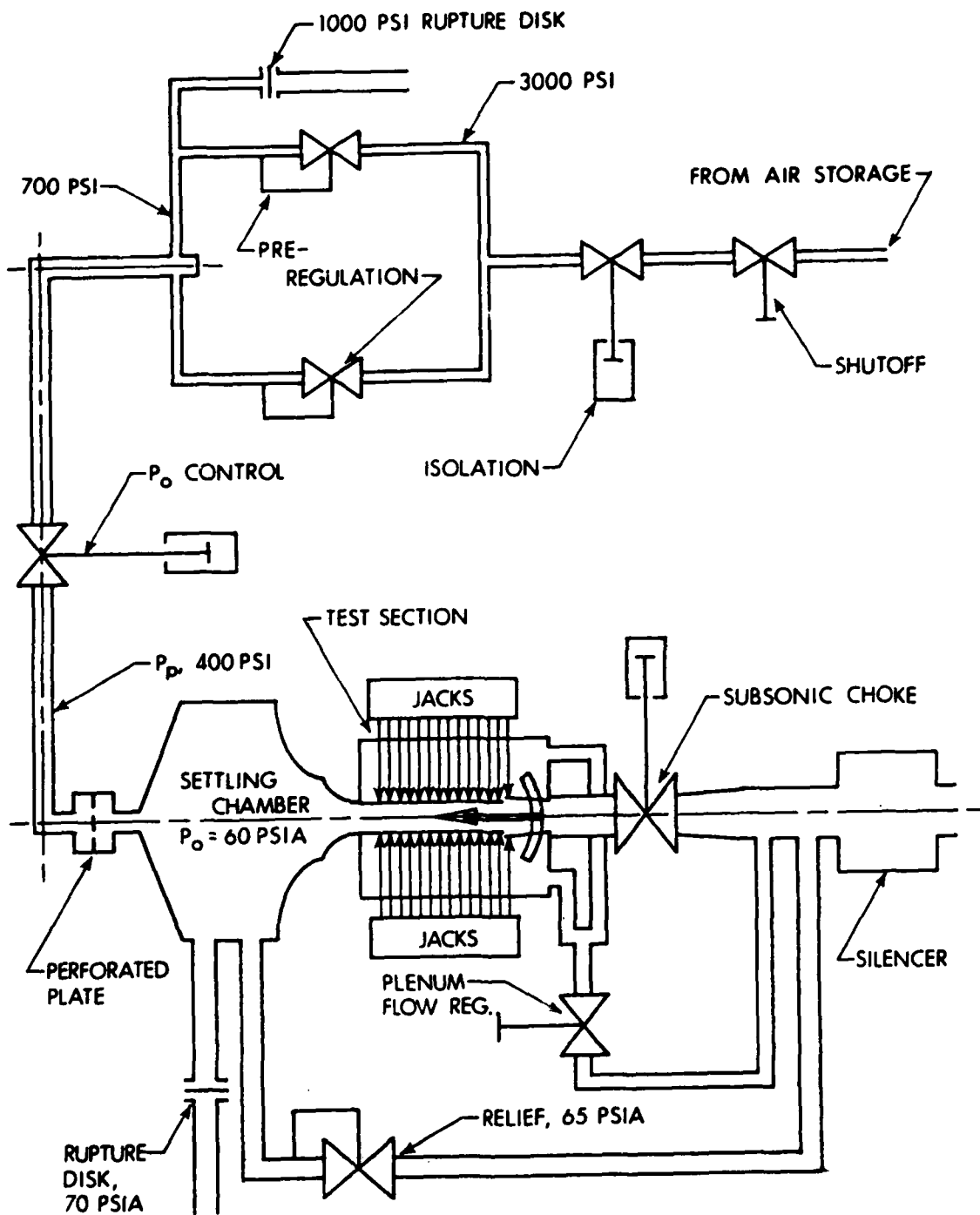


Figure 1. Overall Schematic of Facility

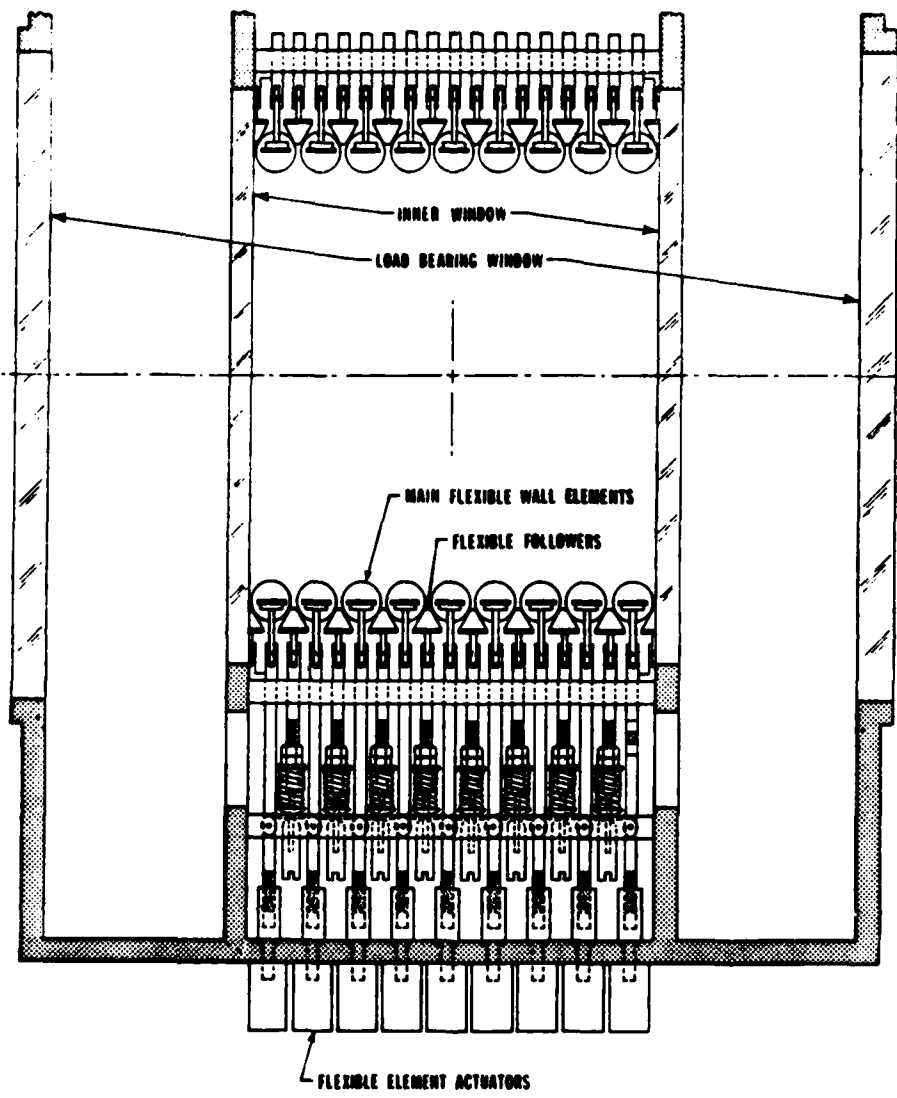


Figure 2. Cross Section through the Center of the Test Region

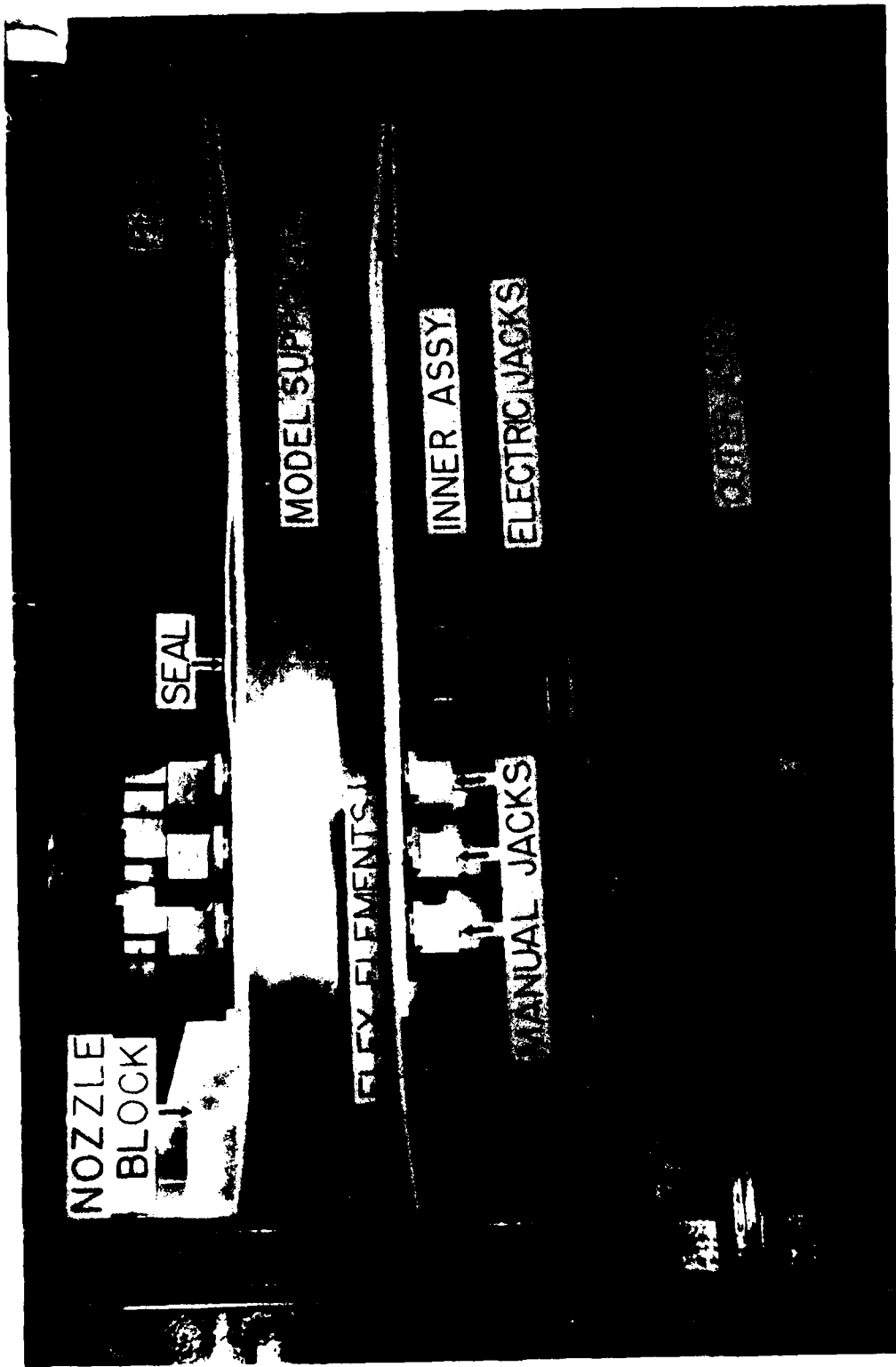


Figure 3. Display of Flexible Wall Test Section with Sidewall Removed.

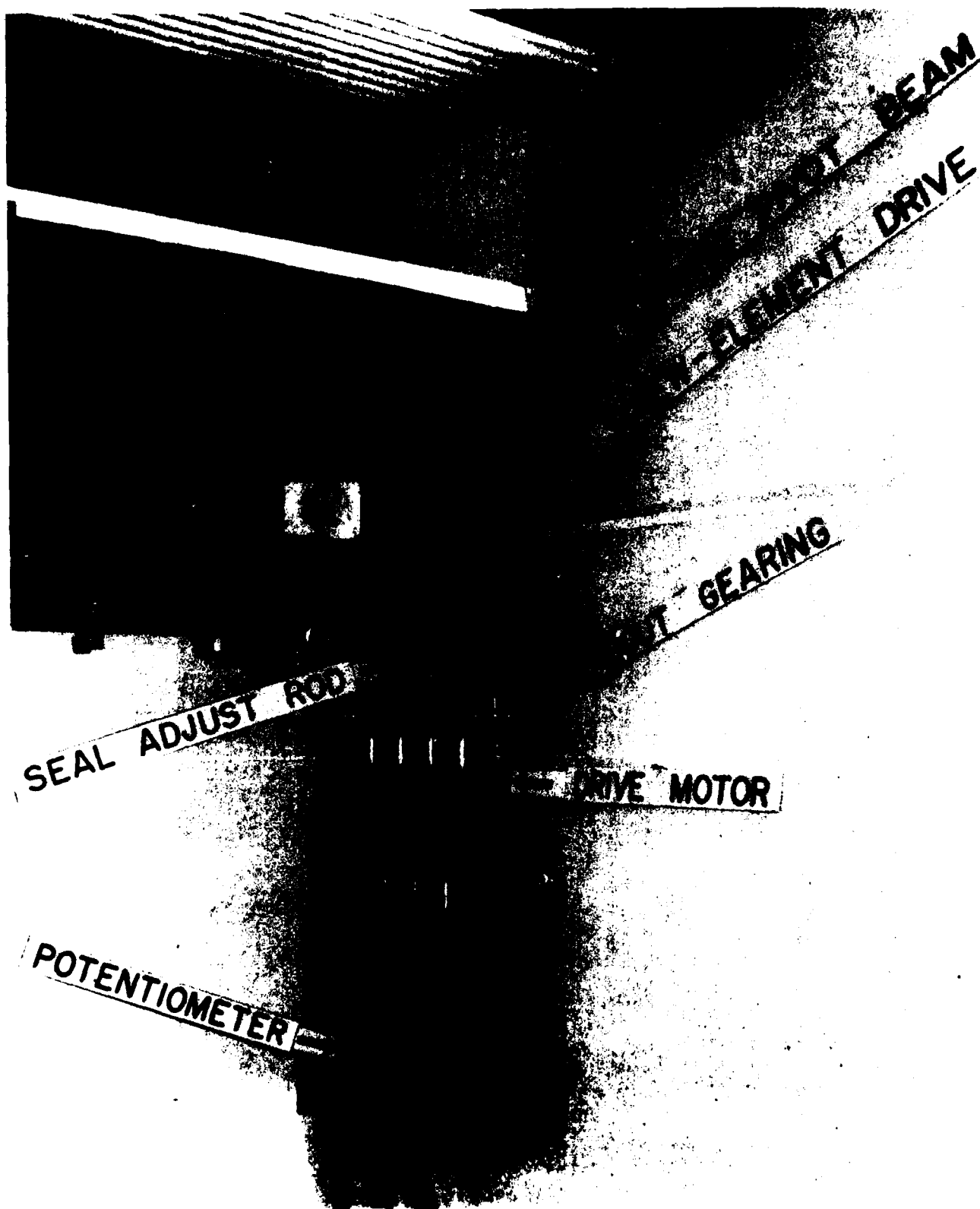


Figure 4. Details of Motorized Jacking Station.

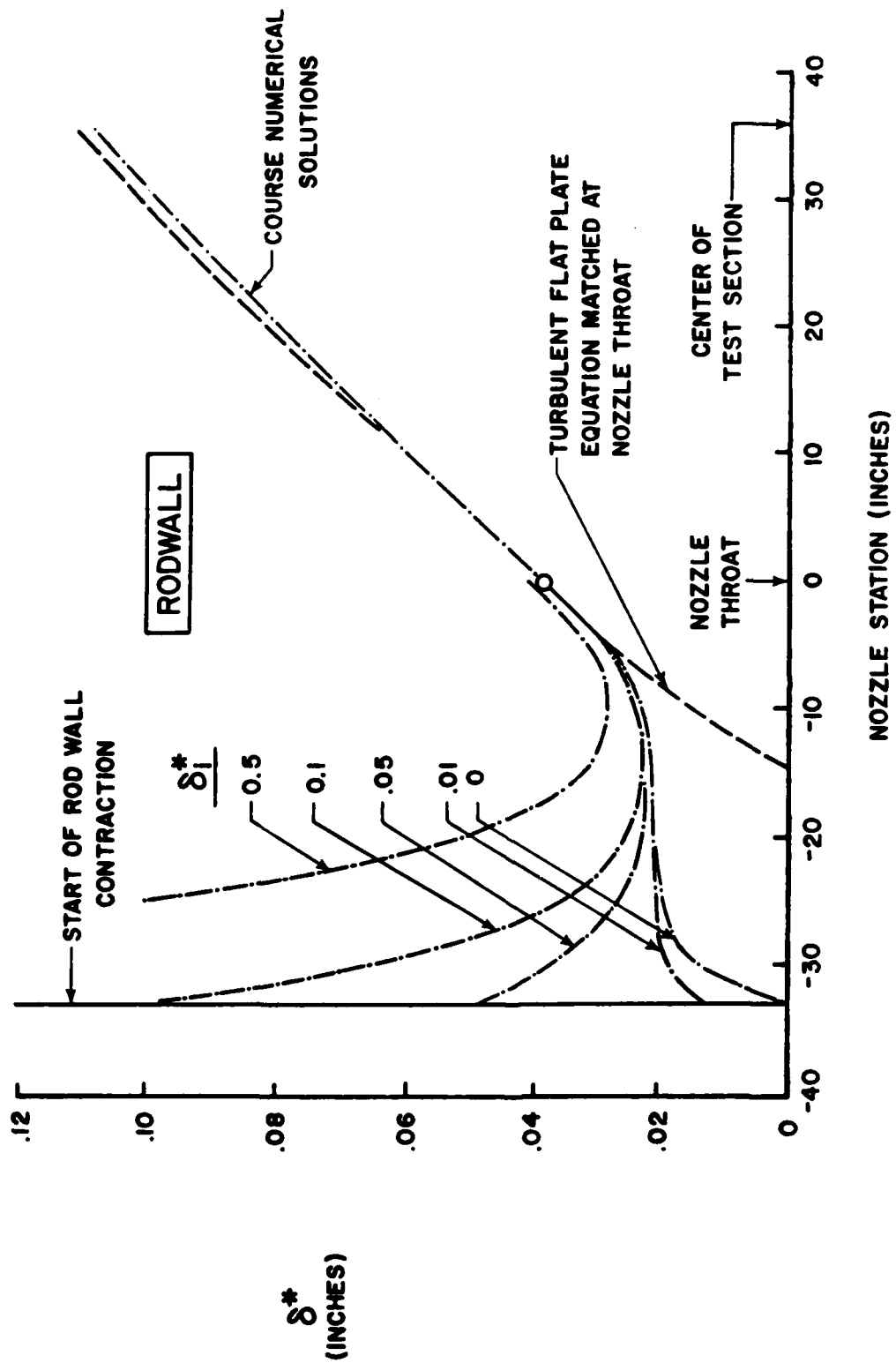


Figure 5. Rodwall Boundary Layer Development through the Nozzle Contraction to the Center of the Test Section

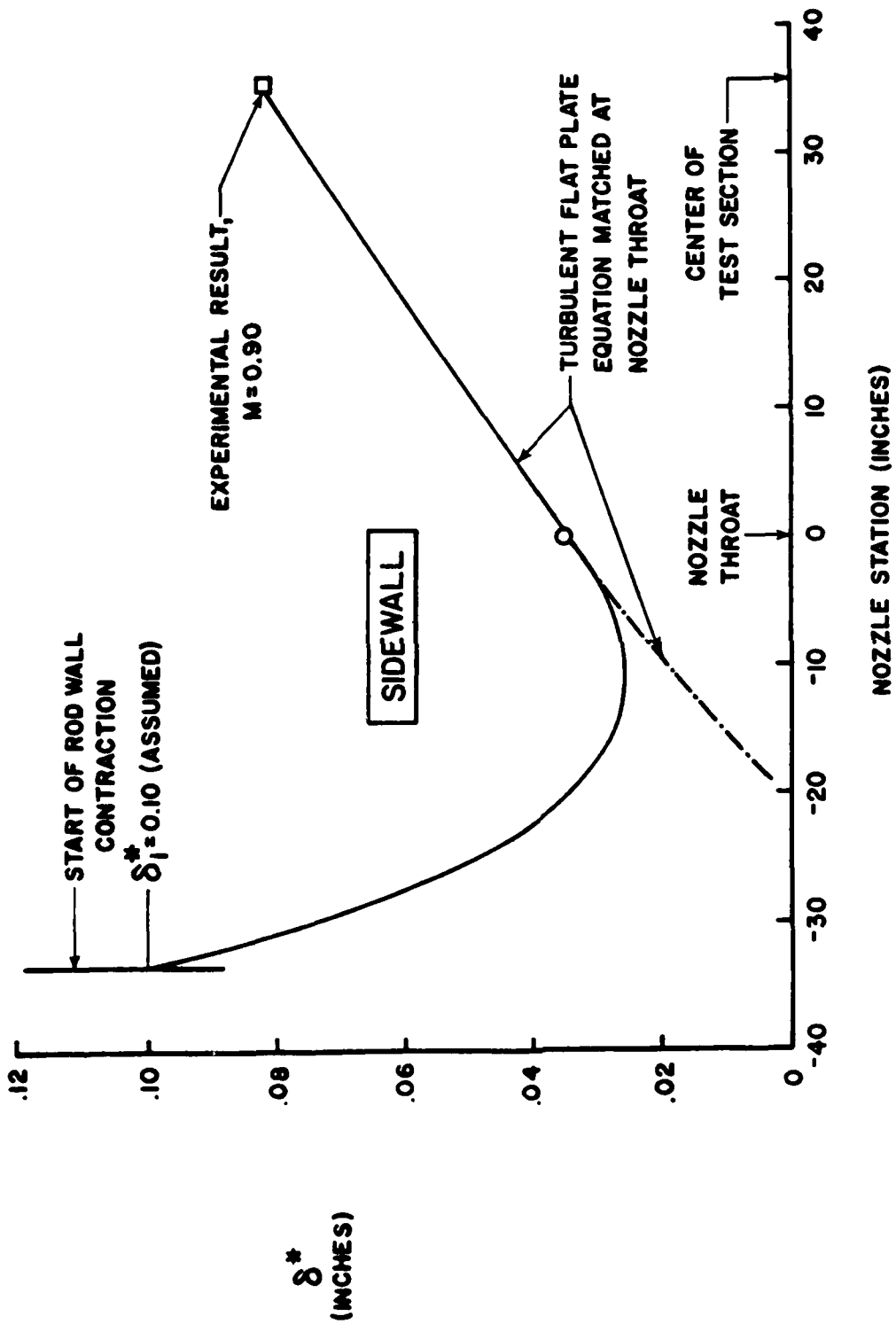


Figure 6. Sidewall Boundary Layer Development

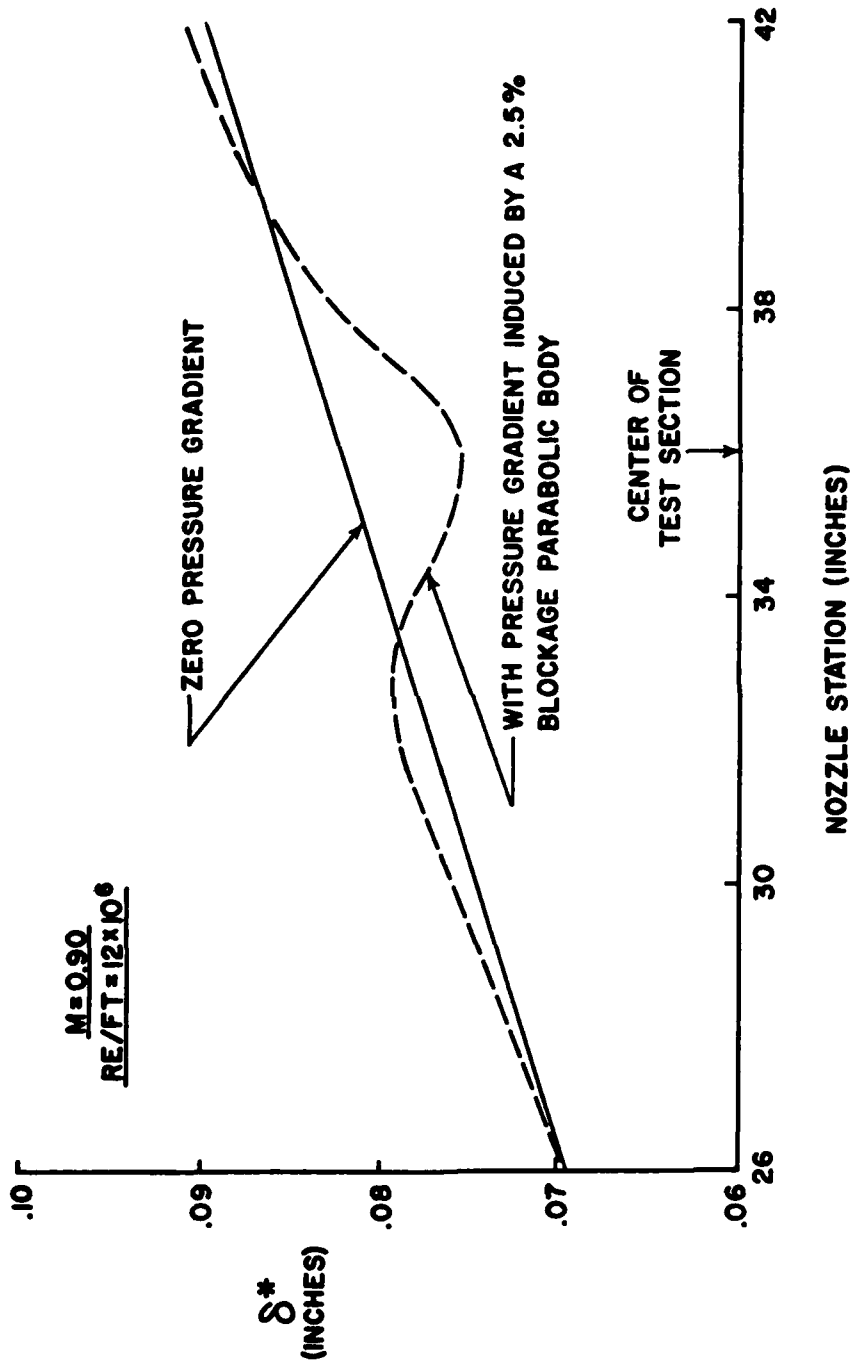


Figure 7. Estimated Effect of Model Induced Pressure Gradient on the Wall Boundary Layer Displacement Thickness.

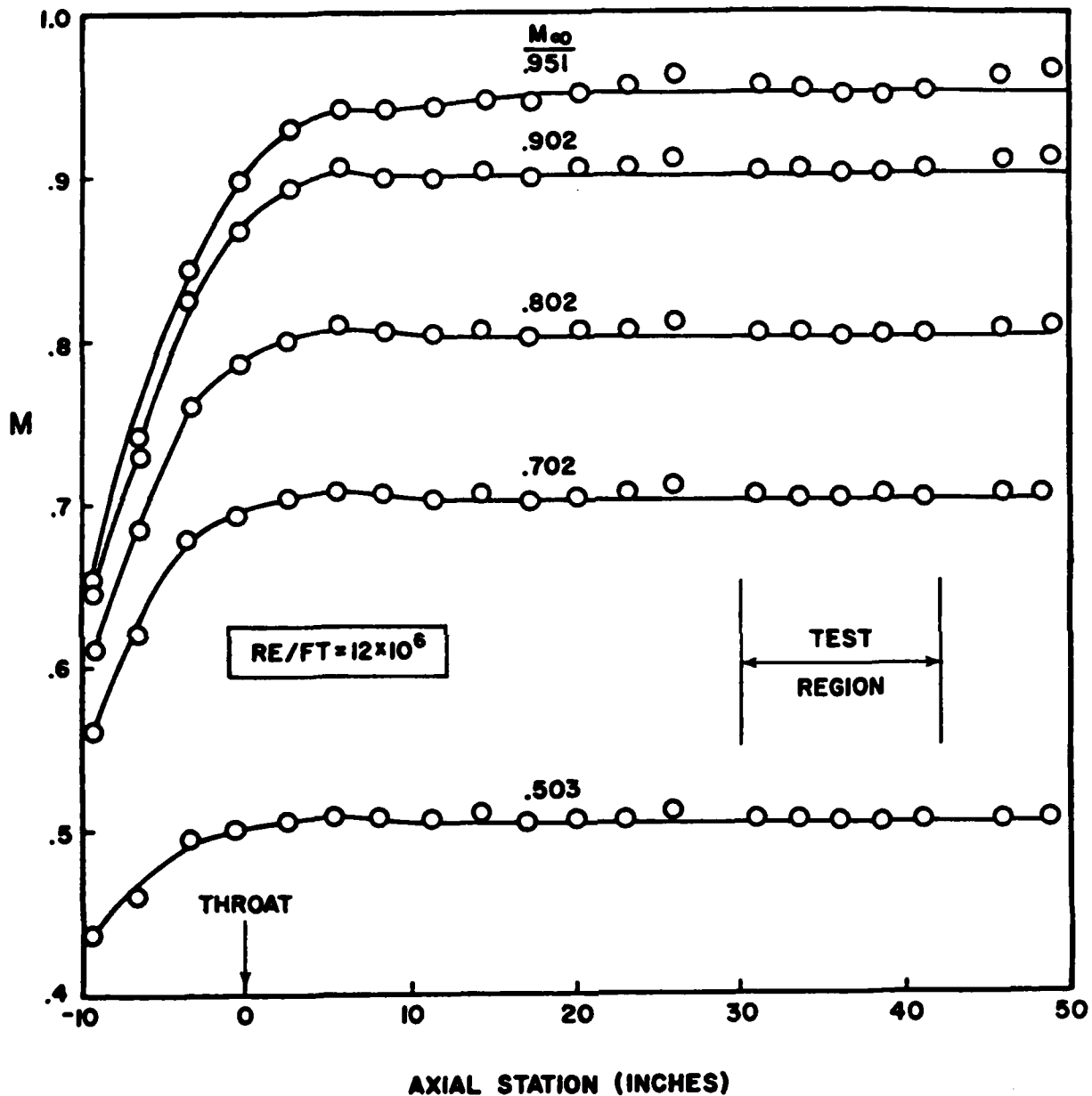


Figure 8. Test Section Empty Calibration after Correction for Wall Boundary Layer

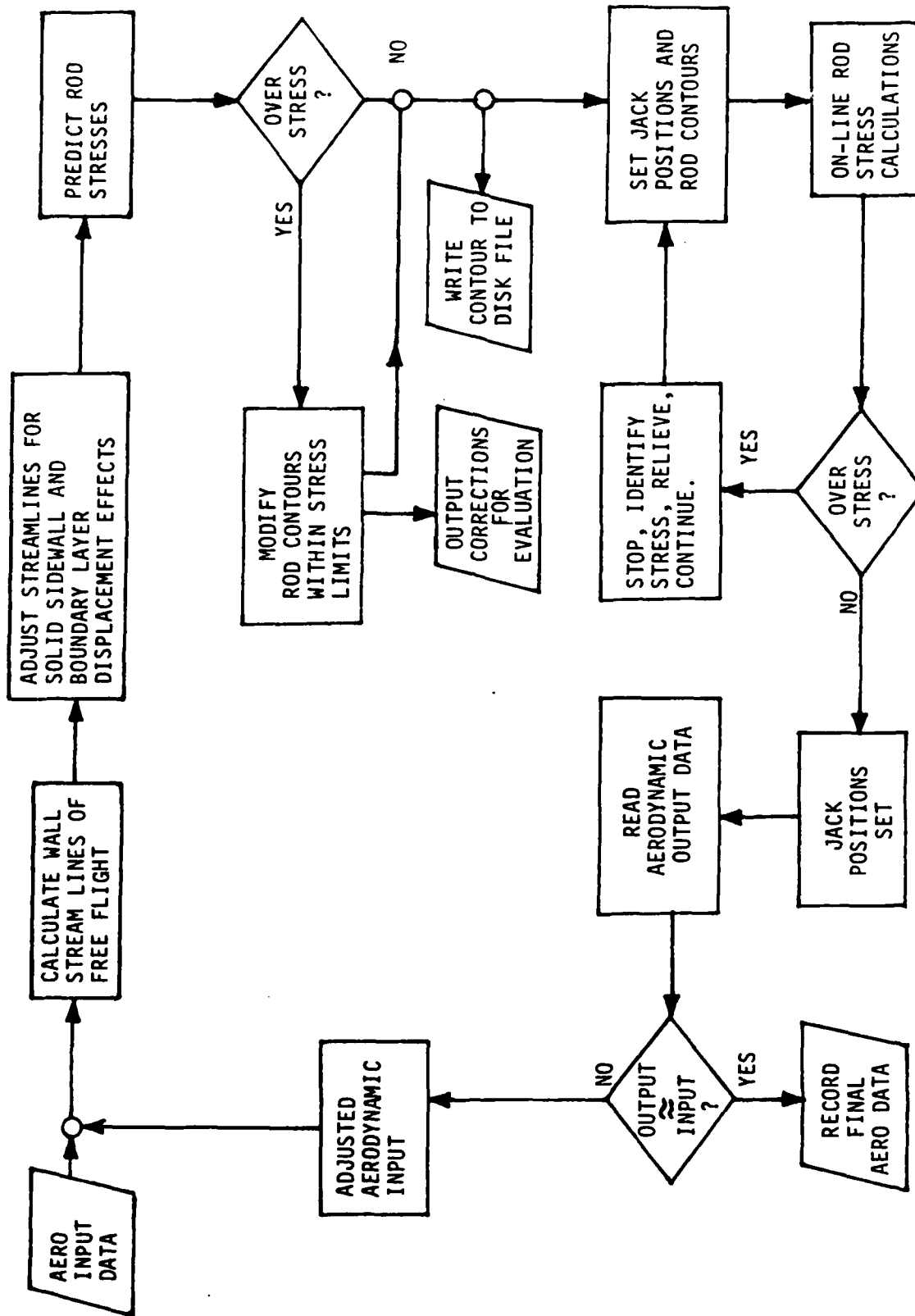


Figure 9. Wall Adaptation Scheme Showing Sequence of Operations.



Figure 10. Parabolic-Arc Body of Revolution Pressure Model.

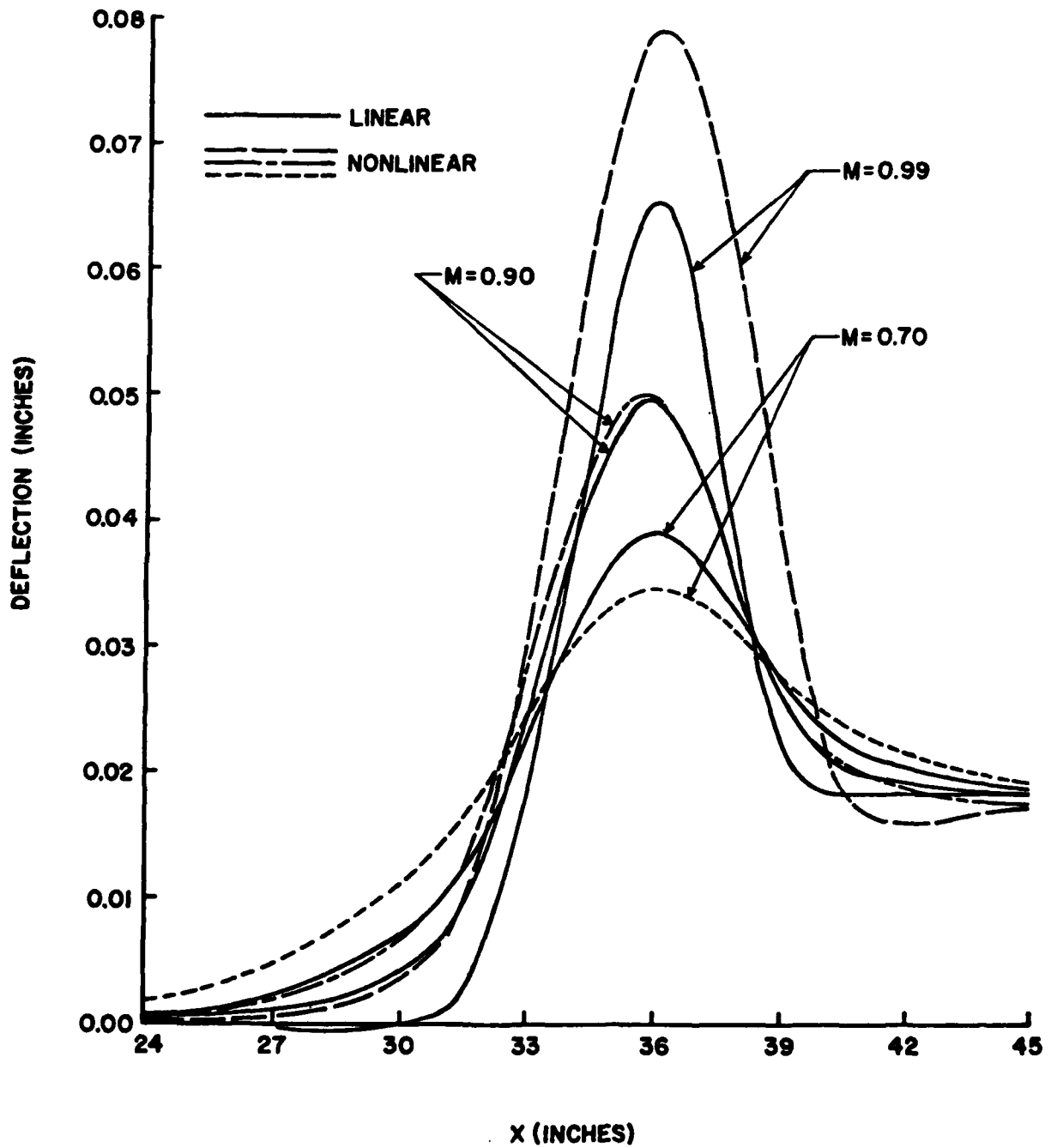


Figure 11. Selected Comparisons of Free-Air Center Streamlines at the Wall Comparing Linear and Nonlinear Potential Flow Calculations

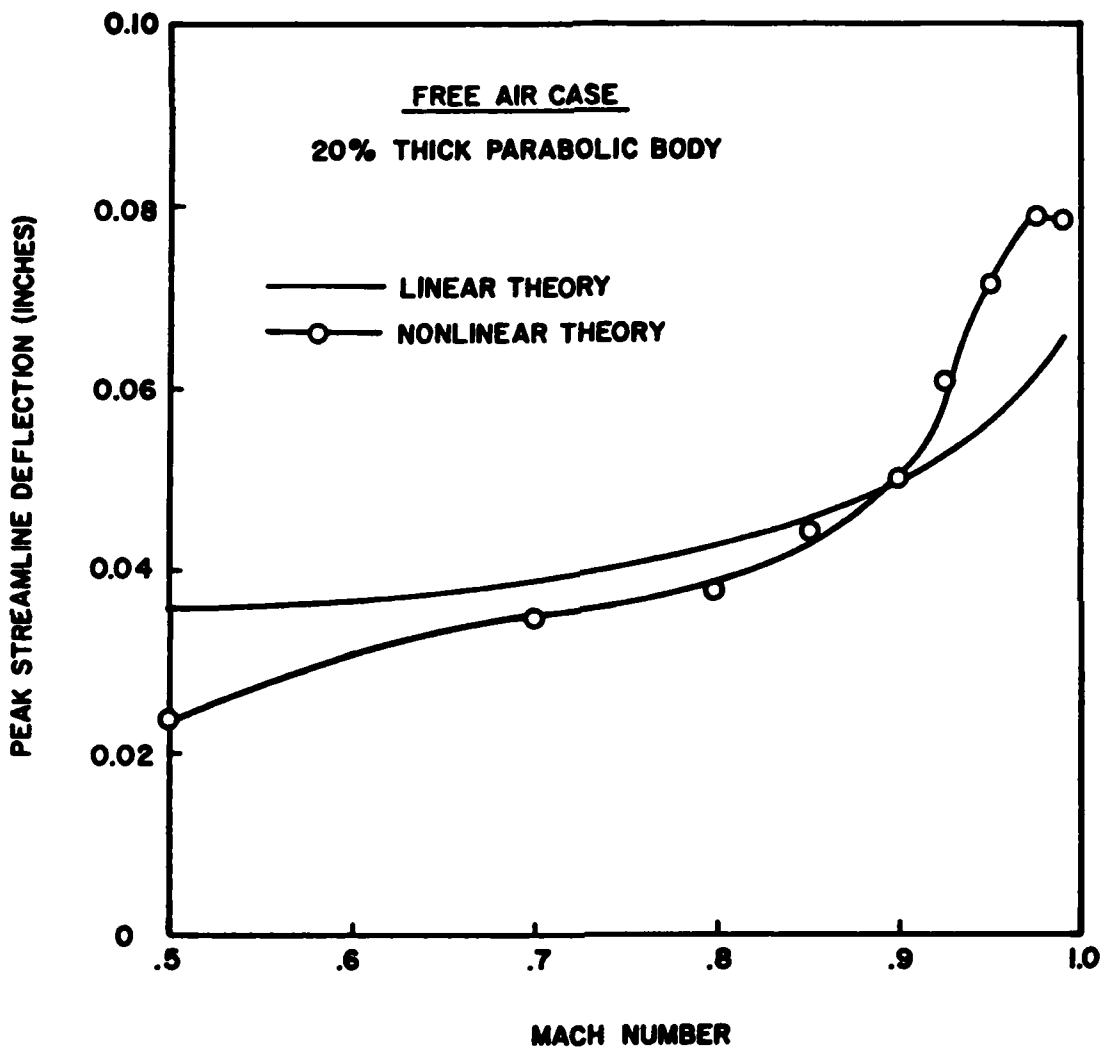


Figure 12. Comparison of Peak Streamline Deflections versus Mach Number Comparing Linear and Nonlinear Calculation Methods

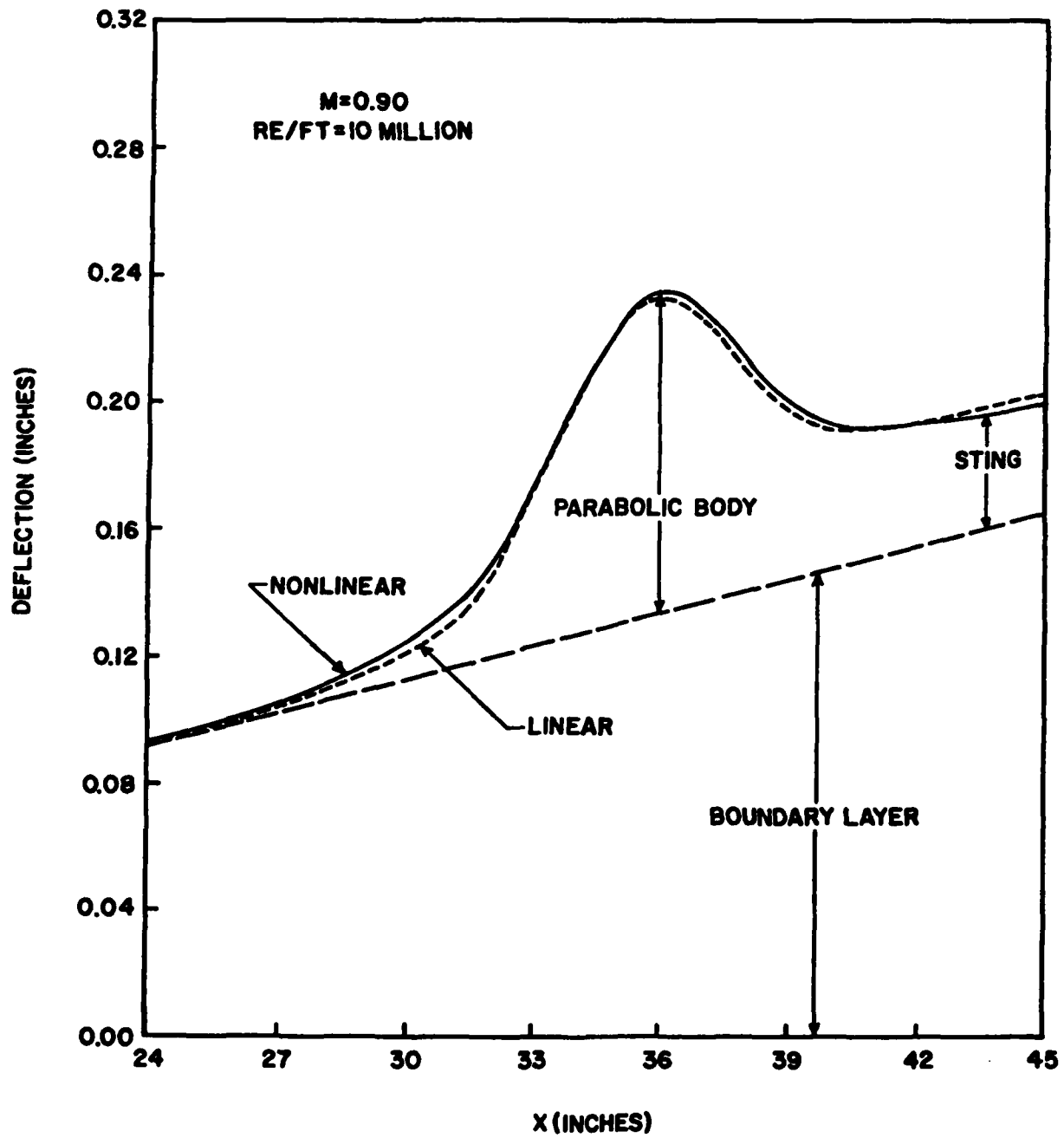


Figure 13. Centerline Rod Deflection Including Boundary Layer Displacement and Solid Sidewall Effects

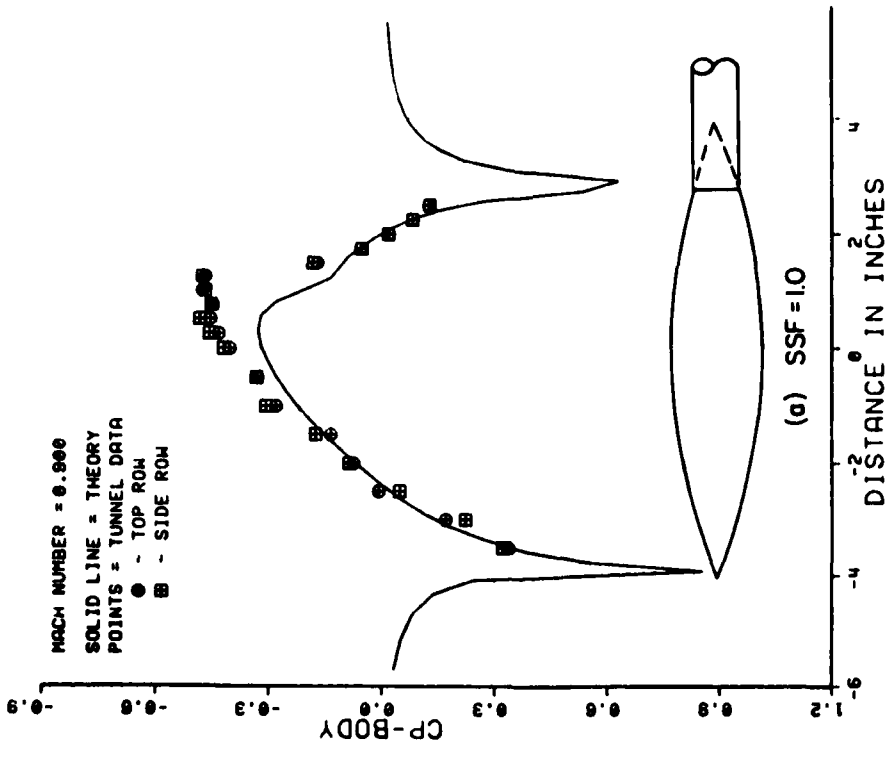
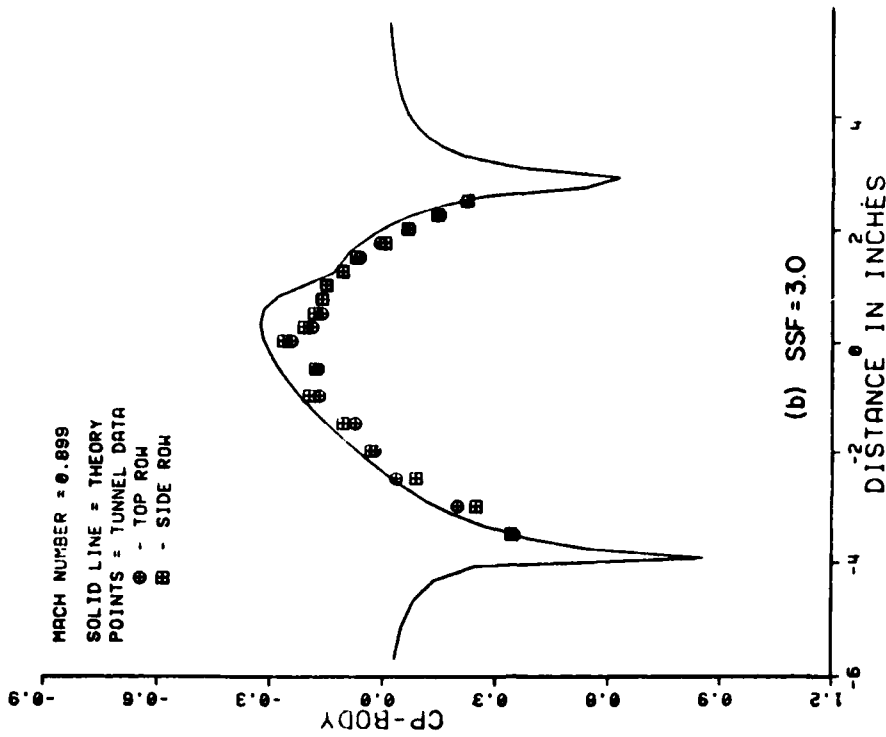


Figure 14. Pressure Distributions on the Axisymmetric Model for Varying Values of the Solid Sidewall Factor

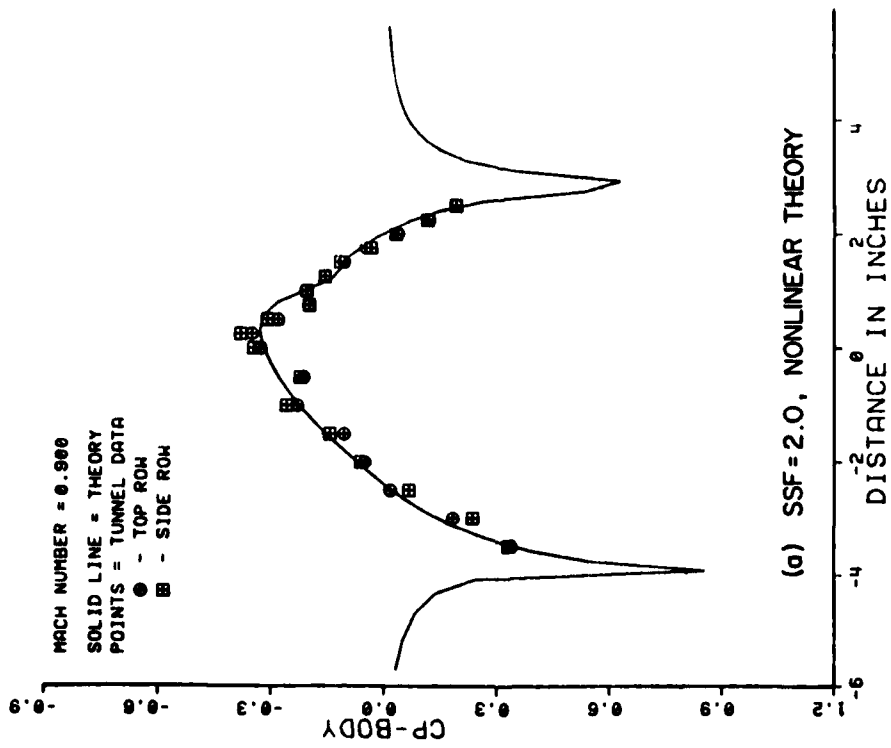
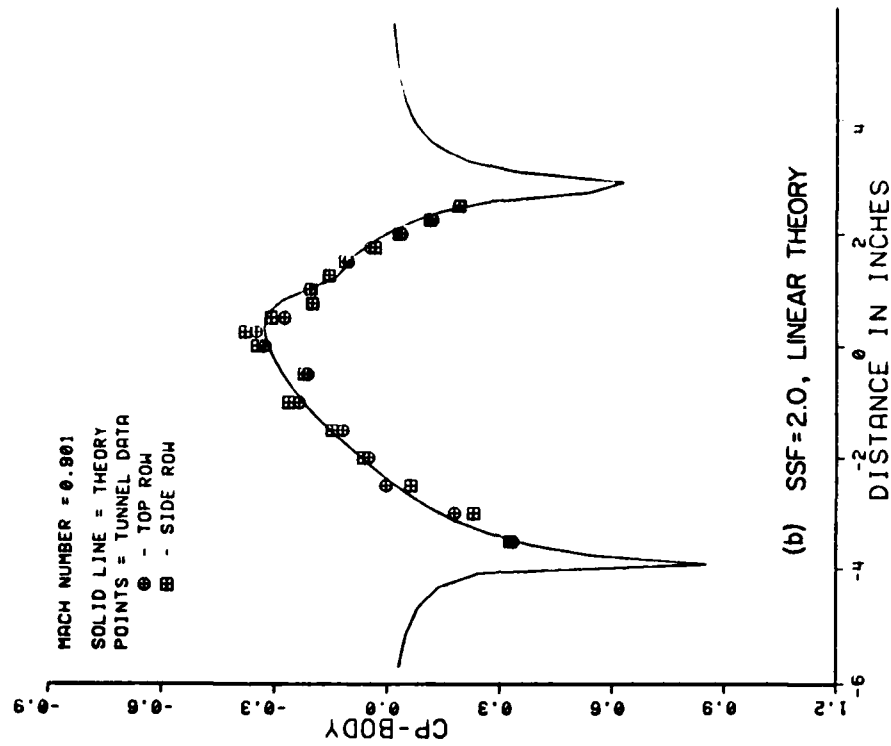


Figure 15. Pressure Distributions for a Solid Sidewall Factor of 2.0
 Comparing Nonlinear and Linear Methods of Calculation

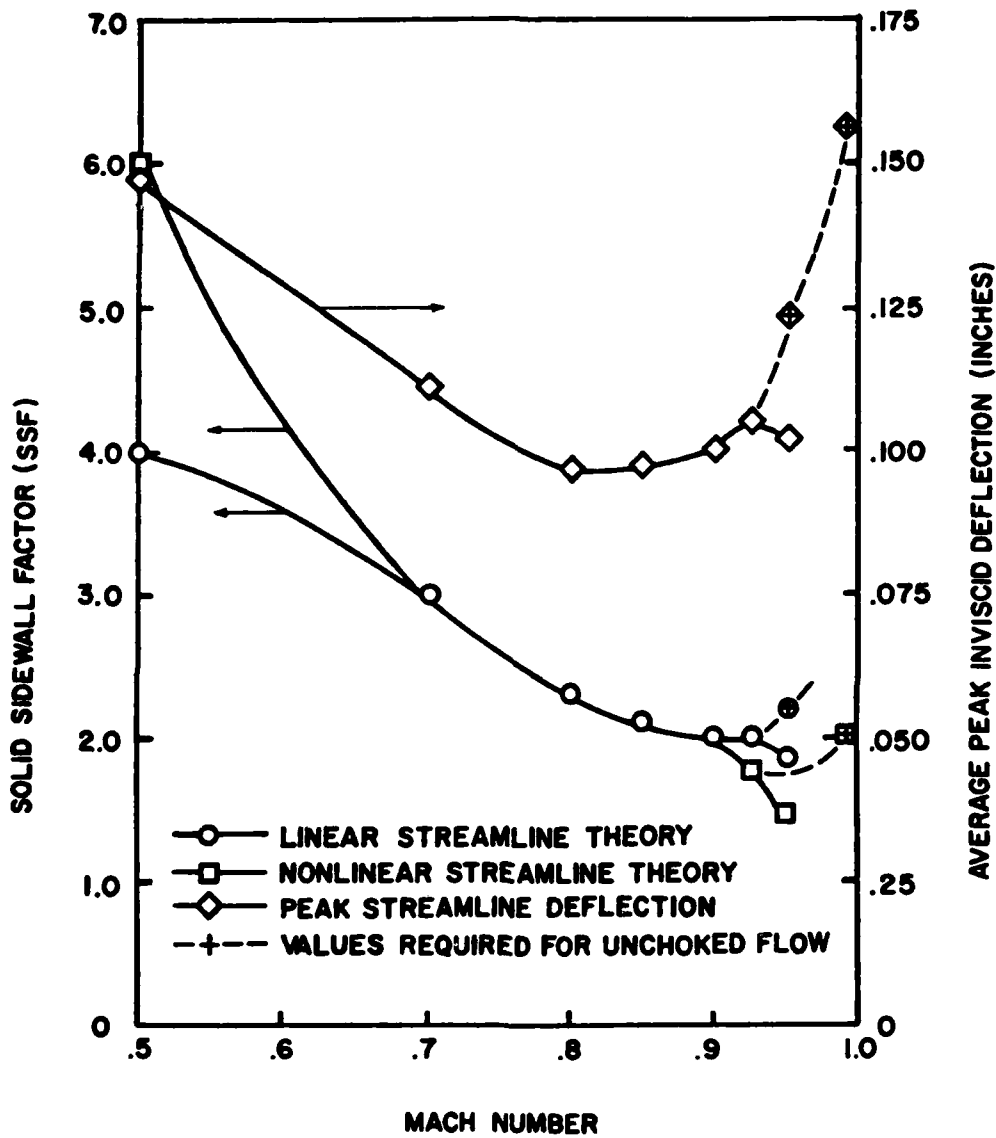


Figure 16. Solid Sidewall Factor and Peak Streamline Deflection Required to Match the Theoretical Pressure Distribution on the Axisymmetric Body

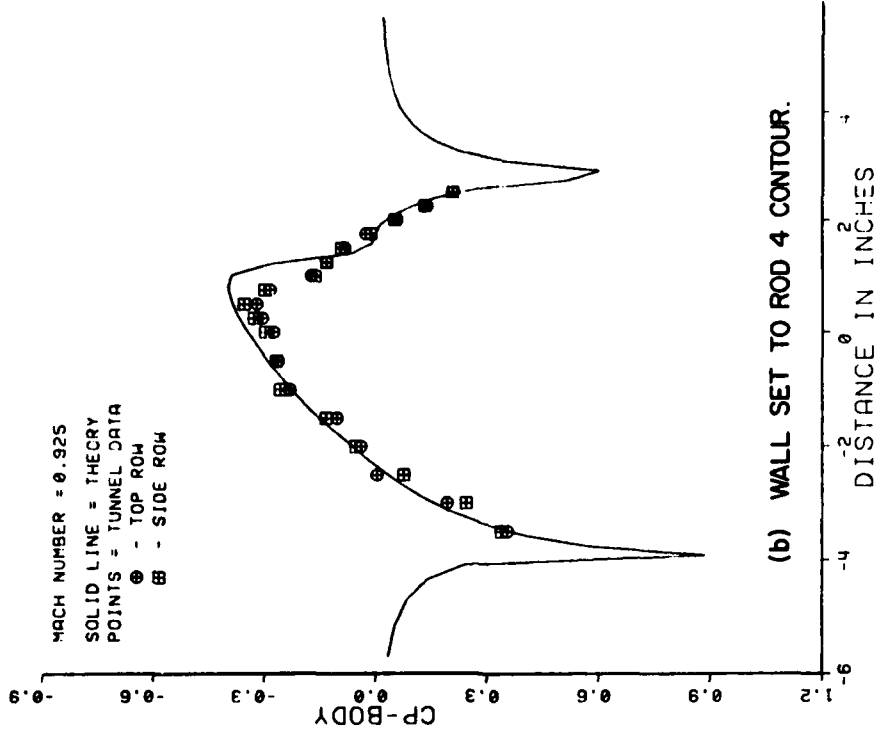
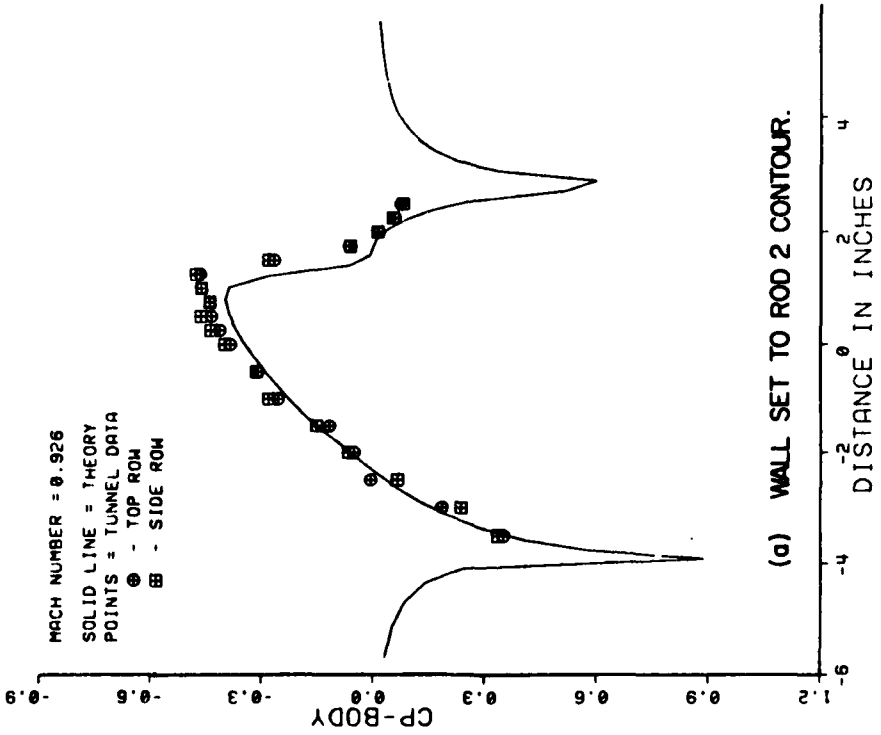


Figure 17. Model Pressure Distributions with Variations in the Two-Dimensional Wall Setting

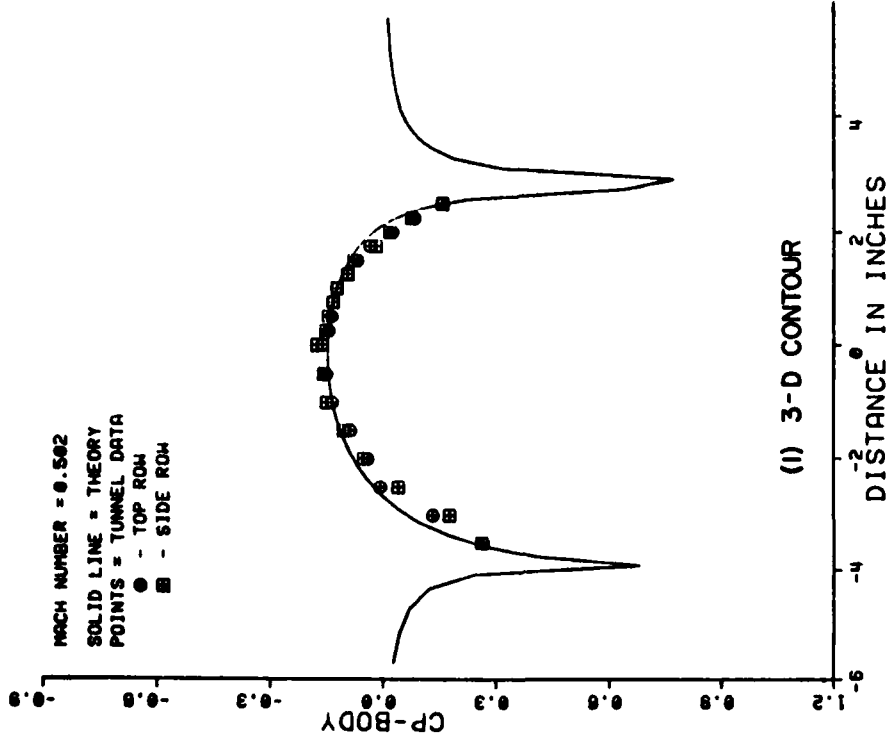
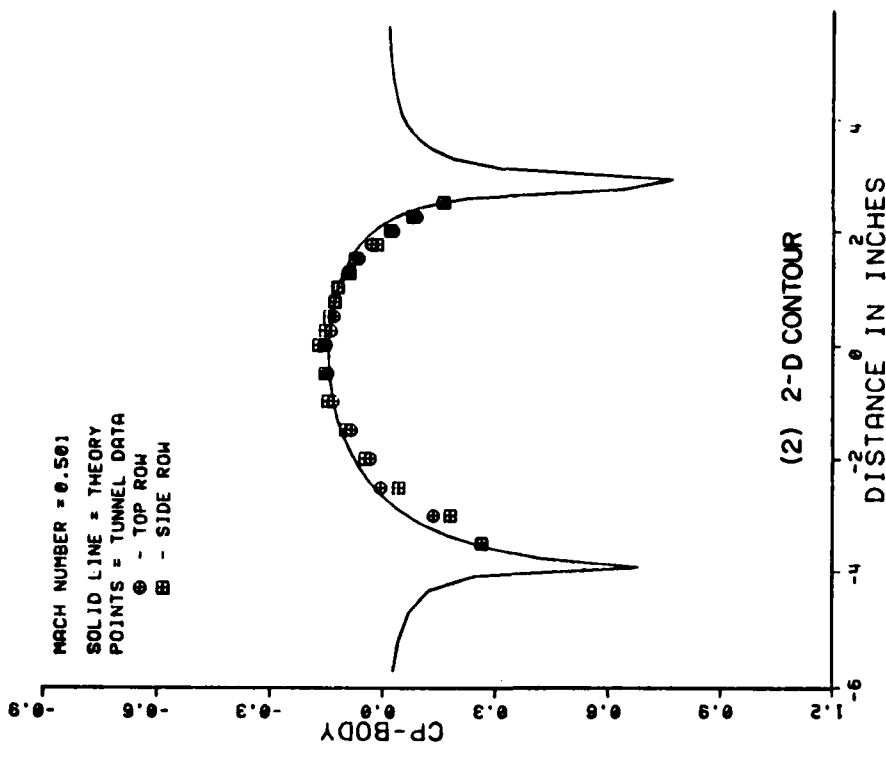


Figure 18. Pressure Distributions on a Parabolic-Arc Body of Revolution. Walls Contoured Using Linear Theory Corrected for Solid Sidewalls. Includes Comparisons of 2-D and 3-D Contours (a) $M = 0.500$

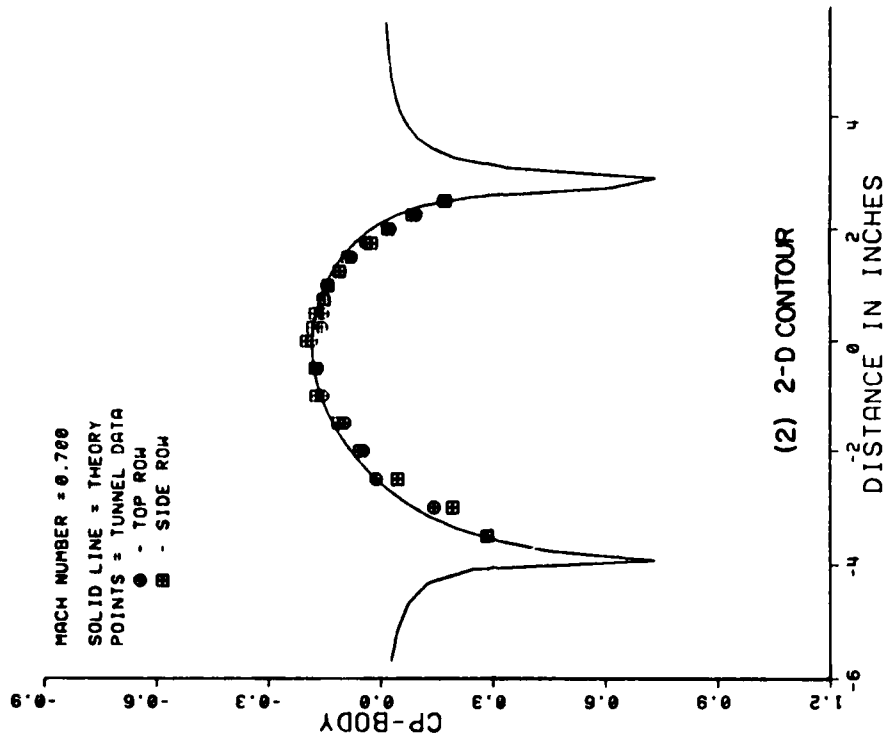
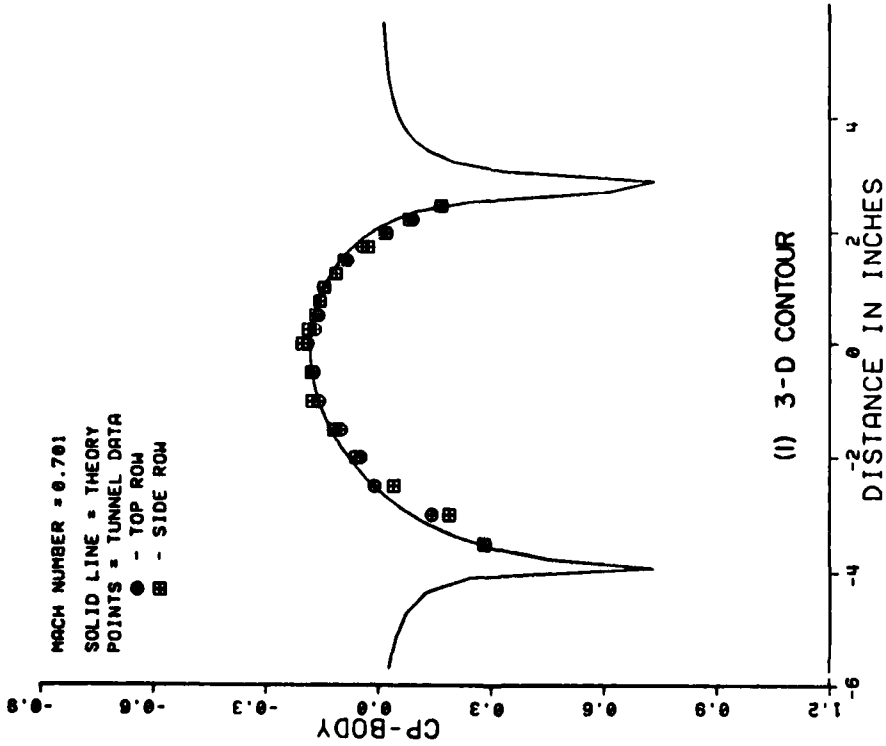


Figure 18. Continued (b) M = 0.700

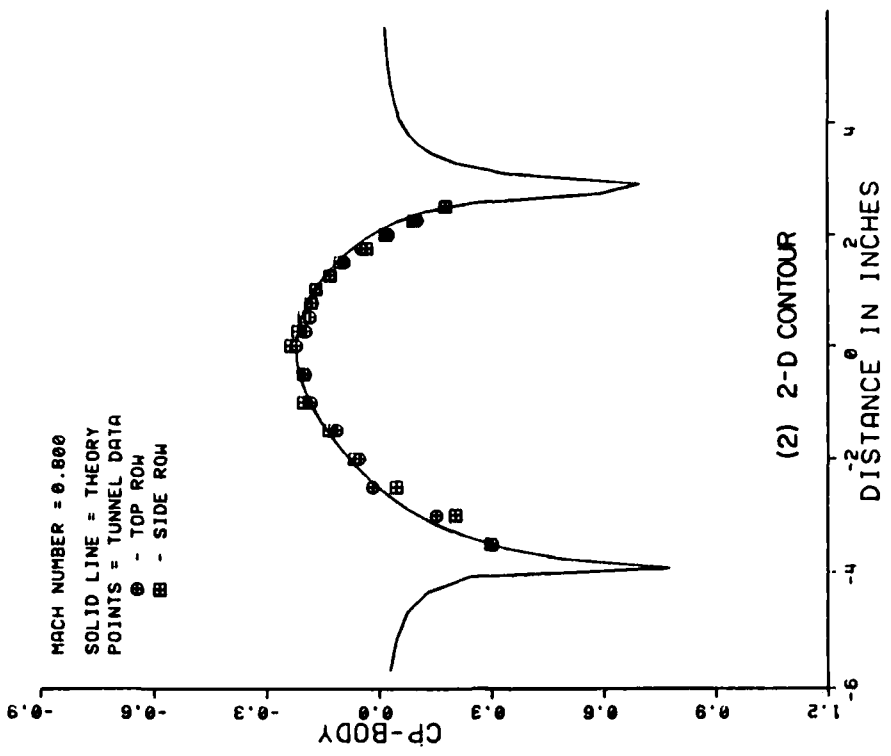
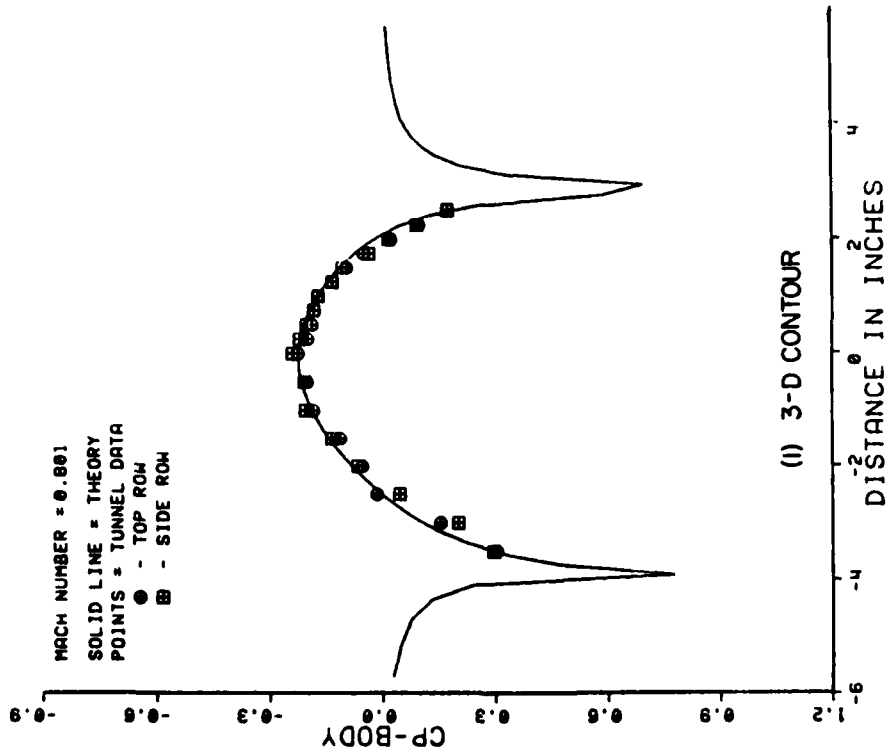


Figure 18. Continued (c) M = 0.800

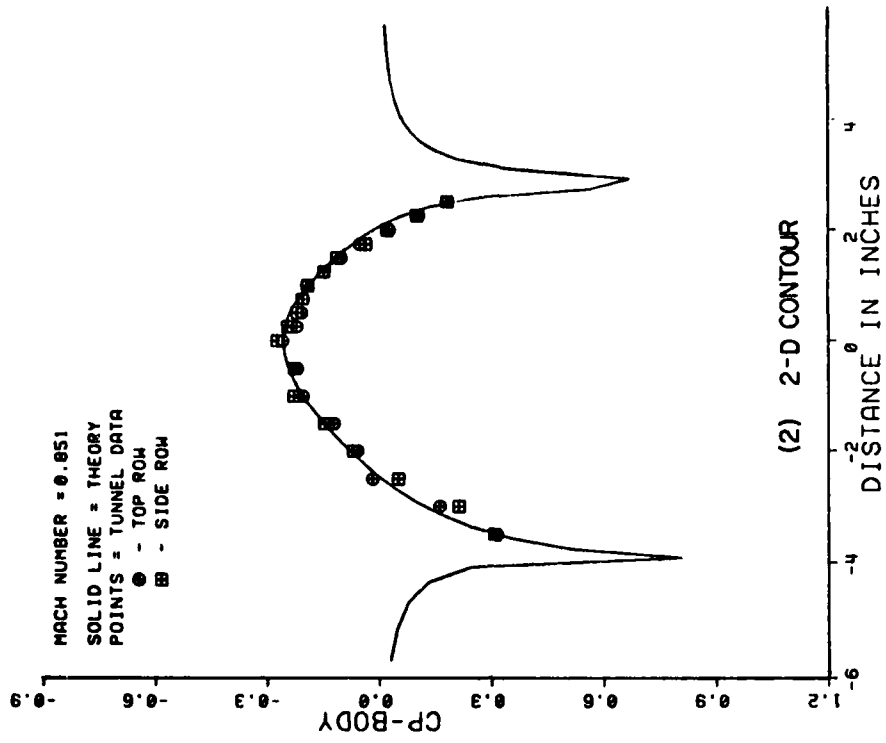
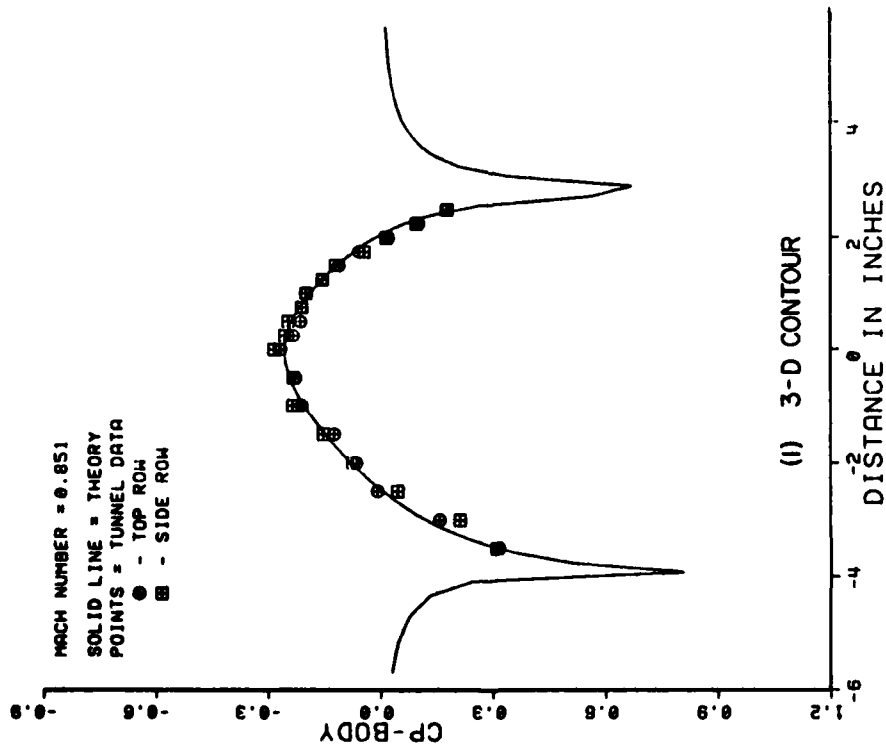


Figure 18. Continued (d) $M = 0.850$

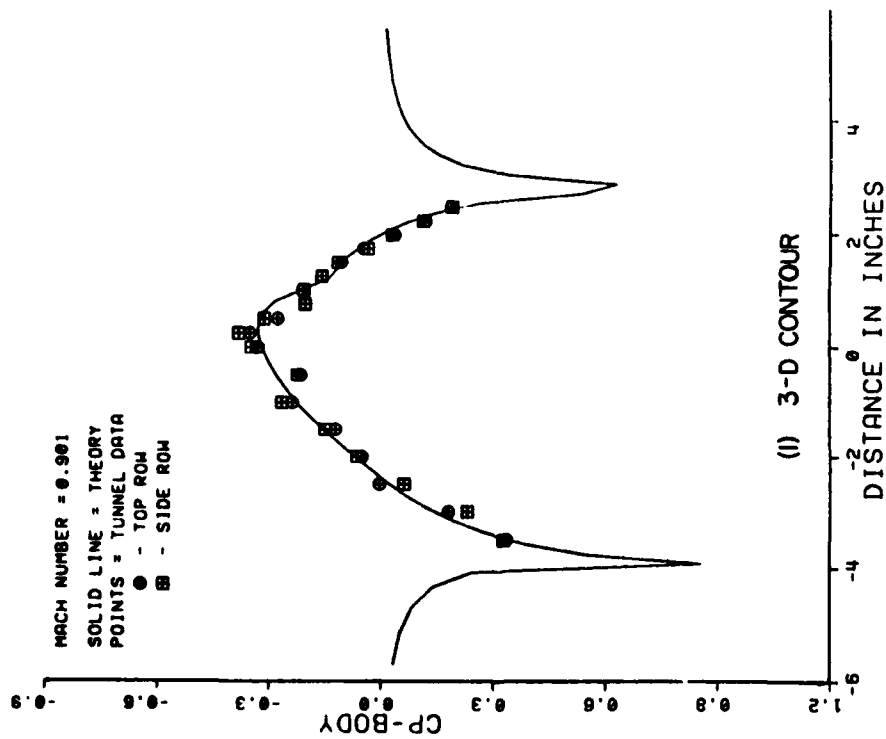
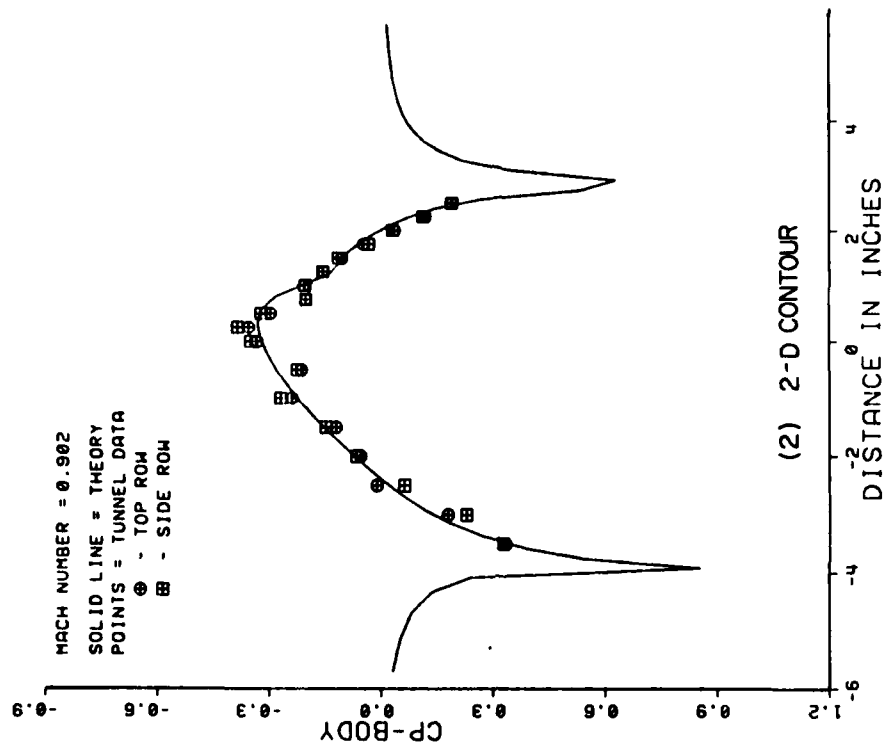


Figure 18. Continued (e) $M = 0.900$

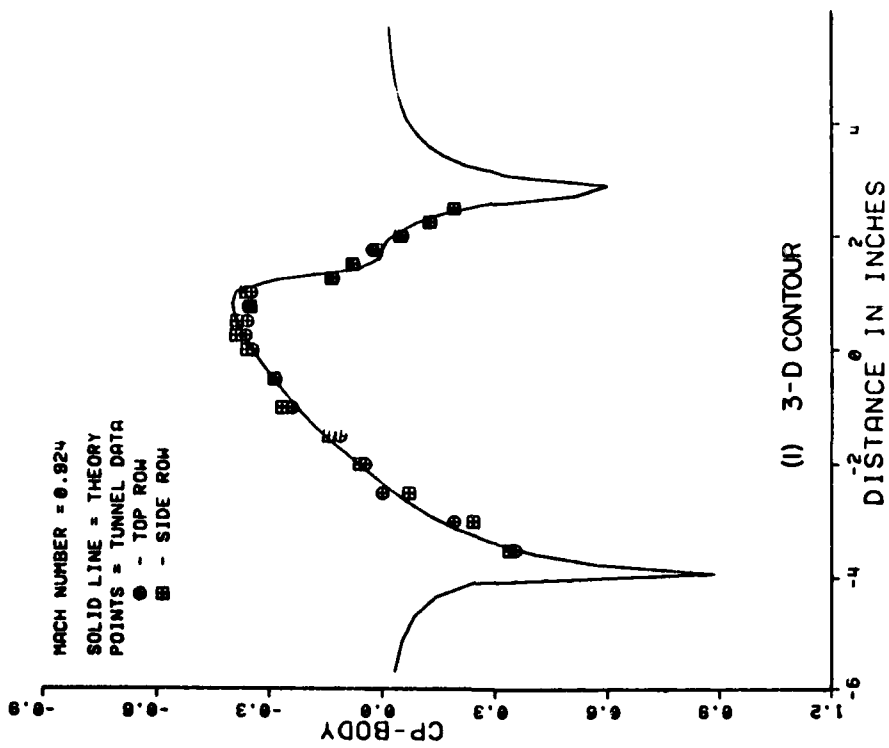
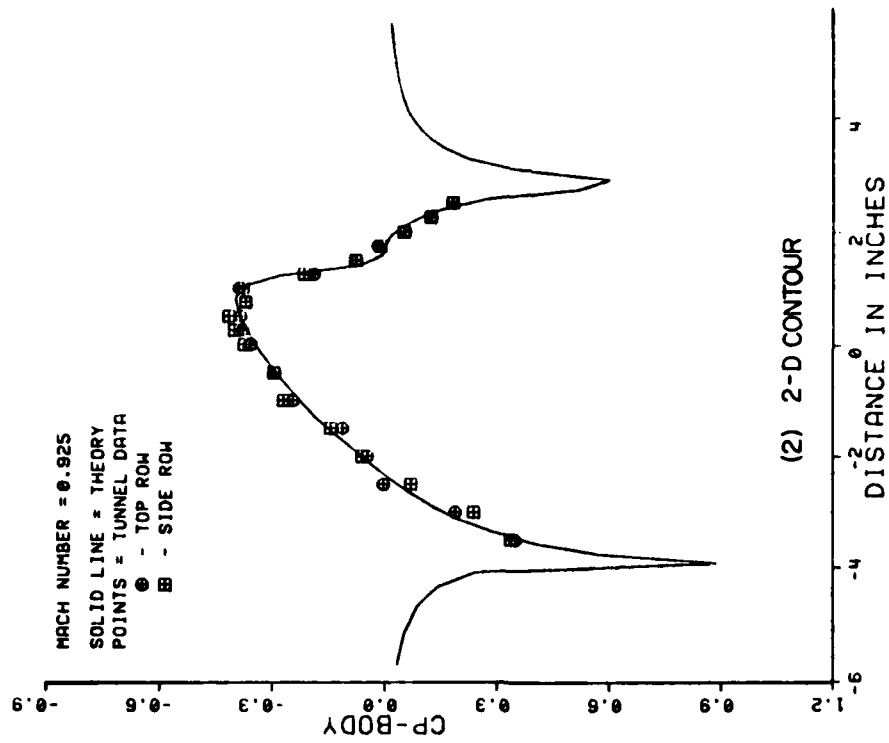


Figure 18. Continued (f) M = 0.925

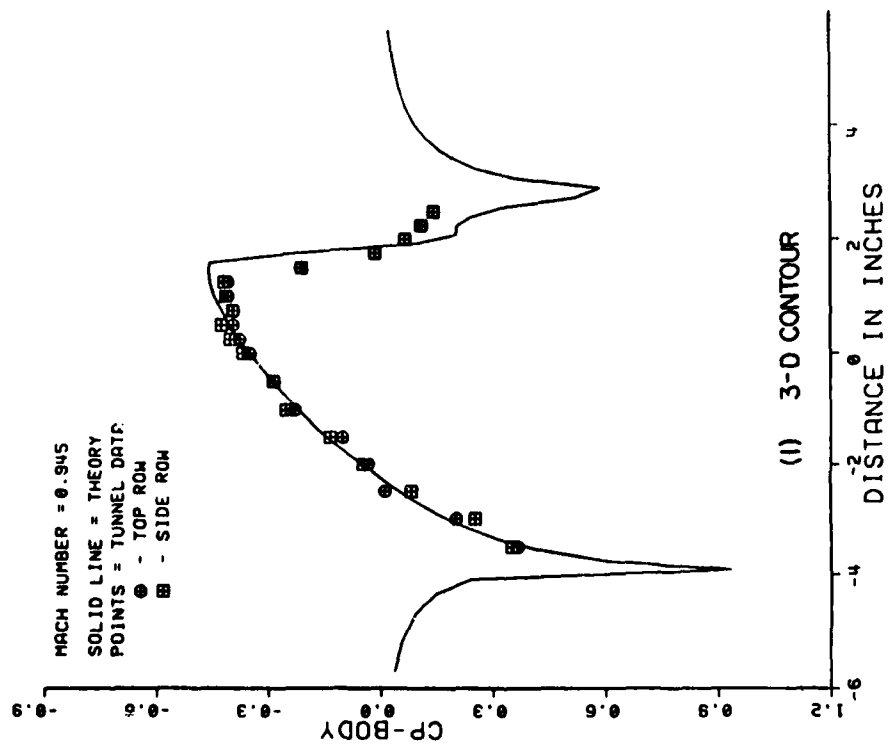
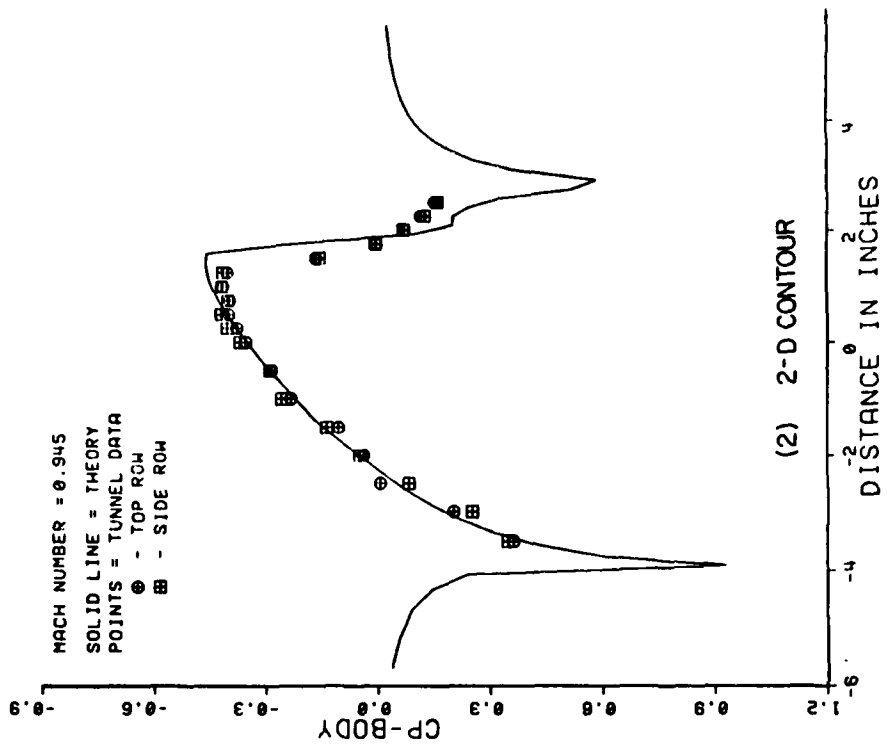


Figure 18. Continued (g) $M = 0.945$

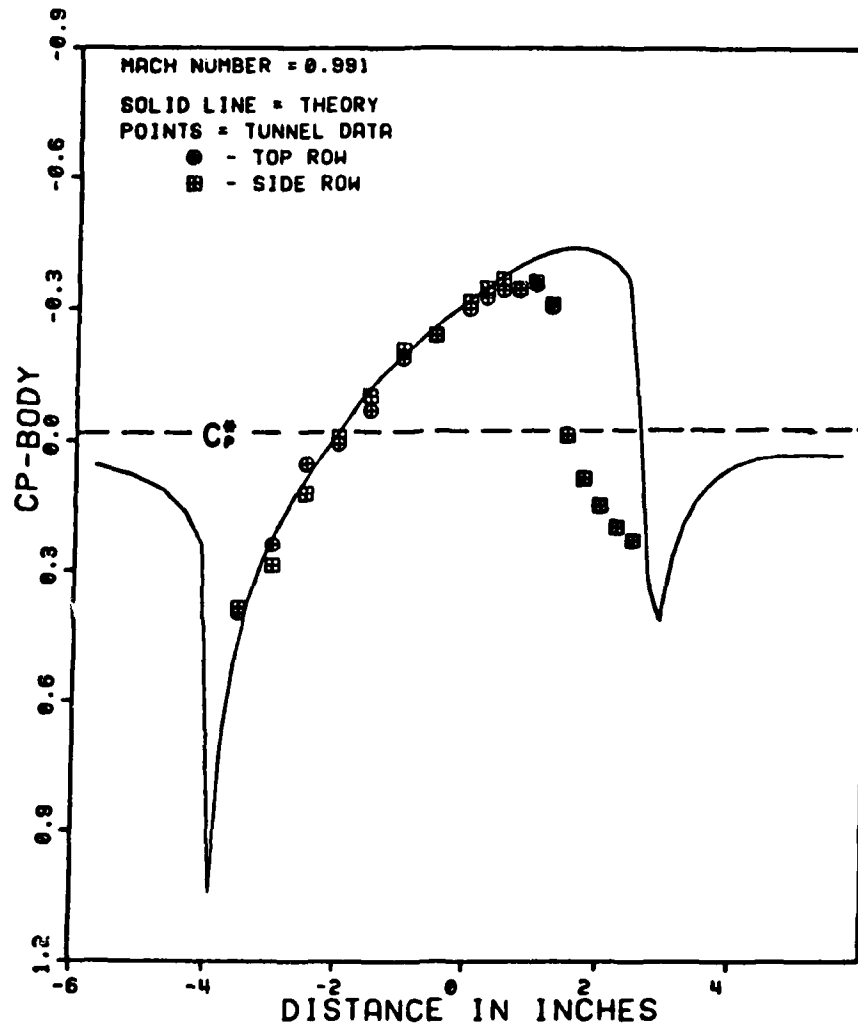


Figure 19. High Mach Number Model Pressure Distribution with Walls Expanded to Relieve Tunnel Choking

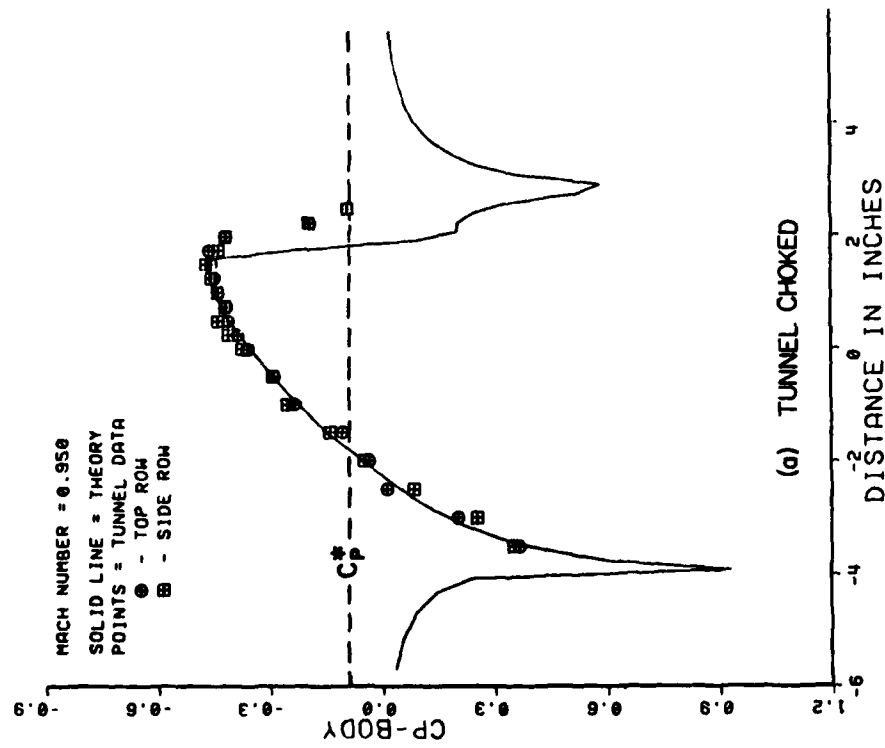
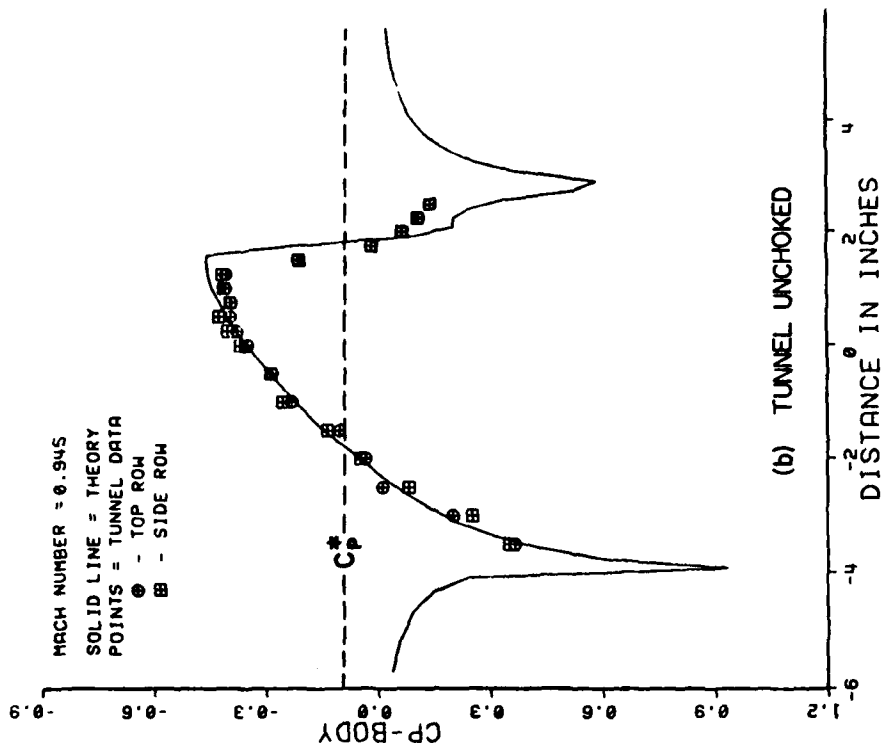


Figure 20. Relief of Tunnel Choking with a Slight Reduction in Mach Number of 0.005

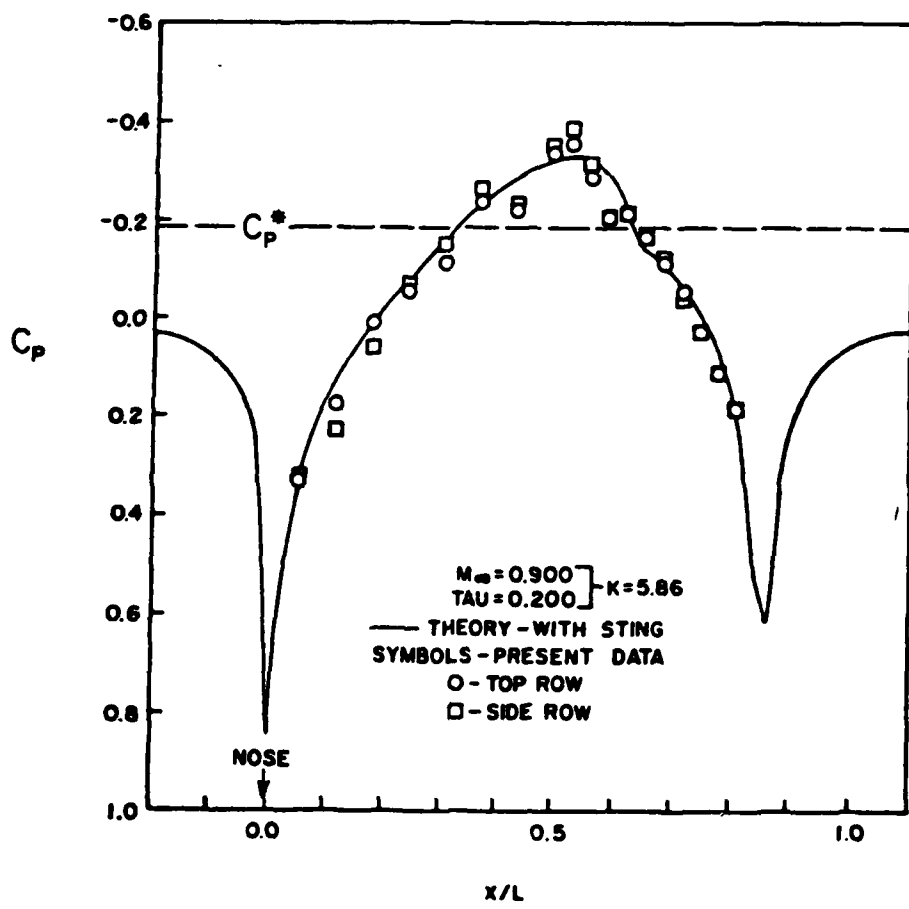
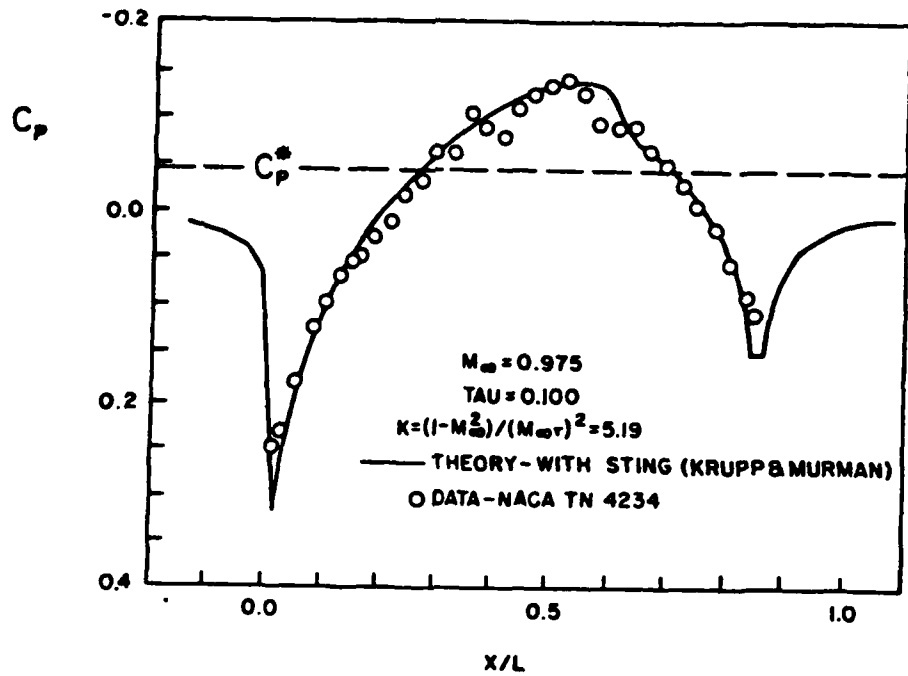


Figure 21. Data Comparison Between a 10% and 20% Thick Model Illustrating a Double Compression



(a) $M=0.850$



(d) $M=0.925$



(b) $M=0.875$



(e) $M=0.935$



(c) $M=0.900$



(f) $M=0.943$ (CHOKED)

Figure 22. Schlieren Photographs of Axisymmetric Flow Ranging from Critical Flow to Tunnel Choking.



Figure 23. Lifting Model Installed in Tunnel

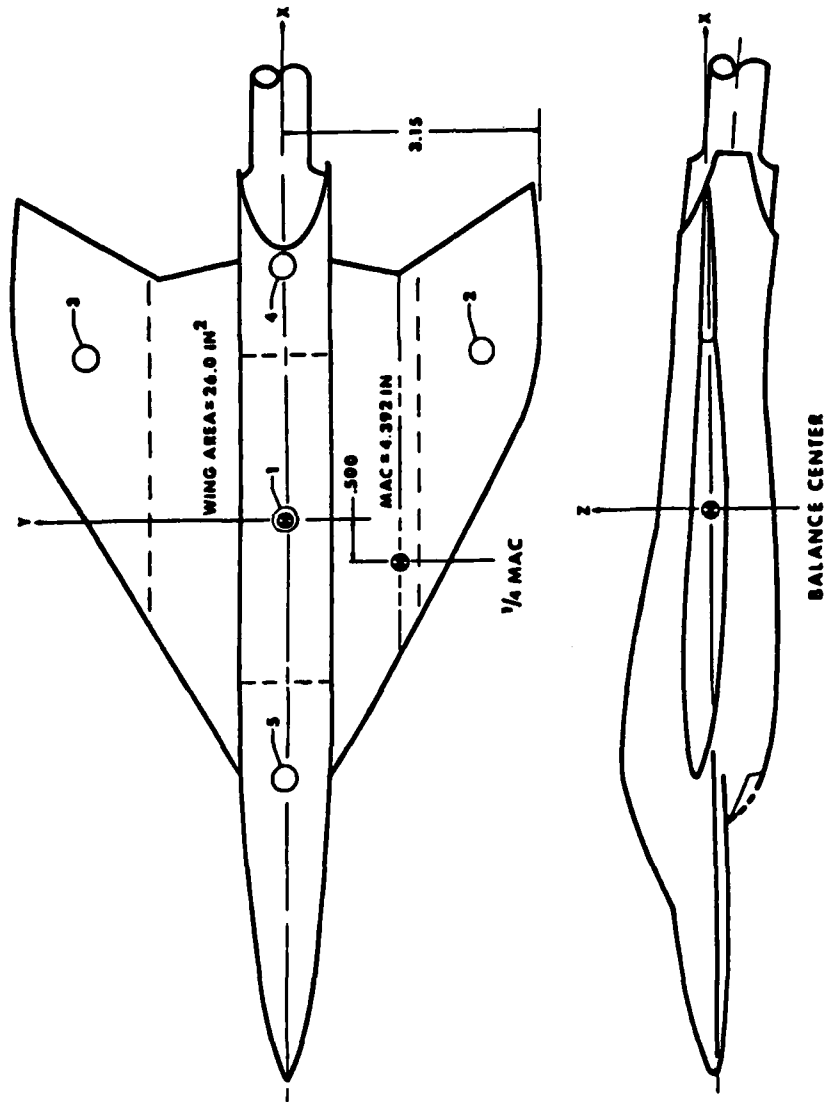


Figure 24. Sectioning of Lifting Model Showing Locations of Representative Singularities

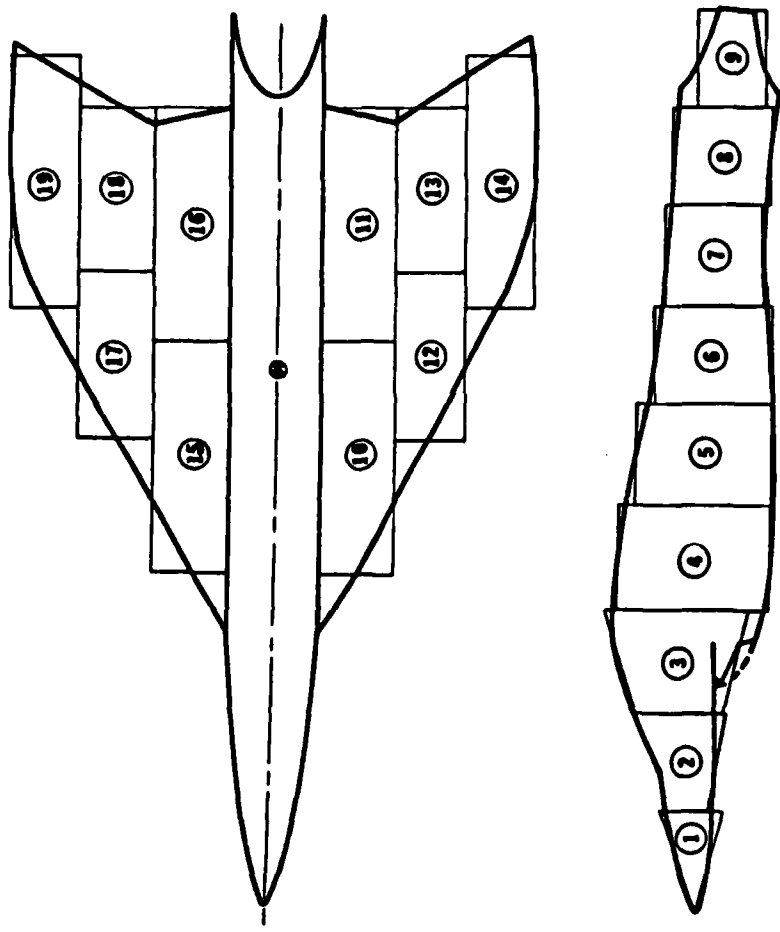


Figure 25. Refined Sectioning of Model for Solid Blockage Effects
Using a Distribution of Doublets

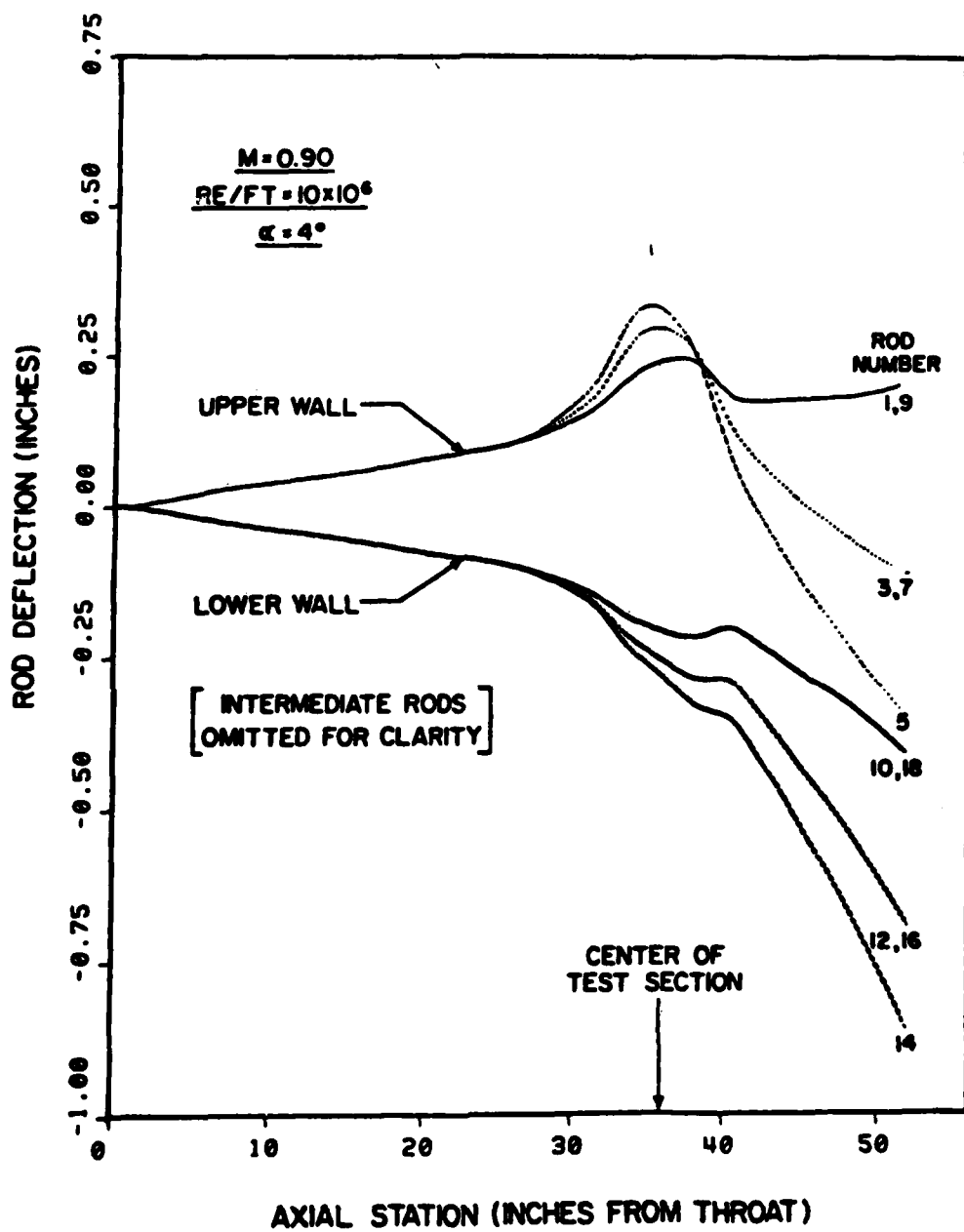


Figure 26. Typical Three-Dimensional Rod Contouring for the Lifting Model

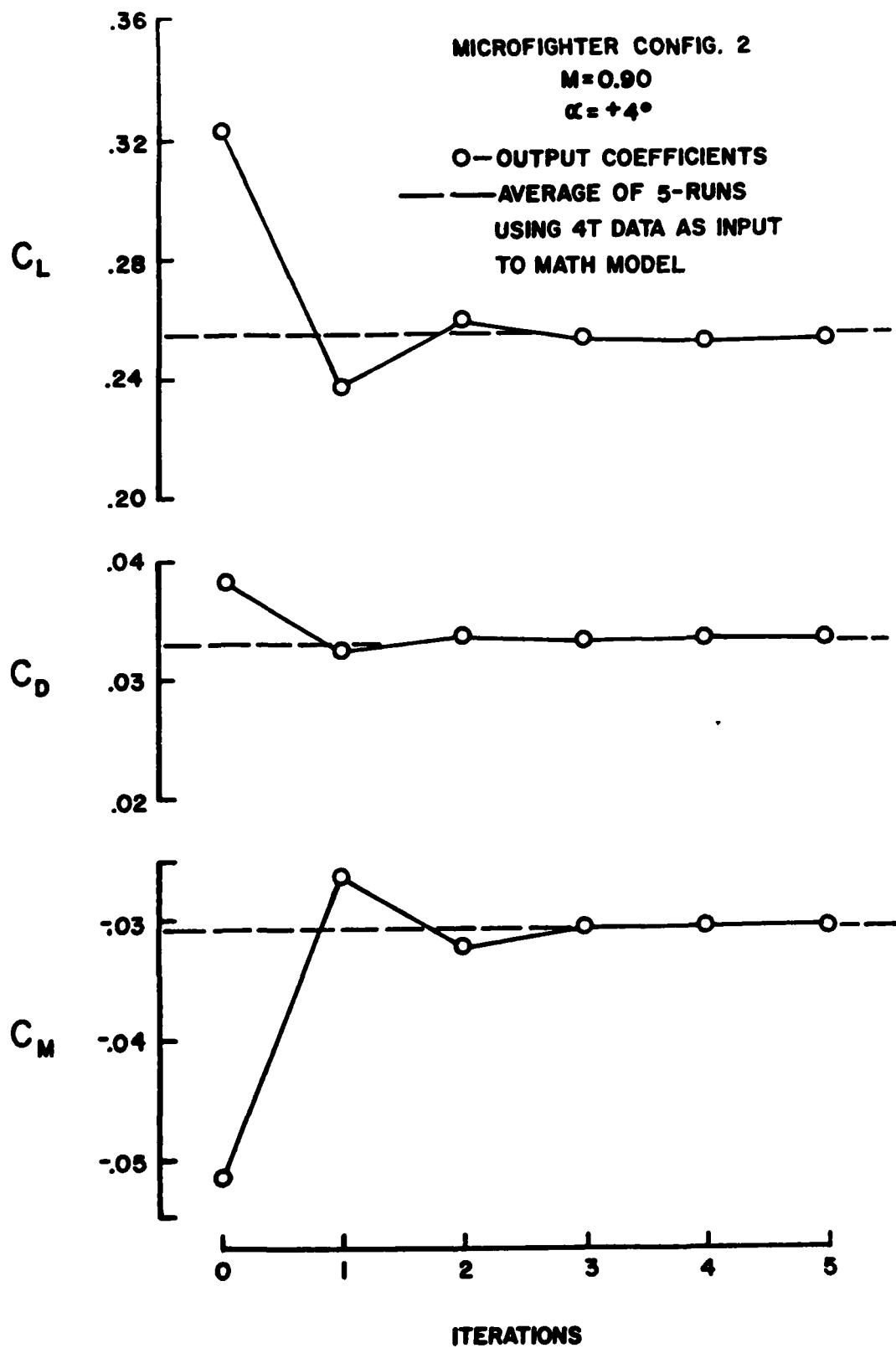


Figure 27. Convergence of Output Coefficients Using Zeros for Initial Input and Measured Values for Iterating.

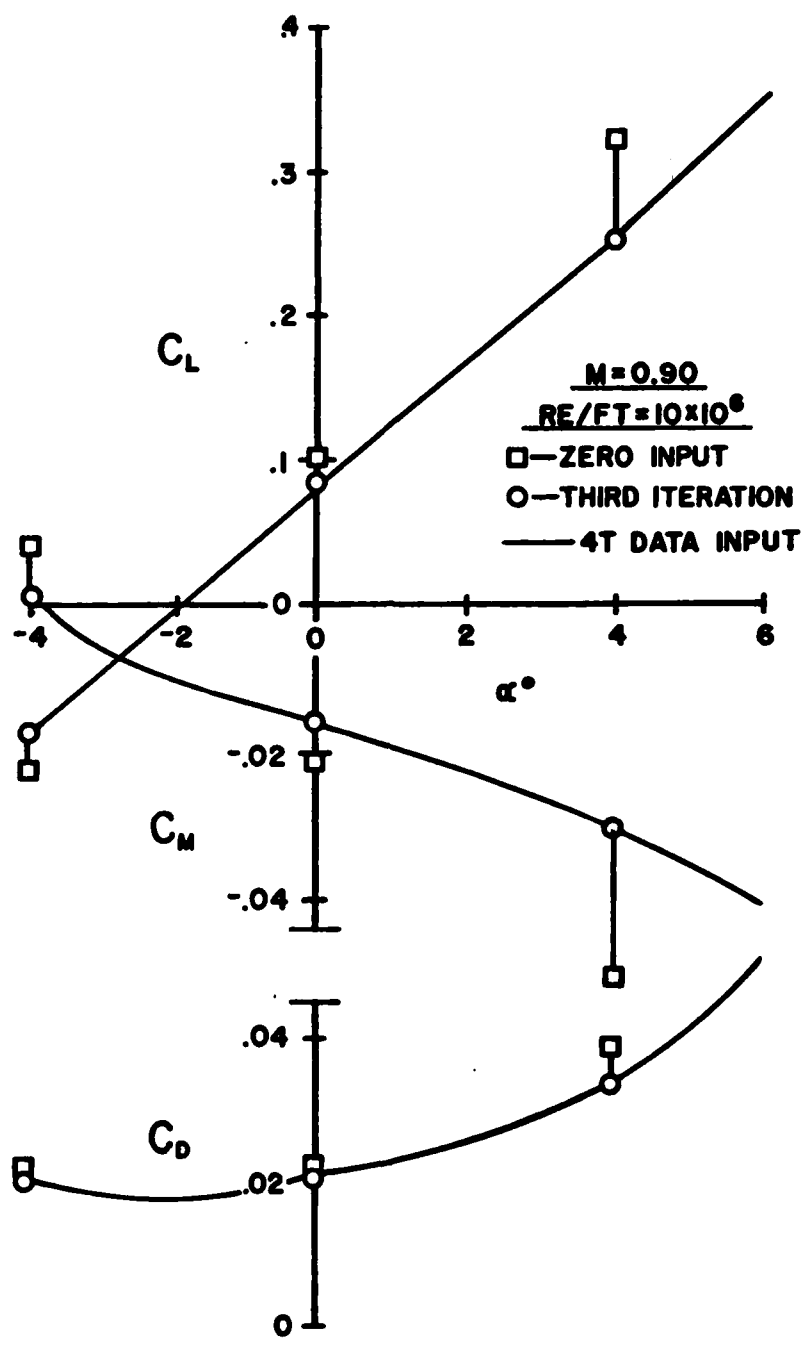


Figure 28. Variation of Convergence with Angle of Attack.

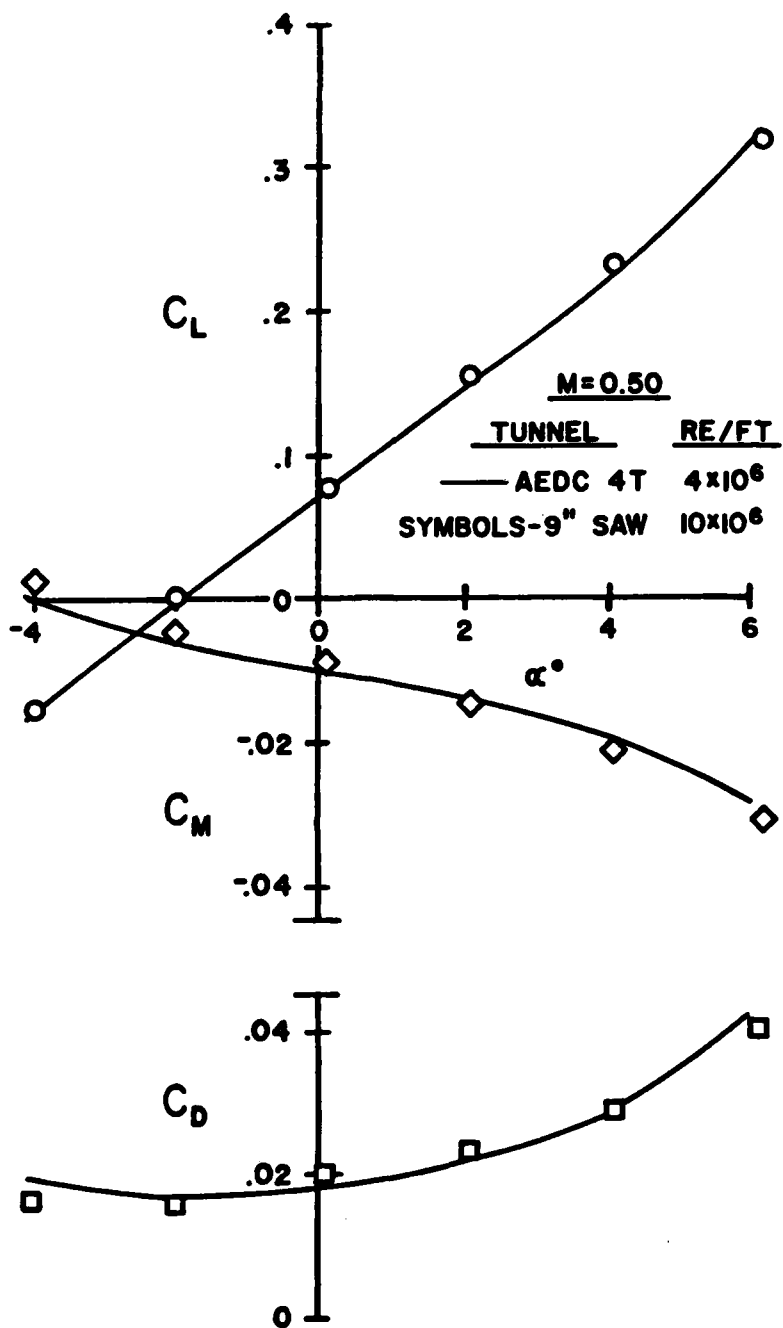


Figure 29. Comparison of Three-Dimensionally Streamlined Wall Output Coefficients with AEDC 4T Data. (a) $M = 0.50$

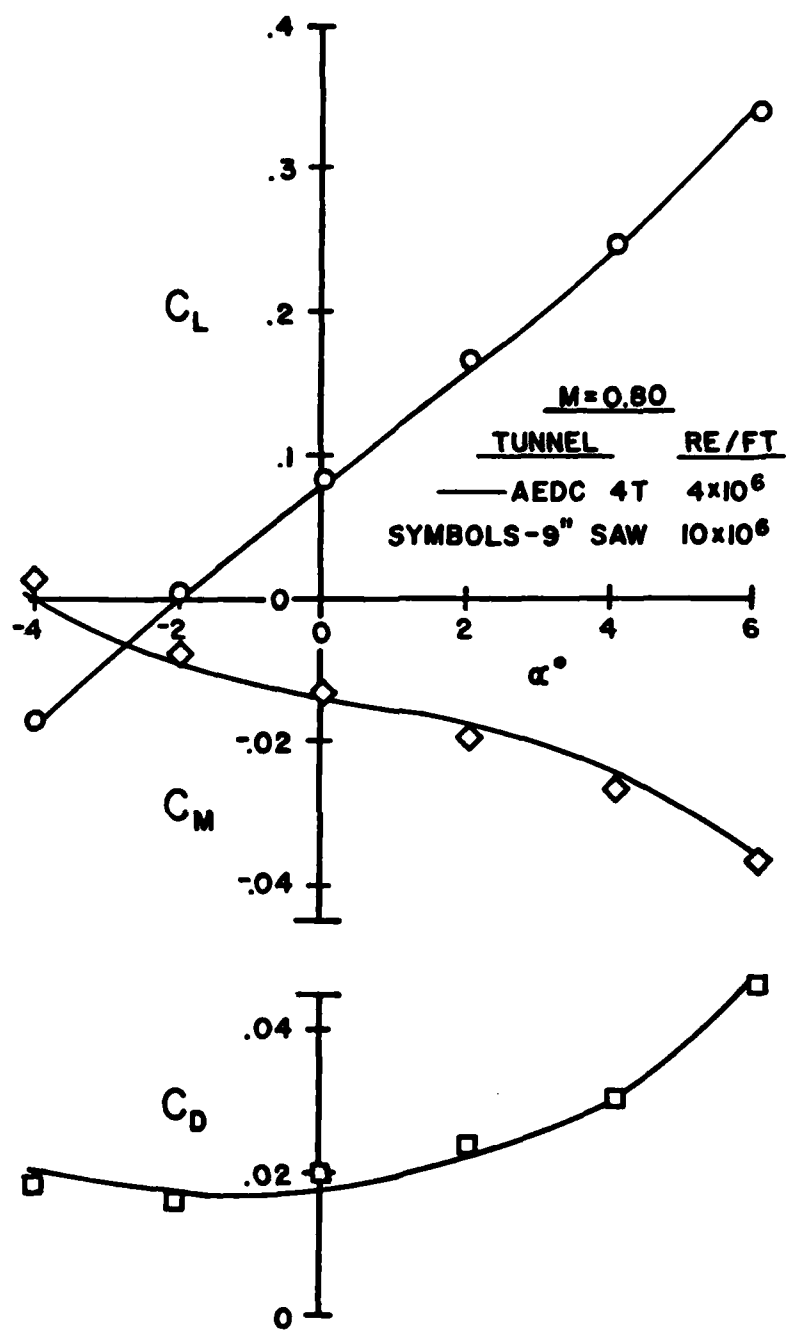


Figure 29 - Continued (b) M = 0.80

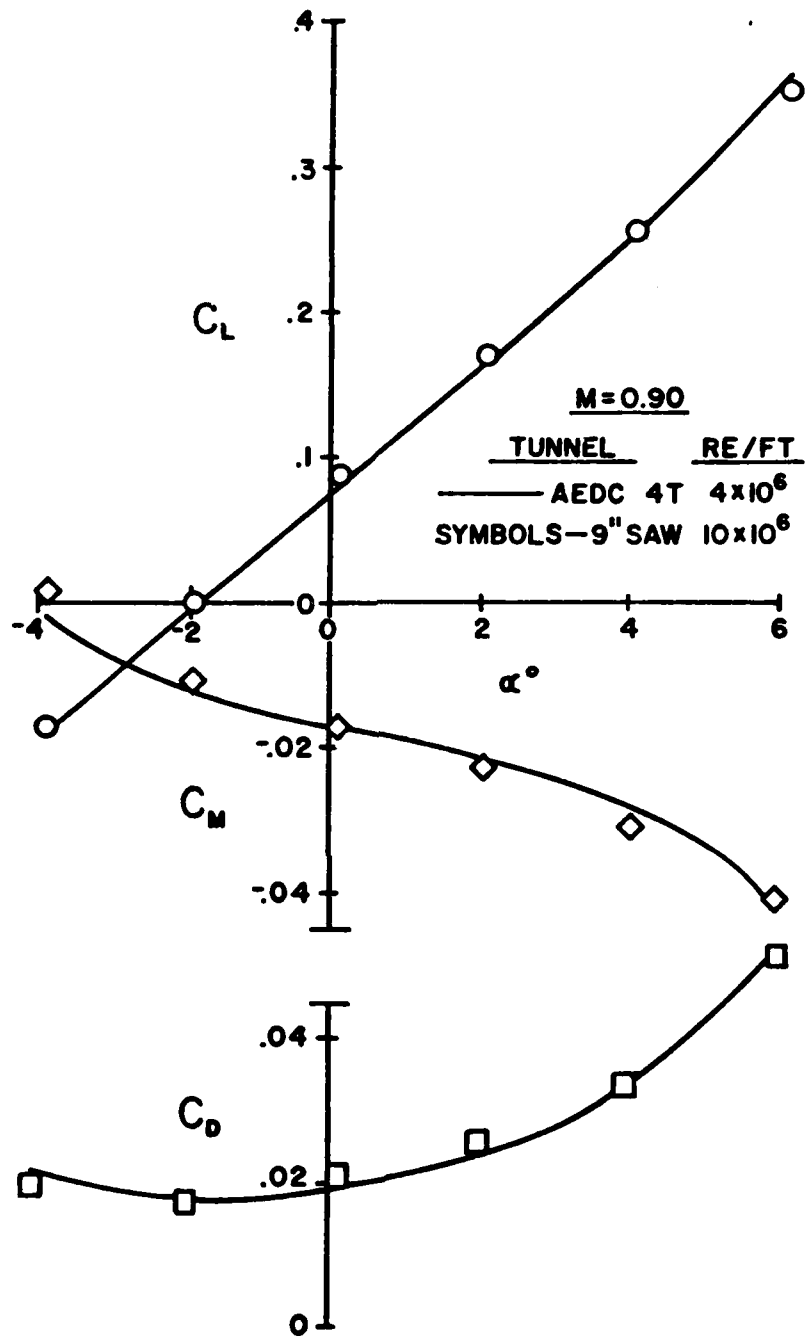


Figure 29 - Continued (c) M = 0.90

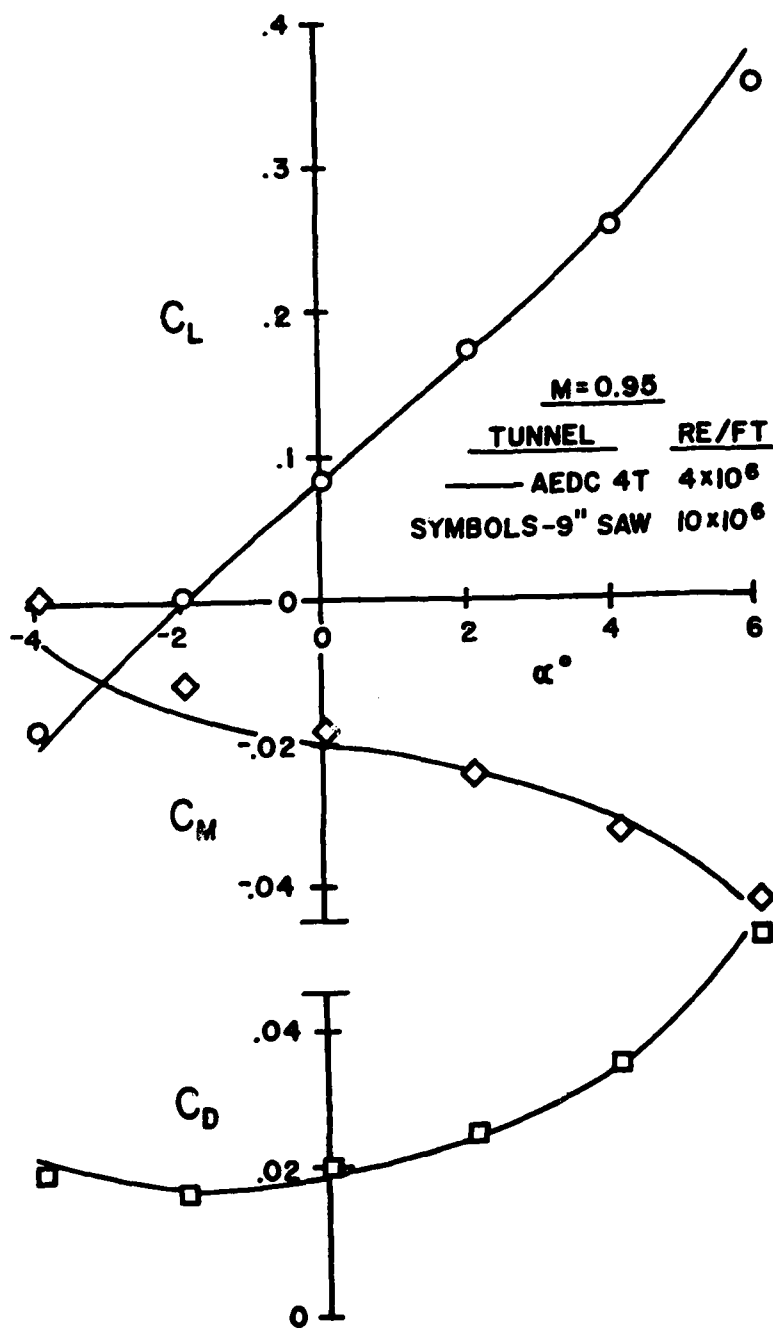


Figure 29 - Concluded (d) $M = 0.95$

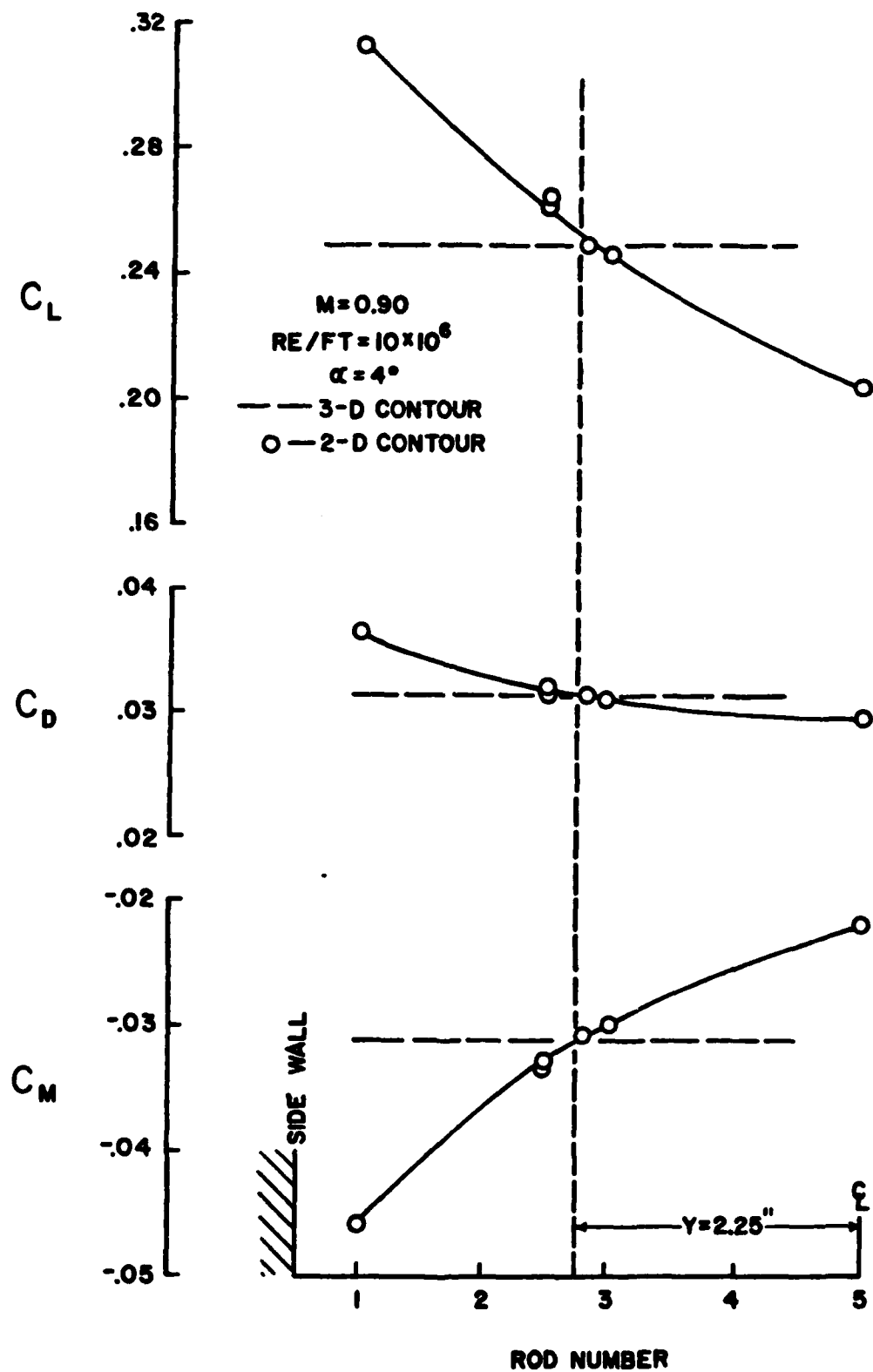


Figure 30. Effect of Varying 2-D Wall Contours in Relation to a 3-D Contour

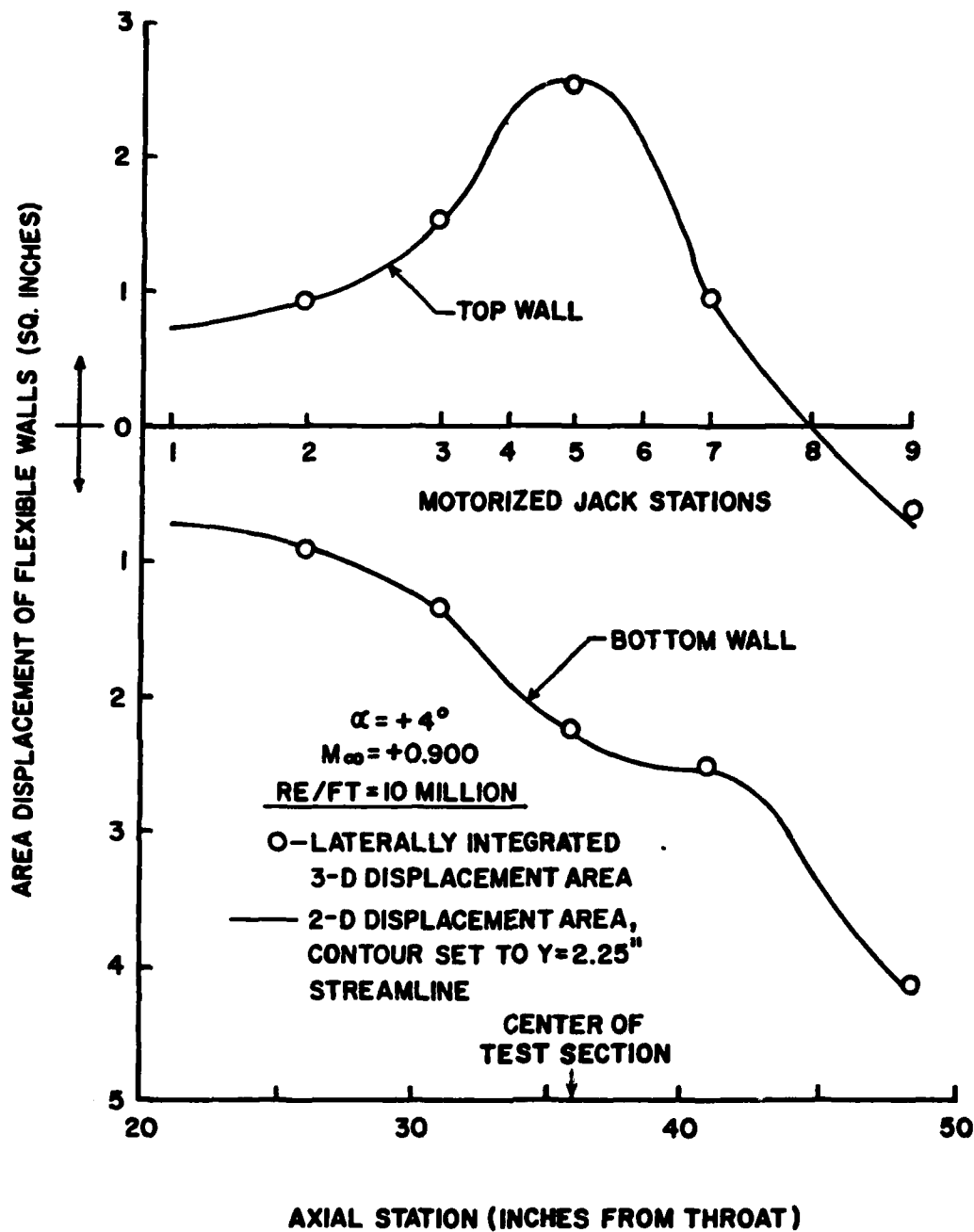


Figure 31. Comparison of the Area Displacement of 2-D and 3-D Wall Contours

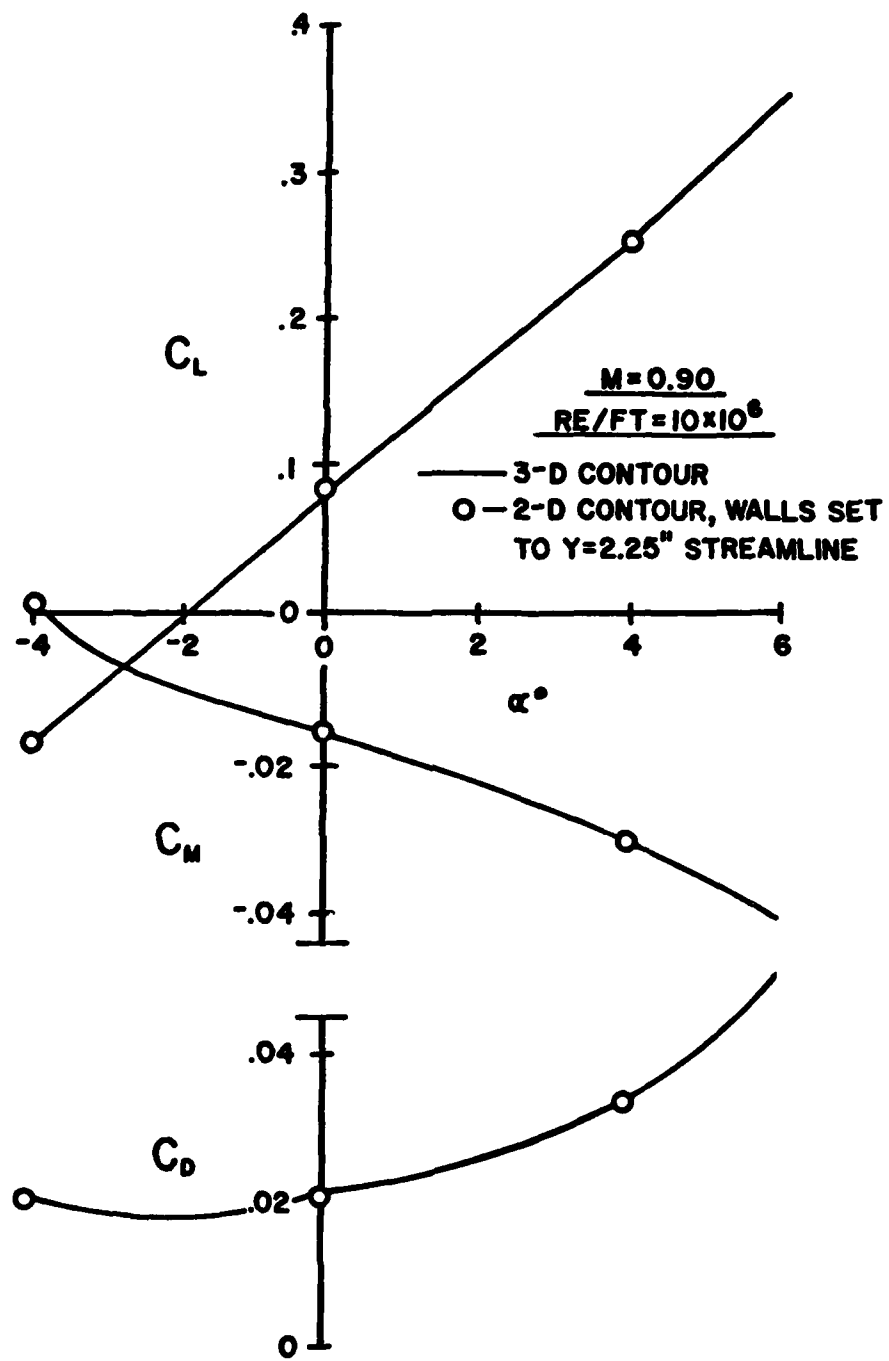


Figure 32. Additional Comparisons of 2-D and 3-D Contouring at $M = 0.90$.

END

FILMED

7-83

DTIC